Experimental Studies on Iron-Based Catalytic Combustion of Natural Gas

by

Kang Pan

A thesis
presented to the University of Waterloo
in fulfillment of the
thesis requirement for the degree of
Master of Applied Science
in
Mechanical Engineering

Waterloo, Ontario, Canada, 2013

Author's Declaration

I hereby declare that I am the sole author of this thesis. This is a true copy of the thesis, including any required final revisions, as accepted by my examiners.

I understand that my thesis may be made electronically available to the public.

Abstract

Catalytic combustion is an efficient method to reduce pollutant emissions produced by a variety of fuels. In this thesis, the use of iron pentacarbonyl ($Fe(CO)_5$) as a catalyst precursor in the combustion of natural gas is experimentally studied. The counter-flow diffusion flame burner is employed as the experimental apparatus. The products of combustion are analyzed by using a Gas Chromatograph (GC) to quantitate the effects of adding the catalyst.

The experimental setup is such that a mixture of methane (CH_4) and nitrogen (N_2) is fed from the bottom burner while a mixture of oxygen (O_2) and air is supplied from the top burner. The combustion of natural gas without catalyst is first characterized. The oxidizer and fuel flow parameters are set up so that a stable, flat blue flame is formed close to the centre plane between the two burners upon ignition. The experimental results agree with the literature data and the numerical predictions from CHEMKIN software.

To investigate and evaluate the performance of iron-containing catalysts on emission reduction, a small amount of separated nitrogen flow is used to carry iron pentacarbonyl into the flame through the central port of the fuel-side burner. Catalytic combustion produces an orange flame. Compared with the non-catalytic combustion data, it is found that carbon monoxide (CO) and soot precursor acetylene (C_2H_2) are reduced by 80% to 95% when 7453ppm iron pentacarbonyl is added.

Acknowledgements

Foremost, I would like to sincerely thank my advisor Prof. John Z. Wen for his continuous support and guidance in my Master study. His patience, motivation and immense knowledge help me smooth the difficulties in the research and acquire satisfied progress for the investigations of the clean-combustion technology. It is a great pleasure to work with Prof. Wen, and I would most like to thank him for bringing me into the combustion area and giving me opportunity to conduct a significant work for environmental protection.

I would specially thank Prof. Zhongchao Tan and Prof. Luis Ricardez Sandoval for being on my thesis committee.

I would also like to thank Prof. Tan and his student Fang Liu for providing me experimental equipment and other help in the process of my research.

I would like to express my appreciation to Prof. Murray Thomson and his students Dr. Tommy Tzanetakis, Dr. Mani Sarathy and Bobby Borshanpour, at University of Toronto. Their energetic help makes me well understand the configuration of the experimental system. Without their suggestions, I can not begin my experimental study.

I would also like to thank Prof. Gregory T. Linteris (National Institute of Standards and Technology, USA) for his help on the design of catalyst supply system and suggestions on how to use iron pentecarbonyl.

Thanks to my colleague Huixiu Qi for conducting the CHEMKIN modeling.

Many thanks for the financial support provided by NSERC and Cestoil Chemical Inc.. Warm thanks to Dr. Samuel Xiong and Dr. Henry Zhu for their suggestions and help on the experimental technologies.

I would also like to thank Tao Xu, Tracey Zhou, Saleh Lavaee, Abhishek Raj, John Rawlins and Jinhee Kang for their help. Thanks for the technical support on the machining from Jason Benninger and Engineering Machine Shop.

Finally, I would like to thank my wife and parents. Their endless love and support motivate me to face difficulties and keep moving forward. I appreciate having the honour of being able to live in such an amazing family.

Table of Contents

List of Tables

List of Figures

Glossary

Al_2O_3 aluminium oxide.

Au gold.

C_2H_2 acetylene.

C_2H_3 vinyl radical.

C_2H_4 ethylene.

C_2H_6 ethane.

C_3H_6 propene.

C_4H_3 vinylacetylene radical.

C_4H_4 vinylacetylene.

C_4H_5 1,3 butadienyl radical.

C_6H_5 phenyl radical.

CF_3Br halon 1301.

CH_4 methane.

CI compressed ignition.

CO carbon monoxide.

Co cobalt.

CO_2 carbon dioxide.

Cu copper.

EPC electronic pneumatic control.

$Fe(CO)_5$ iron pentacarbonyl.

FGR flue gas recirculation.

FID flame ionization detector.

FTIR Fourier transform infrared spectroscopy.

GC gas chromatograph.

GSV gas sampling valve.

H_2 hydrogen.

H_2NCONH_2 urea.

H_2O_2 hydrogen peroxide.

HC hydrocarbons.

HCN hydrogen cyanide.

IC internal combustion.

LIF laser-induced fluorescence.

MFC mass flow controller.

Mn manganese.

MvK Mars and van Krevelen.

N_2 nitrogen.

NEB National Energy Board.

NH_3 ammonia.

NO nitric oxide.

NO_2 nitrogen dioxide.

NO_x nitrogen oxides.

O_2 oxygen.

OH hydroxyl radical.

PAH polycyclic aromatics hydrocarbon (PAH).

Pd palladium.

PdO palladium oxide.

PF particulate filter.

PM particulate matter.

Pt platinum.

PtO_2 platinum oxide.

Rh rhodium.

SCR selective catalytic reduction.

SI spark ignition.

SiO_2-Al_2O_3 silica-alumina.

SNCR selective non-catalytic reduction.

SO_2 sulfur dioxide.

TCD thermal conductivity detector.

TiO_2 titanium oxide.

TOF turnover frequency.

V vanadium.

W tungsten.

ZrO_2 zirconia.

Chapter 1

Introduction

Natural gas is one of the major fuels in the world's energy market. In Canada, it is the second most used energy resource in industrial and residential application. Data published by National Energy Board (NEB) [5,6] about the Canadian energy production from different sources from 2002 to 2011 (shown as Fig 1.1) indicates that the energy generated from natural gas varied from 33.92% to 39.55% of the total compared to petroleum's 35.92% to 44.16%. In addition, the NEB report [12] predicts natural gas to be one of the fastest growing energy source until 2035, with an annual growth rate of 1.9%. This reveals that natural gas will play an integral role in future energy supply.

Compared with the other major energy resources, such as petroleum and coal, natural gas has lots of advantages that make it increasingly popular in the energy market.

- Natural gas is much cheaper than other fuels, such as crude oil. From 2000 to 2013, the price ratio of crude oil to natural gas based on the equivalent energy generation varied from 1.1 to 5. This is calculated according to the price data from NEB reports [12,13]. Therefore, the use of natural gas as an alternative fuel in the transport engines and the other devices is more economic.

- Natural gas has an abundant domestic production. The data from NEB [14] indicates that natural gas production was and will be always bigger than its demand in Canada from 2011 to 2035, and the difference between production and demand changes from 131 million-m^3/day to 102.3 million-m^3/day, correspondingly. Although the difference will slightly decrease, its production is always enough for daily demand.

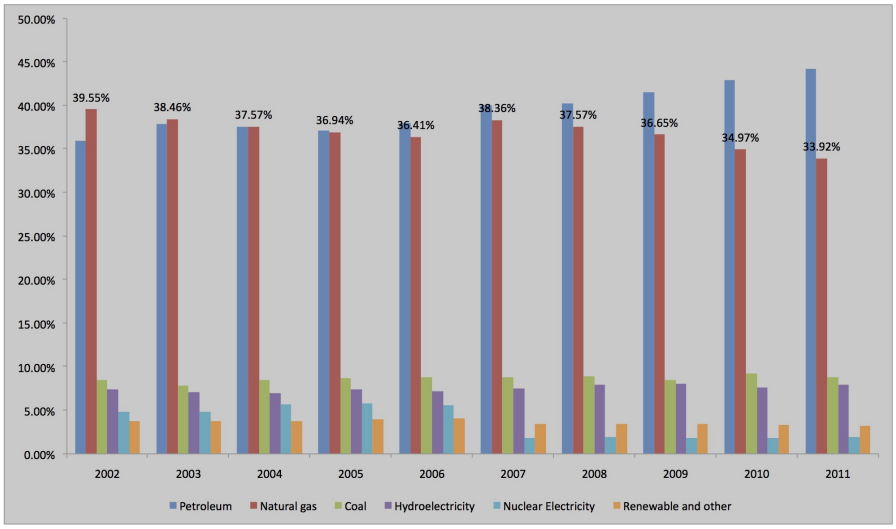

Figure 1.1: Energy production from different energy sources in Canada.(Data sources are from NEB [5, 6])

- Natural gas is one of the safest fuels used in various applications. Compared to petroleum products, such as gasoline and diesel, the ignition of natural gas not only requires a higher temperature but also need its concentration to be within a certain range (from 5% to 15%) [1, 15]. In addition, natural gas is lighter than air, so that it can be easily dispersed to the surroundings. This avoids potential fire or explosion in case of a fuel leak. Consequently, natural gas is safer than petroleum for delivery and storage.

- Natural gas produces less pollutant emissions. Studies on natural gas combustion in engines indicate the major emissions can be highly reduced by 40 $\sim$ 87% for hydrocarbons (HC) and 80% for both carbon monoxide(CO) and nitrogen oxides (NO_x), compared with gasoline and diesel [1, 3, 15, 16]. Fig 1.2 shows the emissions produced by the three major fuels: natural gas, coal and gasoline. Compared with the two latter fuels (coal and oil), natural gas combustion produces much lower NO_x, CO, carbon dioxide(CO_2) emissions, and almost zero sulfur dioxide (SO_2) and particulate matter (PM).

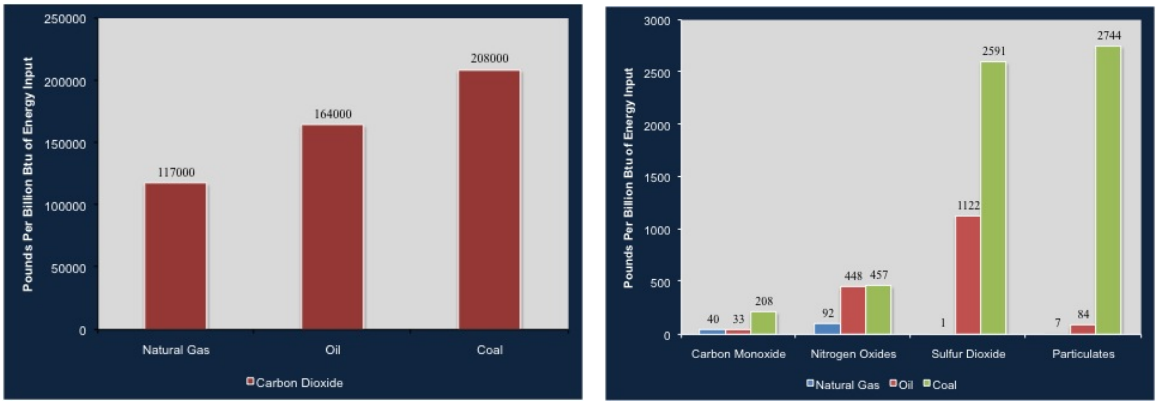

(a) (b)

Figure 1.2: Comparison of the major emissions produced by natural gas, coal and petroleum. a) CO_2 levels. b) Other pollutant emissions. (Data sources are from Energy Information Administration [7])

1.1 Research Motivation

Although natural gas has numerous benefits, its combustion still produces a significant amount of pollutant emissions, as shown in the Fig.1.2. Since the environmental standards and regulations are becoming more and more strict, future reduction of these emissions is critical for the natural gas fired power plants to achieve their environmental and economic goals.

Among different clean-burning technologies, the concept of catalytic combustion has been established as an efficient method for reducing CO and particulate matter (especially soot), through increasing the combustion efficiency and introducing the oxidation pathways on the catalytic surface [10, 17]. Normally, the catalysts used for emissions reduction in combustion are based on noble metals (such as platinum and palladium) and metal oxides (such as single and mixed metal oxides). Although noble metal based catalysts are better catalytic agents for complete combustion, they are toxic, easily vaporized, expensive and also limited in source. Metal-oxides based compounds are thereby developed as the alternative catalysts. However, they usually have lower activity and/or strong sintering tendency that renders them less useful for the high temperature application [18].

Compared to other catalysts, iron-oxide based catalysts are considered as a promising candidate for the intermediate and high temperature application. This is because they are much cheaper than noble metals and have a higher sintering temperature than the other metal oxides [19, 20]. Furthermore, the chemical solution iron pentacarbonyl ($Fe(CO)_5$) can

be treated as the precursor of the iron-oxide based catalysts, and it is expected to be applied for controlling the pollutant emissions generated from natural gas combustion. However, research on the performance of the iron-oxide based catalysts for reducing the pollutant emissions is not available in the literature, especially in the case of using $Fe(CO)_5$ as the catalyst additive. Therefore, the experimental studies on natural gas combustion with $Fe(CO)_5$ addition are important for developing and optimizing the novel clean combustion technologies based on iron-containing catalysts.

Due to its non-premixed, one dimensional and easy controlled, the counter-flow diffusion flame, which is one basic technology to investigate the fundamentals and kinetic mechanism of combustion [21], is chosen to study the emission control by iron-based catalysts. However, for such an open experimental system, how to diminish the experimental uncertainties and obtain an accurate measurement of gas profiles generated from the diffusion flame is critical for conducting further combustion studies. In addition, as the numerical simulation can not only save experimental cost but also guide the potential combustion studies and application, the use of an appropriate numerical model is always favored for the combustion study. Among different numerical softwares such as COMSOL and CFD, CHEMKIN is a good tool which can simulate the chemical reaction in a counter-flow flame and predict its gas structure. In order to make sure the simulated results give a correct conclusion, the modeling results need to be validated by experimental data to confirm its correctness. Therefore, comparison of the results obtained from experiments and modeling are necessary for developing and improving the numerical model.

1.2 Research Objective

In this thesis, the goals of the experimental measurements on catalytic and non-catalytic combustion are to characterize the emission profiles of a natural gas combustion generated in a counter-flow flame apparatus and to investigate the effects of iron-based catalysts. The specific objectives of this study are:

- To build up the counter-flow flame apparatus as well as finalize its gas diagnostics system;
- To establish the experimental database of the non-catalytic combustion of natural gas and compare with the CHEMKIN simulated data;

- To investigate and evaluate the performance of iron pentacarbonyl on the reduction of the pollutant emissions (especially CO and soot precursor C_2H_2) from the natural gas combustion.

Chapter 2

Literature Review

Natural gas is a gaseous mixture composed of different hydrocarbons and some other gas compounds. The primary composition of natural gas is methane(CH_4) whose content can be more than 90%, and there are also several different alkanes such as ethane, propane and very few amounts of other components including nitrogen and carbon dioxide [15, 22]. Table 2.1 gives the typical composition of natural gas.

Table 2.1: Composition of natural gas (Based on literature data [1–4])

Components	Examples	Content
Methane	CH_4	90% ∼ 95%
Ethane	C_2H_4	0∼5%
Propane	C_3H_8	0∼1%
Other Hydrocarbons	C_4H_{10}, C_5H_{12} and C_{6+}	0∼1%
Carbon Dioxide	CO_2	0∼1%
Nitrogen	N_2	0∼5%
Others	O_2, CO, etc.	0∼0.2%

As the major composition of natural gas is methane which has a higher H/C ratio, its combustion products are less CO_2 and more water compared with other fossil fuels. Consequently, natural gas is much more friendly to the environment. Instead of the conventional fossil fuels, it is widely used in various areas, especially in industry and transportation.

2.1 Emissions Characteristics of Natural Gas Combustion

The combustion of natural gas (especially methane) can be described as the overall reaction 2.1, where the reaction temperature can reach above 1600 °C. The final products from the combustion are expected to be only CO_2 and water, however, it still produces some pollutant emissions such as NO_x, soot and CO, due to the complicated operation conditions in different applications.

$$CH_4 + 2O_2 \rightarrow CO_2 + H_2O, H_{298} = -802.7kJ/mol \tag{2.1}$$

To efficiently use natural gas, a great number of studies have been conducted in the past to understand the characteristics of natural gas combustion. These studies were not only experimentally conducted in various systems such as engines and bench-size burners but also numerically simulated by the specific modeling softwares such as CHEMKIN. According to these studies, the emission profiles of natural gas combustion are well known.

Studies [3, 23, 24] on internal combustion (IC) engines (including spark ignition (CI) and compressed ignition (CI) engines) indicated that natural gas produced several pollutant emissions such as NO_x, CO and PM, which have much lower levels compared with those generated from petroleum. As the fuel injection time varied, the concentrations of the major emissions from the combustion of natural gas in the direct-injection engines can reach 100 to 500 ppm for HC, 0.1% for CO and 100 to 600ppm for NO_x [25]. These emissions can also be affected by the engine operation conditions, which made NO_x can be above 1000ppm when a CI engine worked at the high-load condition [26].

Research on natural gas combustion was also conducted in the bench-size systems to study the generated species. Puri et al. [27] compared the chemical structure of a methane/air counter-flow diffusion flame measured from the experiments with the numerical simulation. The profiles of CH_4, oxygen(O_2) and nitrogen(N_2), CO, CO_2, acetylene(C_2H_2), ethylene(C_2H_4) and ethane(C_2H_6) were measured by a gas chromatograph (GC) via a quartz microprobe. The experimental measurements matched with the numerical simulation well. Moreover, Khanna et al. [28] experimentally investigated the CO and NO_x emissions from a methane/air premixed flame using a porous medium burner. The results indicated that the methane combustion in the porous burner were very low with the values of approximately 31ppm for NO_x, 26ppm for nitric oxide (NO) and 125ppm for CO under all the experimental

conditions. The study also found that NO increased as the flame speed increased but the total emissions of NO_x (NO and nitrogen dioxide (NO_2)) were kept constant if the equivalence ratio was fixed. In addition, CO emission was kept constant first and then would be increased when the flame speed was increased to a certain level.

2.1.1 NO_x Formation

NO_x Formation Mechanism

NO_x is a major source contributed to the formation of smog, acid rain and tropospheric ozone. It is one of the major pollutant emissions produced from the combustion process, mainly coming from three mechanisms: thermal NO_x, prompt NO_x and fuel NO_x [29, 30].

- The first source is the thermal NO_x generated from the oxidation of atmospheric nitrogen, which was first suggested by Zeldovich and then extended by Hanson and Salimian. The thermal NO_x mechanism can be described as the following reactions:

$$O_2 \leftrightarrow 2O \tag{2.2}$$
$$N_2 + O \leftrightarrow NO + N \tag{2.3}$$
$$N + O_2 \leftrightarrow NO + O \tag{2.4}$$
$$N + OH \leftrightarrow NO + H \tag{2.5}$$

  Based on these reactions, it is found that the formation of the thermal NO_x depends on the O_2 dissociation, which needs a high temperature. Therefore, the formation rate of NO_x is highly affected by the reaction temperature, the concentrations of N_2 and O_2, and their residence time under the reaction temperature. Moreover, the concentration of hydroxyl radical (OH) is another key factor that affects the NO_x formation, shown as the reaction 2.5.

- The second source is the prompt NO_x coming from the reactions of N_2 with the hydrocarbon radicals including C and CH. Under a fuel rich condition, these reactions usually occur at the earliest stage of the combustion with a low temperature and a short residence time. N_2 will react with the radicals to form some intermediate species such as hydrogen cyanide (HCN), shown as the reaction 2.6. Then these species are oxidized to NO_2. Compared with the thermal NO_x, the prompt NO_x is negligible as

the concentrations of the hydrocarbon radicals are usually very low.

$$CH + N_2 \leftrightarrow HCN + N \tag{2.6}$$

- The third source is the fuel NO_x which is attributed to the oxidation of the fuels containing the organically bound nitrogen. Usually, the nitrogen bonds in the fuels, such as coal and oil, are easily broken to release free radicals which will then react with oxidizers to form NO_x. The fuel NO_x mechanism contribute to 50% to 70% of the total NO_x emissions in the combustion of coal and oil [31], however, it is not a big problem for natural gas due to its low nitrogen content.

NO_x Emission in Natural Gas Combustion

Hahn and Wendt [32] studied the flame structure of methane diffusion flame in a counter-flow burner by both experiments and numerical simulation. The kinetic mechanism of NO_x formation was validated by comparing the experimental measurements with the modeling results. Moreover, the profiles of other components such as CO and CO_2 were also investigated. The results has shown that the opposed diffusion flame was a good tool to conduct the fundamental studies of fuel combustion.

Blevins and Gore [33] used GRI-Mech 2.11 chemical mechanism to simulate a methane/air counter-flow flame with a low strain rate. In the chemical model, methane partially mixed with air were directed from one side, and the pure air was injected from another side. In this study, the combustion products including CO, CO_2 and hydrogen(H_2) were predicted to study the flame structure. The modeling results investigated the profiles of NO and some radicals such as CH_i in the flame with different fuel-side equivalence ratio, where it has demonstrated the importance of CH_i and the equivalence ratio for NO destruction and formation.

The experimental and numerical studies on the soot and NO formation in a CH_4/O_2 enriched counter-flow diffusion flame was conducted by Fridman et al. [34]. The profiles of C_2H_2, C_2H_4 and C_2H_6 were measured in the experiments, in order to develop and validate the GRI-Mech 2.1 numerical model for predicting the soot formation. The NO formation was then numerically investigated by studying its distribution in the diffusion flame, which revealed the importance of thermal and prompt mechanisms on NO production and destruction. The authors also investigated the changes of NO and soot profiles affected by the varied oxygen content and strain rate.

Dupont and Williams [35] investigated the NO_x formation mechanism in the rich methane/air double flames. Comparison of the experimental measurements of NO profile in the co-flow flame with the modeling results revealed the importance of prompt mechanism for NO formation. A counter-flow flame model was also used in this study and revealed that the high equivalence ratio and high strain rate were preferred for controlling NO emission. However, the emissions of CO, unburnt hydrocarbons and soot were increased simultaneously.

2.1.2 Particulate Matter Formation

PM, one of the most important pollutants generated from the combustion process, is the collection of small solid particles or liquid droplets with different diameters (usually in micrometer). Typically, PM contains smoke, dust, ash and soot, which had bad effects not only for the environment by reducing the visibility and forming acid rain but also for human health by decreasing the lung function and increasing the respiratory symptoms [36]. As one of the major PM sources, soot has already been paid more attentions in the combustion research.

Soot Formation Mechanism

Soot is actually the tiny carbon particles generated by the incomplete combustion of hydrocarbon fuels. Usually, the formation of soot from the combustion process has four steps including the formation of soot precursors, particle inception, particle growth and particle oxidation [8, 37, 38].

- First of all, the hydrocarbon fuels are broken to form C_2H_2 during the pyrolysis process, especially under a fuel rich condition. C_2H_2 then reacts with the hydrocarbon radicals such as vinyl radical (C_2H_3) to grow into the small aromatic ring such as benzene and phenyl radical (C_6H_5) via several different routes at different temperatures. The dominant pathway, adding C_2H_2 to the vinylacetylene radical (C_4H_3) radical, usually occurs at a high temperature and is the preferred route in a premixed flame. In a diffusion flame, two other pathways under a low temperature occur to form the aromatic ring, where the alternate route A and B are to add C_2H_2 to 1,3 butadienyl radical (C_4H_3) and vinylacetylene (C_4H_4) respectively. Moreover, there is one more route, regarded as the alternate route C, to form the small aromatic ring (C_6H_5)

via the rapid pyrolysis of allene and methyl acetylene. After the small aromatic ring is formed, it finally grows into the larger aromatic ring (polycyclic aromatics hydrocarbons (PAHs)) via C_2H_2 addition and H_2 abstraction. All of these soot formation routes are shown in Fig 2.1.

- Once the PAH is formed, the primary soot particles with the diameters of less than 1.5 nm can be formed by coagulating these lager aromatic rings. This process actually is to transform the molecular gas species to the three dimensional solid particles.
- The primary soot particles will then continue growing to the larger aggregates by the surface growth reaction and coagulation. The surface growth can increase the soot amount but keeps the soot particles with a constant number, and the coagulation keeps the soot amount constant but reduces the amount of the soot particles via the particle collision and coalescence.
- Finally, the oxidizers mainly including O_2 and OH radicals will then oxidize the soot particles to determine the final soot emission generated in the combustion process.

Soot Precursors

Based on the soot formation mechanism, the soot precursors are found including benzene and PAH, among which C_2H_2 is considered as an important one [8,37,38]. Fig 2.1 has shown the importance of C_2H_2 for the soot growth as it participates in almost the whole process of soot formation, where C_2H_2 is generated first and then reacts with other hydrocarbons to form the soot particles. Therefore, the studies on the C_2H_2 concentration in the combustion process is critical for investigating the final soot production.

Soot Emission in Natural Gas Combustion

Senkan and Castaldi [39] compared the PAH formation in the premixed methane flame with those in two other flames fuelled with ethane and propane. Hydrocarbons including C_2H_2, C_3 species and PAH were experimentally measured by a gas analyzer GC-MS from a porous bronze burner. The results indicated that methane flame had the higher benzene and PAH production than ethane flame, but their levels were lower than those generated from propane flame. Moreover, C_2H_2 and soot produced from the methane flame were found less than those from the other two flames. These findings indicated that the hydrocarbons

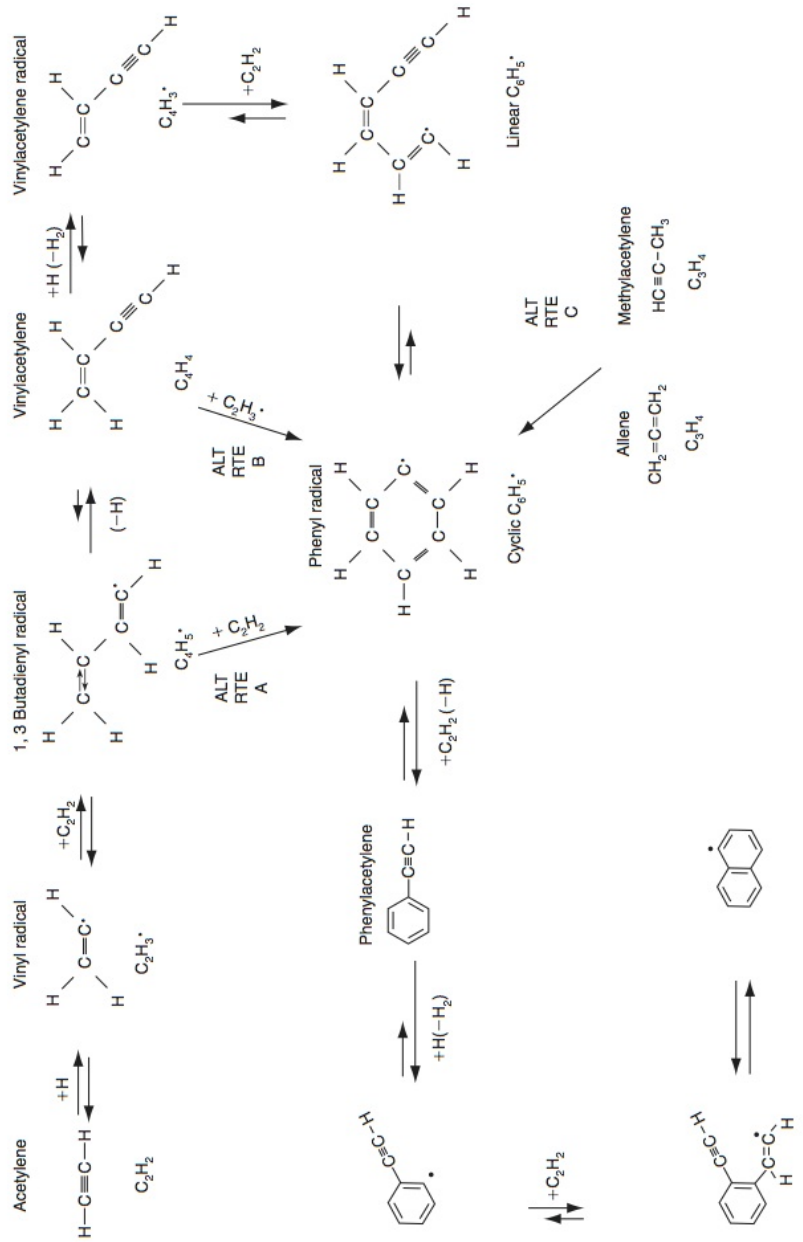

Figure 2.1: Schematic of the general soot formation mechanism [8].

with odd number of carbon atoms were significant for the PAH formation in a premixed methane flame.

A chemical modeling of an opposed diffusion flame fuelled with methane was studied by Marinov et al. [39]. The detailed chemical reaction pathways of different soot precursors, especially PAH and aromatics, were well understood and found consistent in this study. The predictions of PAHs, aromatics and other large compounds by modeling agreed with the experimental results, however, the prediction of four ring PAHs did not match the measurements well.

Smyth et al. [40] used a co-flow burner to experimentally study the soot formation in a methane/air diffusion flame. The measured peaks of the intermediate hydrocarbons including C_2H_2 and C_6H_6 were found consistent with the positions of the earliest soot particles. This finding indicated these components were the important precursors for the soot formation. Moreover, the study also measured the profiles of CO, CO_2 and other C_2 species in order to investigate the chemical reactions in this diffusion flame. The investigation suggested that the chemical growth process was critical for the formation of soot and its precursors.

2.1.3 CO Formation

CO Formation Mechanism

CO is another major pollutant emission produced from the combustion, as it is highly toxic that it can harmfully affect the human's respiratory system. Compared with NO_x and soot, the mechanism of CO is much easier that it is actually the product from the incomplete combustion of hydrocarbon fuels [29]. In the hydrocarbon flame, the hydrocarbon fuels will be oxidized to form CO first, and then it is further oxidized to CO_2. This process can be described as the following reactions (Reaction 2.7 and 2.8). However, in a fuel rich condition, the oxidizer is not enough to oxidize all the CO to CO_2 that it will form a certain amount of CO as one of the final products.

$$C_mH_n + O_2 \leftrightarrow mCO + \tfrac{n}{2}H_2O \tag{2.7}$$

$$CO + \tfrac{1}{2}O_2 \leftrightarrow CO_2 \tag{2.8}$$

CO Emission in Natural Gas Combustion

A fuel ultra-lean methane/air premixed flame was studied in an homogenous combustion reactor by Wang et al. [41]. The combustion reaction process was studied by measuring the concentrations of the major gas components like CO and CO_2 by using both GC and Fourier transform infrared spectroscopy (FTIR). The measurements indicated that CO_2 was mainly oxidized from CO at the high temperature, and a small amount of CO_2 can also be directly produced from methane oxidization at the low temperature simultaneously. A enhancement for the methane combustion was also found by increasing the gas contact area through adding a monolith to the reactor. Based on the experimental results, the study developed a simplified methane combustion mechanism as well.

Kolzov et al. [42] simulated the characteristics of CO in a lean methane/air premixed flame by using the GRI-Mech 3.0 chemical mechanism. The modeling results indicated that more CO was produced as the mixture was leaner only when the flow residence time is shorter than 13 ms, otherwise the CO tendency was totally opposite. The authors also studied the effects of temperature on CO emission by adding two different kinds of boundary conditions to the bulk combustion chamber. The results demonstrated that the low temperature can increase CO production due to the incomplete combustion of methane.

2.2 Pollutant Reduction Technologies

As the major pollutants generated from the combustion process are harmful for both the environment and human health, numerous technologies for pollutant control have been studied and developed in the past years.

2.2.1 NO_x Control Technologies

The methods for reducing NO_x actually can be divided into two types, which are identified as the pollution prevention and the add-on technologies [30, 43]. The add-on controls are to reduce or change the NO_x back to nitrogen by adding some agents. The major applications contain selective catalytic reduction (SCR), selective non-catalytic reduction (SNCR) and the oxidant injection. The pollution prevention technologies, which typically include catalytic combustion, water injection and flue gas recirculation (FGR), are to change the combustion process to inhibit the formation of NO_x.

Add-on Technologies

SCR is a kind of technology to pass the boiler flue gas through a catalyst bed, where the reaction of NO_x and the injected ammonia (NH_3) is promoted by the catalyst to generate nitrogen and water. Ammonia is the key reductant that can react with NO_x at the dominate routes shown as the reactions 2.9 and 2.10 [44]. Catalyst is another key agent which usually consists of a carrier and an active component. The common material used as carrier is the ceramic ones (especially titanium oxide). For the active component, the precious metals such as platinum (Pt) and palladium (Pd) can be used when the temperature varied from 170 to 300 °C. Moreover, the base metals like vanadium (V) and tungsten (W) are used when it was from 260 to 430 °C and Zetolites can stand a higher temperature range from 450 to 600 °C [30]. The catalysts are mainly manufactured as a honeycomb form, where an extruded carrier is homogeneously merged with or surfacely coated with the active components, or a plate form, where the active components are coated on the support materials. SCR has already been widely used in the power plants [45, 46] and engines [47, 48].

$$4NO + 4NH_3 + O_2 \rightarrow 4N_2 + 6H_2O \tag{2.9}$$

$$2NO_2 + 4NH_3 + O_2 \rightarrow 3N_2 + 6H_2O \tag{2.10}$$

Similar to SCR, there is another technology using ammonia or urea (H_2NCONH_2) to reduce NO_x with the absence of catalyst, called SNCR. Instead of ammonia, urea is the common reducing agent in SNCR which will release ammonia in the first step (shown as the reaction 2.11) and then reacts with NO_x. Since there is no catalyst, SNCR needs a higher operation temperature to promote the reactions. However, if the temperature is too high (above 1050 °C), ammonia can be oxidized to NO (shown as the reaction 2.12) so that it decreases the efficiency of NO_x reduction. Consequently, there is an appropriate temperature range from 850 to 1050 °C to achieve the maximum NO_x reduction [30, 49, 50]. SNCR is widely used in the power plant [51] and diesel engine [52]. In the meanwhile, some other studies [53, 54] also investigated the combination of SNCR and SCR in order to obtain the ultra-low NO_x emission.

$$H_2NCONH_2 \rightarrow NH_3 + HNCO \tag{2.11}$$

$$4NH_3 + 5O_2 \rightarrow 4NO + 6H_2O \tag{2.12}$$

The oxidation of NO_x is another method for NO_x removal [30,55]. One kind of technology

using this method is to inject the oxidants, such as ozone or hydrogen peroxide (H_2O_2), into the exhaust gas, where NO_x can be oxidized to N_2O_5 and then absorbed by water. A typical reaction mechanism for this technology is shown as the following reactions (2.13 $\sim$ 2.15). Another technology based on this method is to use the non-thermal plasma to produce some active radicals which can oxidize NO_x to N_2O_5. These NO_x oxidation technologies have already been widely used in the industrial boiler [56] and the internal engine [57, 58] with the NO_x removal efficiency of approximately 95%.

$$NO + O_3 \rightarrow NO_2 + O_2 \tag{2.13}$$

$$NO_2 + O_3 \rightarrow N_2O_5 + O_2 \tag{2.14}$$

$$N_2O_5 + H_2O \rightarrow HNO_3 \tag{2.15}$$

Pollution Prevention Technologies

Most of the pollution prevention technologies are essentially based on reducing the reaction peak temperature to control the NO_x emission. Water or steam injection is such a method used in the power plant and engines that it can lower the flame temperature by forming a heat sink after introducing water or steam to the combustion chamber. Moreover, NO_x is also reduced by the increase of the reducing agents via the dissociation of steam into hydrogen and oxygen [59–61]. Reduced air preheat is another application of controlling NO_x emissions by reducing the peak temperature. Usually, air will be preheated by the flue gases in order to reduce the heat loss and save energy. However, preheated air will absorb less heat in the combustion process and increase the peak temperature, so that it leads to the NO_x formation [62, 63]. Therefore, this method is a good way to inhibit the formation of NO_x.

Over-fire air and fuel reburning are two similar technologies used for control NO_x. In the over-fire air technology, there will be a primary flame zone which is under the fuel rich condition and then a second zone downstream where an additional air is injected into the unburnt fuel. The reaction temperature is always kept low at both of the two combustion zones due to the off-stoichiometric combustion, so that it inhibits the NO_x formation [64, 65]. Similarly, an additional fuel will be added into the second zone (reburning zone) to reduce the NO_x which is formed in the primary zone back to the molecular nitrogen. The produced gas species will then go into the burnout zone and be completely oxidized by an additional air. This technology is known as fuel reburning, where the temperature in the reburning and burnout zone is low [66, 67]. Furthermore, another technology, named flue gas recirculation,

is to reduce NO_x emission by recirculating the flue gas into the combustion air in order to lower its temperature and decrease its oxygen concentration [68]. Based on the over-fire air or fuel reburning technologies, the low NO_x burner was developed to achieve a low NO_x emission level of 90∼140ppm. In addition, an ultra low NO_x burner combining the applications of flue gas recirculation with the staged air or fuel technology can reduce the NO_x emission to 10∼15ppm [69].

Catalytic Combustion Technology

Catalytic combustion is a kind of flame-less reaction that it can oxidize fuel completely under a low temperature and thus produces less thermal NO_x [43]. Different with SCR, catalytic combustion prevents the formation of NO_x by lowering the activation energy to reduce the reaction peak temperature (shown in Fig.2.2) but not by reverting NO_x back to nitrogen. With the presence of catalyst (usually the noble metal or their metal oxides), the reaction temperature can be reduced below 1400 °C or even lower, so that it can significantly inhibit the formation of NO_x in the combustion process [70,71]. The ability of catalytic combustion achieving an ultra-low NO_x emission has already been studied in different equipments. A study conducted in a gas turbine engine by Enga and Thompson [72] indicated that a metal supported Pt catalyst can reduce the emission of NO_x as low as 0.44 ppm, which was much lower than the emission level of 58 ppm from a conventional engine without the catalytic system. Vatcha [73] also tested the NO_x emission was below 1 ppm from Pd-based catalytic combustion in the gas turbine, which was one to two magnitude less than that from the conventional thermal combustion.

Gastec and Vaillant [74] developed both the completely and partially catalytic natural gas burners with the honeycomb catalysts. The experimental results revealed that NO_x were 5ppm and 0 ppm in the partially and completely catalytic boilers, respectively. A study on the Cu-based catalyst for the methane combustion in a fluidized bed reactor was conducted by Iamarino et al. [75]. No NO_x, CO and particulates were detected in the exhaust gas, as methane was completely combusted at the temperature below than 700°C. Another experimental study on the fluidized bed reactor also investigated the effect of Pd-based catalyst on emission reduction of natural gas combustion [76]. Different from other supported catalysts, the Pd-based catalyst introduced into the combustion reactor was a powder. The experimental results from the study found that methane can be completely combusted at the temperature of 500°C to produce 0∼1 ppm NO_x and CO.

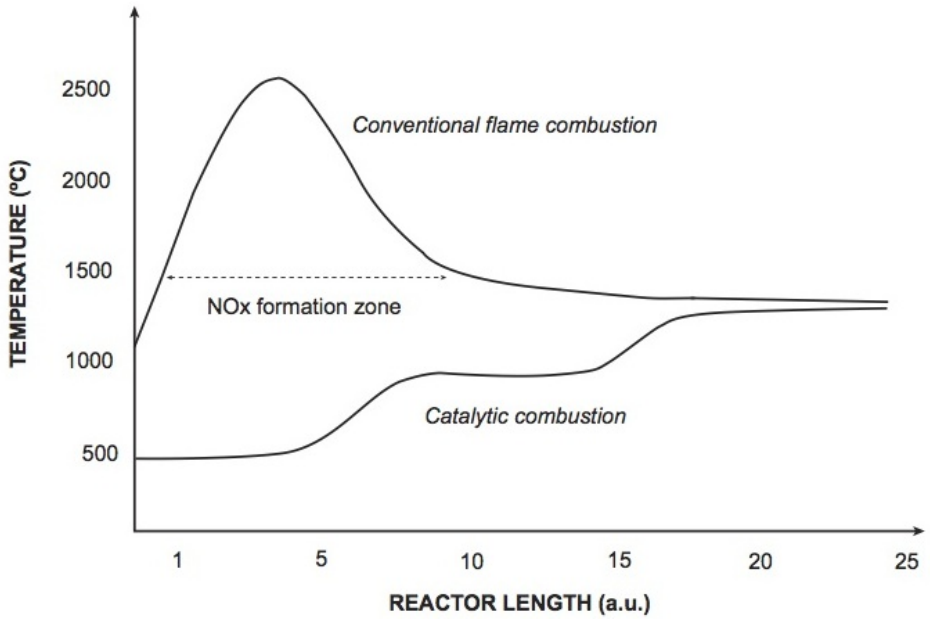

Figure 2.2: Comparison of the temperature profiles between the catalytic combustion and the conventional combustion [9].

2.2.2 PM Control Technologies

To reduce the emission of PM (mainly soot), catalytic combustion is one efficient technology to oxidize the fuels or particulates to CO_2 and water with the presence of catalyst, reducing 10%∼40% PM and 70%∼90% HC. Particulate filter (PF) is another major technology used in different systems (especially in diesel engines) to collect and remove the particulates from the exhaust gas, with the reduction efficiency of both PM and toxic HC greater than 90%. [77–79].

Catalytic Combustion for Particulate Reduction

Catalysts, mainly noble or base metals like Pt and metal oxides like Fe_2O_3, are usually coated on the support materials such as a metallic or ceramic honeycomb structure. Studies on the catalytic combustion found that catalysts can change the reaction routes of the hydrocarbon fuels to inhibit and reduce the formation of soot particles [10, 80, 81]. With the presence of catalysts, methane can be absorbed onto their surface and then oxidized to CO_2 directly. Shown as Fig.2.3, this surface reaction can reduce the generation of some intermediate gaseous hydrocarbon species (which may lead to soot formation) in the regular reaction pathways . Studies also found that catalysts can also oxidize the particulates to

CO_2 and water at a low temperature, via the gas-solid catalyzed hydrocarbons oxidation and sometimes the solid-solid catalyzed graphitic carbon combustion [82–84]. The catalytic combustion of graphitic carbon is favoured for the catalysts with the low melting point, such as V_2O_5 and CuO. In addition, the activities of catalysts for the particulate oxidation depended on their surface area and also the metal-oxygen bond strength (for metal oxide catalysts).

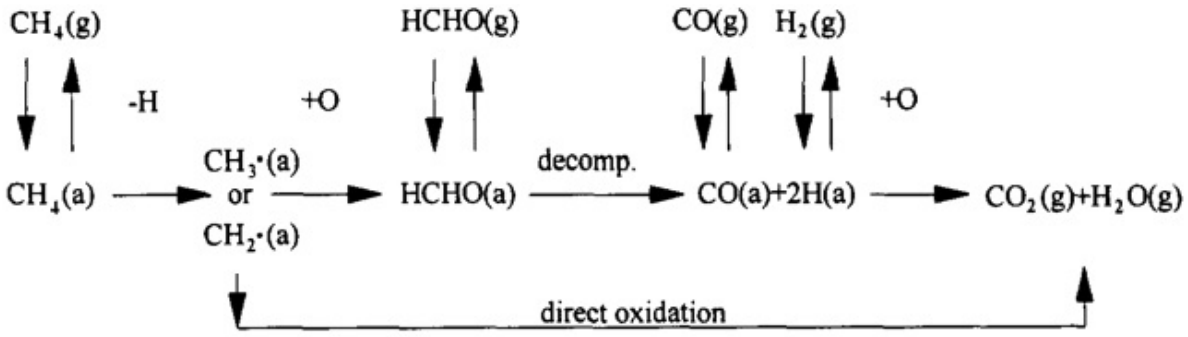

Figure 2.3: The proposed reaction pathway for Methane oxidation on catalyst surface. (a) absorbed; (g) gas phase [10].

In diesel engines, catalysts can also reduce the particulates by some other ways besides oxidizing the particulates and hydrocarbons directly, when they are used as the regeneration catalysts to remove soot particles from the diesel particulate filters [77, 78]. On one hand, soot can be combusted by the generated heat from catalytic oxidation of unburnt hydrocarbons and CO existed in the exhaust gas. On the other hand, the regeneration of the filters is to use the catalysts oxidizing some NO in the exhaust gas to NO_2, which then burns the soot particles at a lower temperature than oxygen.

Particulate Filters

High efficiency filters (wall flow filters), usually based on a porous wall, honeycomb structure with blocked end at each alternate channel, are the most common type that can trap the particulates when the exhaust gas pass through the alternate channels [77,78,85,86]. These filters can be made of different ceramic materials, such as cordierite, aluminium titanate and silicon carbide, which have the high strength and thermal durability. Since the soot particles are continuously deposited on the porous walls of the filter channels, it will cause a pressure

drop over a certain time to affect the performance of the filters. As a result, the accumulated particulates need to be removed from the filters, which is known as regeneration.

The regeneration of particulate filters can be accomplished by burning or oxidizing the soot particles via several different methods: 1) the soot particles can be burnt off at a low temperature with the help of coated surface oxides and metal catalysts on the filter substrate, known as passive regeneration; 2) the particulates can also be burnt off at an increased temperature by means of introducing an oxidation catalyst or a temporary change to the engine operation such as fuel injection and an external heating, namely active regeneration; 3) a small amount of fuel-borne catalysts including iron and platinum containing compounds can be added into fuel prior to combustions. The catalysts will be well mixed with soot particles and lead to the ignition of the particulates at a low temperature. During this process, the catalysts remain left on the filter as ash and need to be removed in the regular filter maintenance.

Flow through filters (partial filters) are another type using metal wire mesh structures or metal foil substrates with porous metal fleece layers to remove the soot particulates, when the exhaust gas flows through the filters. The retained particulates then can be burnt off or oxidized with the assistance of coated catalyst or upstream oxidation catalyst. Usually, the flow through filters does not need a cleaning procedure as the inorganic ash generated from the catalyst can pass through the filters without deposit. The particulate reduction can reach 30% to 60% by these partial filters.

2.2.3 CO Control Technologies

Carbon monoxide can be reduced by some clean combustion technologies or by thermal combustion. Since CO is a major product generated from the incomplete combustion of hydrocarbon fuels, it can be reduced by avoiding the fuel rich flame or using a clean fuel, such as biodiesel which usually contains oxygen component [87]. Besides these technologies, catalytic combustion is another efficient method to help reduce CO emission.

Usually, catalysts can reduce the CO emission not only by lowering the reaction activation energy to promote the complete oxidization of hydrocarbon fuels or CO at a low temperature, but also by absorbing hydrocarbon or CO species to introduce the new reaction pathways of forming carbon dioxide and water [17, 88, 89]. An example of the catalytic combustion of CO on Pt particles is shown as the following reactions 2.16 and 2.17 [90]. It was found the Pt catalyst can be reacted with oxygen first to form a layer of platinum oxide (PtO_2) on

its surface, which can then oxidize the later absorbed CO species to generate CO_2. After these reactions, Pt can be oxidized back to the gaseous and then solid PtO_2 again. In the meanwhile, it was found that the activation energy for these reactions were lower than the conventional CO oxidation. Catalysts have already been used to reduce CO emission in different areas, such as boiler [74], fluidized bed reactor [76] and IC engines [72]

$$PtO_2(s) + 2CO \leftrightarrow Pt(g) + 2CO_2 \tag{2.16}$$

$$Pt(g) + O_2 \leftrightarrow PtO_2(g) \rightarrow PtO_2(s) \tag{2.17}$$

2.3 Catalytic Combustion of Natural Gas

Catalytic combustion can be used to simultaneously reduce the major pollutant emissions, such as NO_x, soot and CO, generated from the combustion process by lowering the reaction temperature and changing the reaction pathway [10, 17, 76]. Various catalysts, mainly including noble metals and metal oxides, have already been investigated and used for the combustion of natural gas [18]. The noble metal based catalysts were thoroughly explored for natural gas combustion, as they were found having the highest potential for reducing the pollutant emissions. Since noble metals are easily vaporized, toxic, scarce and also expensive, alternative catalysts are necessary to be developed. It is found that metal oxides can catalyze the natural gas combustion to reduce the generated pollutant emissions, although their catalytic activities are lower and their light-off temperatures are higher. Numerical metal-oxide based catalysts, such as single metal-oxides and doped metal-oxides, have already been investigated and used for natural gas combustion. However, most of these catalysts (no matter noble metals or metal oxides) are not suitable to be employed in the high temperature combustion, in respect that they will become vaporized or sintered to lose their activities under the high temperature. Thanks to their high thermal stability and low cost, iron oxides (mainly Fe_2O_3) are paid certain attentions to their potentials as the medium and high temperature catalysts [19, 20, 91], although studies on combustion added with iron-oxides based compounds (especially iron pentacarbonyl) are inadequate.

2.3.1 Catalysts for Natural Gas Combustion

Noble Metal Catalysts for Natural Gas Combustion

Noble metals are the most popular materials as catalysts for combustion, due to their high activities and great resistance to sulfur poisoning. This kind of catalyst used for natural gas combustion includes Pd, Pt, gold (Au) and rhodium (Rh) and so on [18].

Pd based catalysts are considered as the most active materials for the complete combustion of methane. Most of studies [92–94] found the activities of the Pd based catalysts were structure sensitive, meaning that the turnover frequency (TOF) is generally increased as the Pd particle size increases. TOF, defined as the number of molecular product per catalytic site in a unit time, is used for describing the activity of catalyst. However, the activities of the Pd catalysts were also determined by the chemical composition of the species on their surface and some other factors. The Mars and van Krevelen (MvK) mechanism can explain the catalytic combustion process of methane over the Pd catalysts [95–97]. The palladium oxide (PdO) layer formed on the metallic Pd surface is identified as the active part for oxidizing methane. After the reaction with methane, Pd will be re-oxidized by oxygen to form PdO for maintaining the activities of the catalysts. The studies also found that both the concentration and position of the PdO on the partially oxidized catalyst determined the oxidation rate of methane.

Although Pd based catalysts are more attractive under most conditions for the catalytic combustion of natural gas, Pt based catalysts have been found more active in some certain conditions, such as with the addition of hydrogen sulphide and presence in the multi-metallic catalysts [98, 99]. Similarly, the Pt based catalysts are generally thought to be structure sensitive. Meanwhile, the kinetic and other studies also indicated the importance of the surface PtO_2 for the catalytic oxidation process [90,92]. Furthermore, some studies [100–102] found that Pt-Pd bi-metallic catalysts were superior for the oxidation of methane than the individual Pt or Pd based catalysts, in respect that they were more active, durable and more stable during the reaction process.

Some other catalysts based on the noble metals including Rh and Au are also used for the methane combustion. Studies on the Au based catalysts [103–105] indicated that the increase of the oxidized Au can enhance the methane oxidation rate. The methane oxidation activity was also affected by the Au particle size, illustrating that smaller Au particles were preferred for reducing the reaction activation energy. In addition, Rh based catalysts were investigated to promote the oxidation of methane by researchers, who found

that their activities were sometimes higher than Pt based catalysts [98]. A study [106] also suggested that the catalytic activity can be improved due to the higher dispersion of Rh^{d+} specie, when using a Rh/ZrO_2 catalyst for the methane oxidation. Besides these studies, Au and Rh were mixed with Pd or Pt used as the multi-metallic catalysts. The investigations demonstrated that these catalysts can get an enhanced catalytic activity sometimes for the complete oxidation of methane [107–109].

Metal Oxide Catalysts for Natural Gas Combustion

The metal oxides are receiving more and more attention due to their lower price. The metal-oxides based catalysts mainly contain single metal-oxides, doped metal-oxides, perovskites and other mixed metal-oxides.

Various oxides of the base metals, such as copper (Cu), manganese (Mn) and cobalt (Co), were used as catalysts for the methane combustion. CuO based catalysts have already been studied to show that isolated Cu species presented on the support surface were more active than the CuO particles for a total oxidation of methane. Moreover, high Cu loading and high temperature were also found to have an unfavourable effect on the activities of the CuO based catalysts [110, 111]. MnO_x based catalysts with and without support were also investigated to evaluate their performance in catalytic methane combustion. The study indicated that unsupported MnO_x can promote the complete combustion of both methane and CO, however, zirconia (ZrO_2) supported and silica-alumina (SiO_2-Al_2O_3) supported MnO_x have the superior activities for oxidizing CO and methane respectively [112]. Similar study [113] on Co based catalysts pointed out that the zirconia supported Co catalyst had the highest activity for the methane combustion compared with bulk Co_3O_4 and other supported (aluminium oxide (Al_2O_3) and titanium oxide (TiO_2)) catalysts. The activities of catalysts were also found significantly affected by the surface Co_3O_4 but not the bulk species. Major metal oxides supported on $LaAlO_3$ used for the methane combustion were compared and showed that the order of their catalytic activities (from highest to lowest) was Co_3O_4, CuO, NiO, Fe_2O_3, Mn_2O_3 and Cr_2O_3 [114].

Perovskite oxides, with a general structure presented as ABO_3, have been widely investigated recently as the alternative catalysts for methane combustion. This is because they have better thermal stability compared with noble metals and also good activities at the evaluated temperature [115]. In the perovskite oxides, usually A is a rare earth metal and B is a transition metal like Mn and Co, which can be partially replaced by other A' and B' cations described as a formula of $A_xA'_{1-x}B_yB'_{1-y}$. The number of A and

B cations entering into the structure as well as their partial-substitution determine the properties of the perovskite catalysts, and thereby affect the catalytic activities profoundly. Using perovskite oxides, the oxidation of methane is either dominated by the weakly bonded-oxygen adsorbed on the surface of catalysts at the low temperature, or affected by the lattice oxygen of the catalysts at the high temperature when the surface oxygen is desorbed [116, 117]. However, the low surface area and the strong sintering tendency of perovskite oxides are the major issues reducing their catalytic activities. Thus, these disadvantages lead to the use of various supports, such as alumina and magnesia based metals, to enhance their performance [118, 119].

Doped metal oxides (which have the higher activities than perovskite oxides) and hexaaluminates (which have superior thermal properties) are two other major catalysts based on the mixed metal-oxides. Studies [120, 121] found that the crystal defects of metal-oxides catalysts can be increased when they were doped by transition metals. This enhanced the mobility of the lattice oxygen and thereby lead to an increase of its reactivity. However, the catalytic activity was not linearly increased with the content of doped metals based on a study on the Mn-doped zirconia catalyst, which showed there were the best values of both the Mn/Zr ratio and the calcination temperature to get the maximum activity [122]. Hexaaluminates, usually described as $AAl_{12}O_{19}$, have attracted attention due to their potentials of being high temperature catalysts [123, 124]. Similar to perovskite, A site is usually filled with the earth metal cations, while A and Al sites can also be partially substituted by other metal cations. Studies [125–127] have shown that partially substituted hexaaluminates can enhance their activities and simultaneously maintained their high thermal stabilities, whereas their low surface areas induced a lower activity compared with other mixed metal-oxides.

2.3.2 Iron Based Compounds for Natural Gas Combustion

Iron-oxide Based Catalyst Review

Compared with other catalysts, studies on iron-oxide catalysts are limited but have shown their potentials for the medium and high temperature application, in respect that they have a high sintering temperature. In addition, although the catalytic activity of Fe_2O_3 is lower than other oxides like CuO and Mn_2O_3, iron-oxide based catalysts have been found that they can catalyze the complete oxidation of methane, when the iron content which linearly determined the methane oxidation rate was above a certain level [10, 128, 129]. Similar

to other metal based catalyst, iron oxide particles will catalyze the oxidation of methane via the surface reactions with the absorbed hydrocarbon species. Iron oxides can oxidize the gas species first and then be converted back to their initial states via the re-oxidation by oxygen. These conclusions indicated the importance of surface area for the catalytic activities of iron oxides [19, 82, 130]. The calcination temperature has been proved having a critical effect on the catalytic properties of unsupported Fe_2O_3. The high calcination temperature can give a higher stability to these oxides, but reduced their catalytic activities due to the lower surface area. It was also noticed that it can increase the catalytic surface area and inhibit the total oxidation of methane when adding sulphates into the iron-oxide catalysts [131].

A study [132] on the catalytic activities of iron-oxide catalysts showed both the unsupported and supported iron oxides were able to catalyze the oxidation of CO, among which Fe_2O_3 supported on Al_2O_3 had the best performance compared to the others. In the meanwhile, $FeSbO_4$ and $FePO_4$ were observed having a better activity for propene(C_3H_6) oxidation. The Fe_2O_3 nano-particles with the size of 3 nm were found that their higher surface area made them a higher activity for oxidizing methane and CO, compared to the Fe_2O_3 micro-particles with the sizes of 300 nm and 5 μm. Furthermore, it was also found that CO can be removed by iron oxides through either the catalytic oxidation or the direct oxidation (when oxygen was absence) [20, 133].

Iron Pentacarbonyl for Combustion

Iron Pentacarbonyl ($Fe(CO)_5$) has been extensively investigated in the past years, due to its much more efficient performance on reducing the flame burning velocity than the other flame inhibitors such as halon 1301 (CF_3Br) [134–136]. In these previous studies, the performance of $Fe(CO)_5$ on flame inhibition affected by the inhibitor mole fraction and flame structure have already been well understood. In most conditions, $Fe(CO)_5$ can reduce the flame velocity, however, some differences were found in a methane counter-flow diffusion flame [137]. The experimental measurements indicated that there was no obvious flame inhibition when the flame was located in the fuel side. Furthermore, it was found that the oxidizer-side flame was even promoted if the inhibitor was directed from the fuel stream.

In addition, although the inhibition mechanism of $Fe(CO)_5$ are still not very clear, some critical iron oxides generated during the combustion process were found by the previous studies. Rumminger et al. [138] extended the flame inhibition mechanism of $Fe(CO)_5$, which included the catalytic H atoms removal cycle based on the work of Jensen and Jones [139].

In this mechanism, $Fe(CO)_5$ was decomposed to Fe and CO, but it would break the Fe-CO bounds orderly to produce $Fe(CO)_4$, $Fe(CO)_3$,$Fe(CO)_2$ and Fe(CO) first. Then the iron atoms can be formed to various iron-containing compounds, such as FeO, FeO_2, FeOH, $Fe(OH)_2$ and Fe(O)OH. This mechanism was numerically simulated in both a premixed and a counter-flow diffusion flame fuelled with methane, oxygen and nitrogen. The simulated results were validated by the experimental results. The authors [140] also numerically studied the methane/air counter-flow flame with $Fe(CO)_5$ addition, where the simulation revealed that same iron-containing species appeared in the diffusion flame, no matter $Fe(CO)_5$ was added into the flame from the fuel or air side. However, the distributions of FeO_2, FeOH and $Fe(OH)_2$ were different under these two different inhibitor injection conditions.

Based on the mechanism established by Rummingers, Wlokas et al. [141] developed the mechanism on the formation of Fe_2O_3 from $Fe(CO)_5$. The new mechanism was validated by comparing the modeling with experimental results measured by the laser-induced fluorescence (LIF). The experimental measurements demonstrated the generation of Fe_2O_3 and other iron-containing products in the H_2/O_2 low pressure flame. In addition, Kim et al. [142] conducted experiments in the isooctane diffusion flames to study the soot reduction by $Fe(CO)_5$. The experimental measurements indicated that the soot can be increased in the early stage of the combustion due to the presence of the atomic iron, whereas the overall soot emission can be reduced by two-thirds later via the catalytic oxidation by the formed iron oxides (such as Fe_2O_3). The study also introduced that the soot oxidation was dominated by different iron-containing species, which were Fe_2O_3 at the low temperature, FeO and Fe_3O_4 at the intermediate temperature from 1000 to 1200K, $Fe(OH)_2$ and FeO at the high temperature above 1800K.

From these previous studies, it can conclude that iron pentacarbonyl has the potential of creating iron oxides which are considered as the iron-based catalysts, although its kinetic mechanism in the combustion process is still unclear. These iron-based catalysts are able to promote the combustion of natural gas and reduce the production of emissions. However, iron pentacarbonyl is usually used as the flame inhibitor, that investigations on emission control are not available. Therefore, the related research of iron pentacarbonyl on emission control is significant for developing the novel catalytic combustion technology.

Chapter 3

Experimental Apparatus and Diagnostics Methodology

In this chapter, the details of the experimental system and the analytical methodologies used for studying the catalytic combustion of natural gas are introduced. The experimental system is composed of a counter-flow diffusion flame burner, a gas and fuel supply system, a catalyst supply system, a gas sampling system and an online analyzer, shown as Fig 3.1. In this experimental system, a stable laminar natural gas flame is generated between the two burners, where fuel and oxidizer streams are directed from bottom and top burners respectively. The catalyst precursor $Fe(CO)_5$ is added into the flame by the carrier gas (N_2) through the central port of the bottom burner. A microprobe driven by two vacuum pumps is used for collecting and delivering the gas sample into the gas analyzer in order to conduct the online measurements. The profiles of generated gas species are analyzed by a GC, where the inorganic components mainly including CO, O_2 and N_2 are detected by a thermal conductivity detector (TCD) and the organic components such as CH_4, C_2H_2 and other C_2 species are measured by a flame ionization detector (FID).

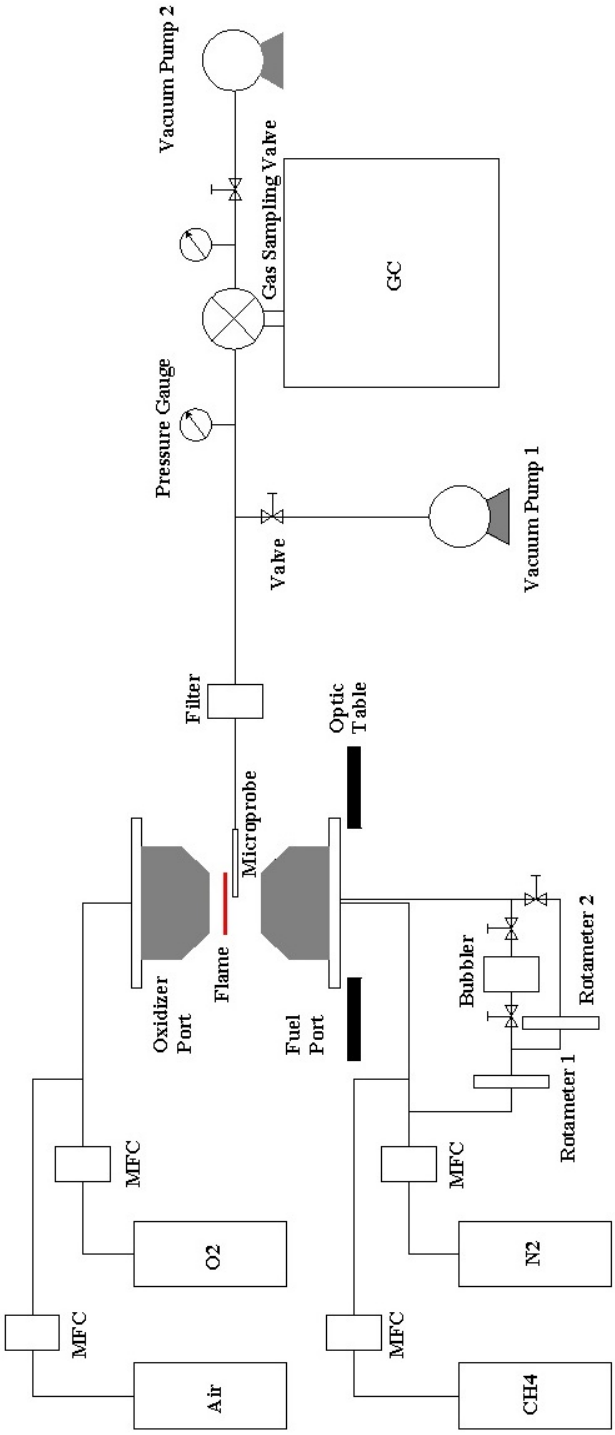

Figure 3.1: Schematic of the experimental system.

3.1 Counter-flow Diffusion Flame Burner

The counter-flow diffusion flame burner is the main body of the experimental system, which consists of two opposed burners[1] containing the enclosed porous sintered bronze matrix. The porous matrix of the burner is divided into the inner and outer coaxial cylinders with the diameters of 60.4 mm and 73.4 mm, respectively [143]. The fuel and oxidizer are directed from the inner annulus to form the flat flame, and the inert gas such as nitrogen can be directed from the outer annulus to form a shroud minimizing the external disturbance to the flame. For the burner used as the fuel-side port, there is a customized central port with the outer diameter of 1/8 inch, through which the catalyst can be injected into the flat natural gas flame.

To get a stable flame, the two burners are separated and supported by a burner mounting system, containing an self-designed aluminum burner holder[2] and a stainless steel optical table[3]. To connect the bottom burner with the gas supply tubings, a 200 mm by 200 mm hole is removed from the centre of the optical table. In the meanwhile, four adjustable aluminum columns are designed and assembled to the optical table to maintain the table at a horizontal level. The burner holder is composed of two 12.7 mm thick aluminum pate and three columns, among which the two plates are used for maintaining the burners and the three columns are used for separating the burners at a distance of approximately 20 mm.

The two counter-flow flame burner is first assembled to the burner holder and then placed on the optical table, as shown in the Fig 3.2. Using this counter-flow flame burner, the fuel is injected from the bottom burner and the oxidizer is simultaneously injected from the top burner. These two streams will meet with each other near the centre of the burners and then form a stable flat flame where the equivalence ratio of fuel and oxidizer is equal to 1.

[1] McKenna Flat Flame Burner (Holthuis & Associates, USA)
[2] Manufactured by Engineering Machine Shop, University of Waterloo
[3] M-TD-23, Optical Breadboard, 600 × 900 × 28 mm (Newport corporation, USA)

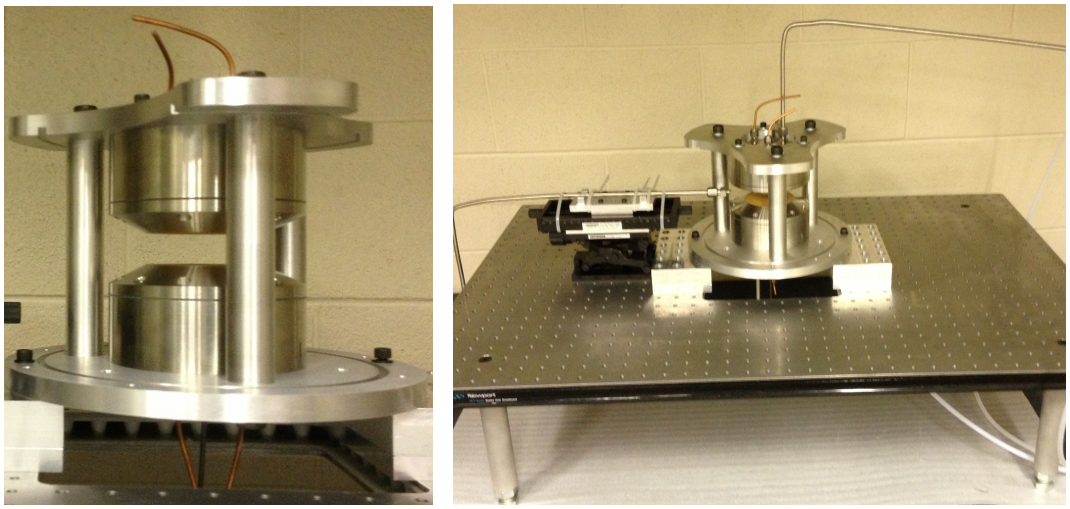

(a) (b)

Figure 3.2: Schematic of the counter-flow diffusion flame burner.

3.2 Gas and Fuel Supply system

In this study, methane[4] is used as the fuel which is mixed with nitrogen[5] before being directed to the bottom burner, and oxygen[6] mixed with air[7] is used as the oxidizer directed to the top burner. The flow rate of these gases are controlled by the mass flow controllers (MFCs)[8], whose accuracies are 1% of the reading. Between the bottom burner and the nitrogen mass flow controller, there is a stainless steel bubbler filled with liquid iron pentacarbonyl that supplies the catalyst to the counter-flow diffusion flame.

3.2.1 Supply of Fuel and Oxidizer

For studying the generated gas profiles of natural gas combustion, a stable laminar flame should be formed near the centre of the burners where the equivalence ratio is 1. This requires that the flow rate of the fuel and oxidizer streams should be set and controlled at the appropriate values. To select these flow rates, several criteria should be followed [38].

[4] 99.97% Pure, Compressed Methane (Praxair Inc.)
[5] 99.998% Pure, Compressed Nitrogen (Praxair Inc.)
[6] 99.993% Pure, Compressed Oxygen (Praxair Inc.)
[7] Zero Extra Dry, Compressed Air (Praxair Inc.)
[8] 1179A Mass-Flo®, Analog, Elastomer-sealed Mass Flow Controller (MKS Instruments Inc., USA)

- The momentums of the fuel and oxidizer streams should be equal to create a stagnation plane at the intersection
- The flow rate ratio of nitrogen to oxygen should be equal to 3.77 for studying the flame under a real air condition
- The flame should not be very hot to prevent damaging the sampling probe
- The flame should be soot-light to prevent blocking the sampling probe
- The Reynold's number of the fuel and oxidizer streams should be lower than 2300 to form a laminar flame

Based on these criteria, the flow rates of methane, nitrogen, oxygen and air are calculated, as shown in the Table 3.1.

Table 3.1: Fuel and oxidizer flow conditions in the experiments

Components	Fuel Side		Oxidizer Side	
	CH_4	N_2	O_2	Air
Flow rate (L/min)	1.395	13	3.448	10.242
Mole fraction	0.097	0.903	0.409	0.591
Velocity (cm/s)	8.37		7.96	
Reynold's number	360		342	

The corresponding Reynold's numbers of the fuel and oxidizer streams are approximately 360 and 342, based on the Equation 3.1. This indicates the fuel and oxidizer streams are laminar flow as their Reynold's numbers are smaller than 2300. In addition, the strain rate, which is defined as the normal gradient of the normal component of the flow velocity, describes the inverse of the characteristic flow time in the counter-flow configuration [144]. For the strain rate at the stagnation plane near to the fuel side, it has a value of approximately

17 s^{-1} in this laminar flame, based on the calculation by the Equation 3.2 .

$$Re = \frac{\rho D u}{\mu} = \frac{4\rho}{\mu \pi D} \sum V_i \tag{3.1}$$

Where, V_i is the flow rate of methane, nitrogen, oxygen or air (m^3/s);

ρ is the density of fuel or oxidizer stream (kg/m^3);

D is the diameter of fuel or oxidizer burner (m);

μ is the viscosity of fuel or oxidizer stream (kg/(m·s));

Note: In this flame, the fuel stream is the mixture of methane and nitrogen, and the oxidizer stream is the mixture of oxygen and air.

$$a = 2\frac{|V_{fuel}|}{L}(1 + \frac{|V_{ox}|\sqrt{\rho_{ox}}}{|V_{fuel}|\sqrt{\rho_{fuel}}}) \tag{3.2}$$

Where, a is the stain rate on the fuel side (s^{-1})

L is the distance between the two burner ports (cm)

$|V_{fuel}|$ is the absolute value of the fuel stream velocity at the fuel boundary (cm/s)

$|V_{ox}|$ is the absolute value of the oxidizer stream velocity at the oxidizer boundary (cm/s)

$|\rho_{fuel}|$ is the density of the fuel stream (g/cm^3)

$|\rho_{ox}|$ is the density of the oxidizer stream (g/cm^3)

3.2.2 Supply of Catalyst

Fig 3.3 shows the structure of stainless steel bubbler which is designed to supply iron pentacarbonyl for the catalytic combustion study. The bubbler has one inlet and one outlet which are both 1/8 inch stainless steel tubings. The inlet tubing is inserted into liquid iron pentacarbonyl through the top cap, and the outlet tubing is installed on the top side of the bubbler which is connected with the bottom burner. In the inlet and outlet of the bubbler, two valves[9] are installed for keeping the bubbler close when iron pentacarbonyl is stored in it before and after the experiments. Before using the bubbler, leak detection must be conducted in order to avoid the potential gas leak during the experimental process. The step is to inject some gas and close both the inlet and outlet valves first, and then monitor the inside pressure of the bubbler by a pressure gauge to check if there is any gas leak.

[9]SS-41GS2, Stainless Steel 1-Piece 40 Series Ball Valve, 1/8 inch Fitting (Swagelok Company, USA)

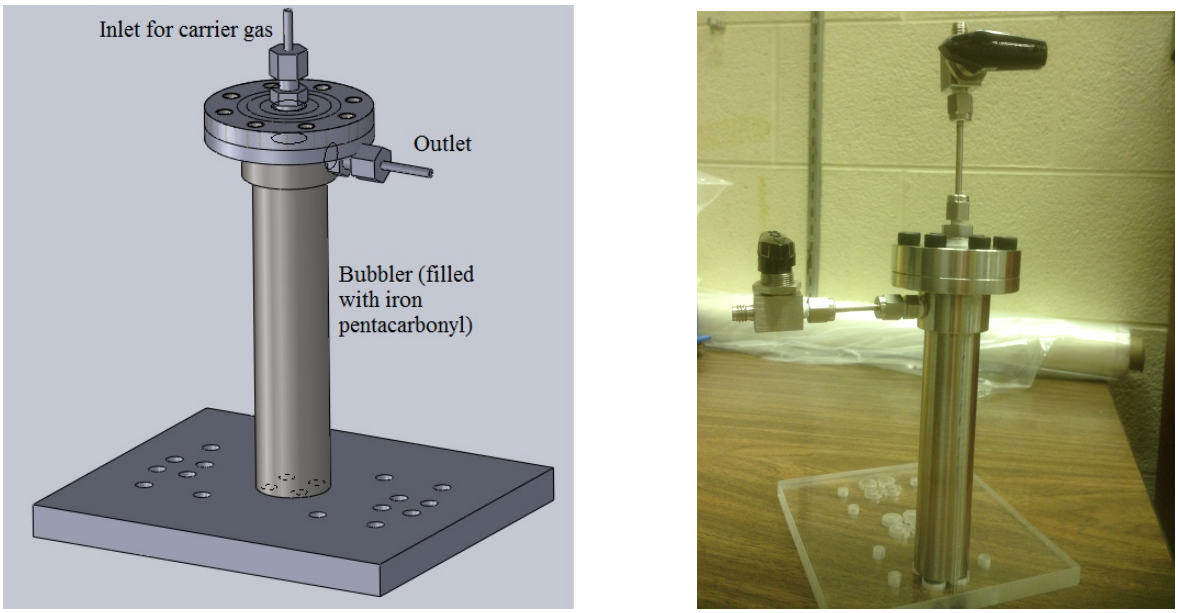

(a) (b)

Figure 3.3: Schematic of the bubbler for supplying catalyst

For keeping iron pentacarbonyl stable, the bubbler is placed into the ice-water bath to maintain its temperature at zero centigrade during the experiments. A two-stage bypass system, consisting of two rotameters with two additional valves[10], are installed for the bubbler to control the flow rate of carrier gas, which is finally directed into the bubbler to evaporate and carry the catalyst into the laminar flame through the central port of the bottom burner. The first flow meter[11] which has a bigger flow range is used for separating and controlling the primary bypass from the nitrogen flow, and the second flow meter[12] is installed to further split the bypass nitrogen flow to determine the amount of carrier gas injected into the bubbler. Since the mole fraction of iron pentacarbonyl in the bubbler outlet is fixed once temperature of bubbler is kept constant, the catalyst concentration in the total carrier gas flow can be adjusted to any values from zero to its maximum (same with the concentration value at the bubbler outlet). In the meanwhile, the total bypass flow (N_2) rate is kept constant, which is critical for investigating the effects of catalyst concentration on pollutant reduction.

[10]SS-SS2 Stainless Steel Low-Flow Metering Valve, 1/8 inch Fitting (Swagelok Company, USA)
[11]RK-03217-12, 150 mm Aluminum/Glass Correlated Flow Meter (Cole Parmer, Canada)
[12]RK-03217-00, 150 mm Aluminum/Glass Correlated Flow Meter (Cole Parmer, Canada)

3.3 Gas Sampling System

3.3.1 Setup of Gas Sampling System

To get an accurate online measurement, a suitable gas sampling system should be used to collect and deliver the gas sample into the analyzers continuously from the counter-flow diffusion flame. A gas sampling line composed of a microprobe, two vacuum pumps, a positioning system and a filter is designed and built up for withdrawing the gas sample of natural gas combustion.

To reduce the errors of the experimental results, several factors should be considered when designing and choosing the components of the gas sampling line. First of all, quenching the continuous chemical reactions inside the microprobe and the gas line is necessary for an accurate measurement. Some previous studies on the gas sampling technologies indicated a low pressure at the entrance of the sampling probe can effectively quench the chemical reactions [58, 145, 146]. In addition, another previous study [147] indicated that it was essential to quench the continuous reaction by a rapid pressure drop combined with the destruction of the chemical radicals but not by only temperature drop in the gas sampling line. In the meanwhile, the counter-flow diffusion burner is an open system that it works at atmospheric pressure. These reasons determine a high vacuum inside the gas sampling line should be generated by the vacuum pump. Moreover, some tests show that the pressure behind the microprobe is not low enough when only one vacuum pump is added after the gas analyzer. For getting enough high vacuum, two vacuum pumps[13] are placed before and after the GC to suck and deliver the sample into the gas analyzer. The maximum vacuum generated by vacuum pump no.1 and no.2 are 25" Hg and 25.5" Hg, respectively. To protect the GC and pumps from being damaged by the particles inside the gas sample, an online filter[14] is installed between the microprobe and the gas analyzer to remove the fine particles bigger than 15 μm.

Second, minimizing the disturbance in the flame caused by the intrusive probe is one of the important factors that need to be considered. A previous study on the microprobe size [38, 148] suggested that the ideal inside diameter of the microprobe was 0.18 to 0.22 mm, as a higher ID would not quench the reaction effectively and a smaller ID would not get enough gas sample through the probe tip for the gas measurements. For these reasons,

[13] DOA-V722-AA, Oilless Diaphram Vacuum Pump (Gast Manufacturing Inc., USA)
[14] SS-4TF-15, Stainless Steel Tee-Type Particulate Filter (Swagelok Company, USA)

a silica microprobe[15] with the dimension of 0.2 mm in ID, 0.34 mm in OD and 6 cm in length is used in this study, which is quite cheap and easily-replaceable. Compared with the flame reaction zone, this microprobe is small enough that it will not cause the visible disturbance to the flow field between the burners.

Third, avoiding the adsorption or absorption of the hydrophilic gas species (such as NO_x) by the condensed water inside the gas sampling line is critical for measuring their real concentrations produced from combustion. In addition, the condensed water will also affect the accuracies of the experimental measurements by increasing the measured concentrations of the hydrophobic gas species (such as nitrogen). For these reasons, it is necessary for avoiding water condensation by using a heated gas line, which adds several heating tapes[16] outside of the stainless steel tubing. The temperature of the tubing is maintained at a temperature of approximately 120 °C by two J type thermocouples and two temperature controllers[17].

Finally, collecting the gas sample from the different positions between the two burners is also necessary for getting the natural gas flame structure. A positioning system mainly containing a vertical translation stage[18] and a linear translation stage[19] is designed and assembled with some self-designed mounting components[20]. The microprobe is first connected with a 1/4 inch stainless steel tubing via a reducing union[21] combined with a adapter[22], and then the 1/4 inch tubing is mounted by the positioning system, shown as Fig. 3.4. Using this positioning system, the microprobe can be inserted into the different positions between the burners by adjusting the vertical translation stage vertically and the linear translation stage horizontally.

[15] 160-2205-10, Deactivated Fused Silica Tubing (Agilent Technologies, USA)

[16] Duo-Tape, Heavy Insulated Heating Tape, High Watt Density (HTS/Amptek Company, USA)

[17] CNi3233, i-Series 1/32 DIN Temperature, Process and Strain PID Controller with Two Relay Outputs (Omega Engineering, Inc., USA)

[18] 124702: Manual Lab Jack Stage, Vertical Travel 60mm, 20 kg Load Capacity (Produstrial, LLC, USA)

[19] 124686: Manual stage, Dovetail Guide Type, with Travel of 125 mm, Lapped Ball Screw, 20 kg Load Capacity (Produstrial, LLC, USA)

[20] Manufactured by Engineering Machine Shop, University of Waterloo

[21] H-EZRU41C, Stainless Steel, External/Internal Reducing Union with 0.25 mm Bore, for 1/4 inch to 1/16 inch OD Tubing (VICI Valco Instuments Co. Inc., USA)

[22] H-FS1.4-5, 1/16 inch Polyimide, Fused Silica Adapter for Tubing between 0.30 and 0.40 mm OD (VICI Valco Instuments Co. Inc., USA)

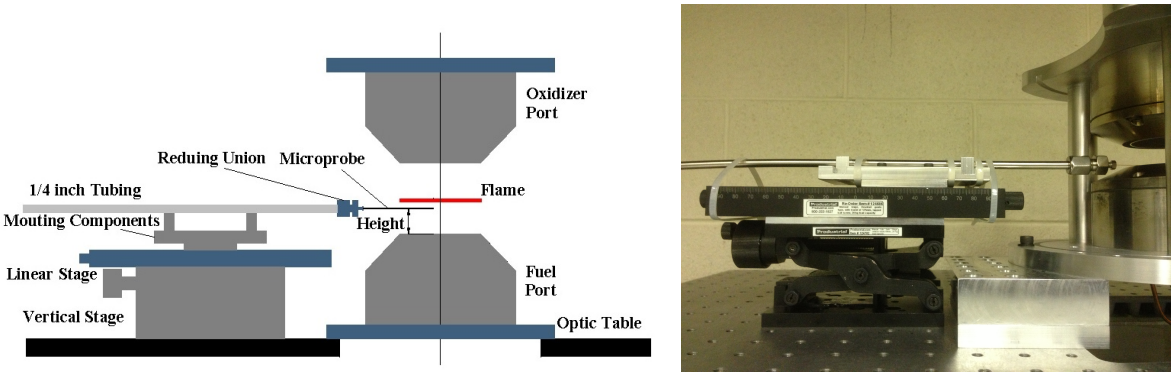

(a) (b)

Figure 3.4: Schematic of the positioning system

3.3.2 Gas Sampling Procedure

In the natural gas combustion experiments, the procedure for collecting the gas sample from the flame is described as follows. To avoid the effect of the potential gas leak in the gas sampling line on the gas measurements, gas leak test should be conducted before doing experiments. A plug is inserted into the sample probe side first and then the two inline valves installed before the vacuum pumps are closed once a low pressure (25"Hg) is generated by the vacuum pumps. The pressure is monitored by the pressure gauges to detect the potential gas leak in the gas sampling line.

After the leak testing, methane is injected from the bottom burner and lighted by the ignitor first. Air, oxygen and nitrogen are injected orderly, and then a stable laminar flame is observed. When studying the gas profiles of the catalytic combustion, the catalyst should be added into the flame by the separated nitrogen. To add the catalyst smoothly, the flow rate of bypass flow (separated nitrogen) should be adjusted to the designed value by opening the bubbler valves slowly. The microprobe which is driven by the two vacuum pumps is then injected into the different positions between the two burners to collect the gas sample. Then the gas sample is injected into the GC when the purge time is around 5∼6 minutes. When measuring gas profile in vertical direction, the tip of microprobe is placed approximately 1 mm behind the central vertical axis of the burners with various heights, in order to collect the gas sample from the central part of the burners.

To optimize the experimental method, two different gas sampling methods are tested and compared for injecting the gas sample into the GC analyzer during the experiments. One way is to inject the gas sample directly into the GC at a specific low pressure of

approximately 25" Hg (method 1), and another is to inject the gas sample when the pressure inside the gas sampling valves (GSVs) raises to atmospheric pressure (method 2) after closing the inline valves. The pressure value is monitored by two pressure gauges, which are installed just before and after the gas sampling valves.

After getting enough data in one position, the microprobe is adjusted to a new location for collecting gas sample, by means of rotating the vertical translation stage (moving vertically) or the linear stage (moving horizontally). Once the full gas profiles of the counter-flow flame are measured, the experiments are finished. The inlet and outlet valves of the bubblers should be closed first to avoid excess catalyst overflowing into the surroundings without burning. Then methane, oxygen, nitrogen and air should be stopped orderly to extinguish the flame.

3.4 Diagnotics Methodolgy

3.4.1 Gas Chromatograph

Gas chromatography is a common technology used in laboratory for analyzing the composition of a mixture sample, which is gas or liquid that can be evaporated to gaseous components [149]. The partitioning difference of different components between the flow mobile phase and stationary phase under certain conditions makes them separated, and then specific detector can identify each component and its amount in the mixture. GC is the instrument using this technology to separate and analyze the mixture sample, which is usually composed of a carrier gas (flowing mobile phase), a column (stationary phase), an oven, a detector and a sample injector.

Shown as Fig.3.5, an Agilent GC6890, which includes two detectors (TCD and FID), two columns, two injectors and two GSVs, is used for analyzing the gas compounds produced from natural gas combustion in this study.

Carrier Gas

Carrier gas is the mobile phase of the GC, which can be helium, nitrogen and hydrogen [149, 150]. The type of carrier gas usually depends on the type of detectors installed on GC and analyzed components in the gas sample. The purity of the carrier gas should be high enough as it may affect the sensitivity and accuracy of the measurements. Moreover,

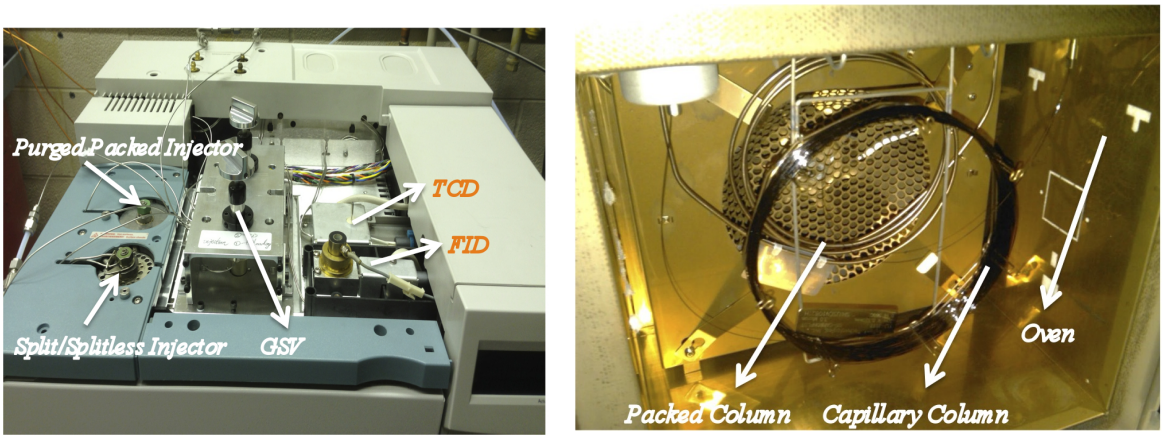

(a) (b)

Figure 3.5: Schematic of the Agilent GC 6890. a) The configuration on GC top; b) The configuration inside GC oven.

the moisture and particles contained in the carrier gas can damage GC. For these reasons, helium[23] with a high purity of 99.999% is selected as the carrier gas. The flow rates of helium used as makeup gas or carrier gas are described in the following parts.

Detectors

Thermal Conductivity Detector (TCD) is a kind of detector to identify the compounds by comparing the thermal conductivity of the carrier gas with those of the sample components [149, 151]. A filament in the detector is electrically heated and maintained at a constant temperature, which is higher than the detector temperature, by supplying a certain power. The power difference used for avoiding the filament temperature changes are detected and recorded when the gas sample passes over the filament. TCD is a good detector to analyze the inorganic components in the gas sample. In this study, it is used for analyzing N_2, O_2 and CO in the gas sample.

Flame Ionization Detector (FID) is another common detector to analyze the compounds by measuring the current produced from the sample addition [149, 151]. A hydrogen-air flame is generated inside the detector first to create some ions, which are attracted by a polarized collector. When the compounds in the sample are burnt by this flame, a current will be generated and detected due to the increase of the collected ions from the sample

[23] HE 5.0 UH-T, Helium (Praxair Inc.)

burning. FID can be used for analyzing the organic components. In this study, it is used to analyze the hydrocarbons, especially CH_4, C_2H_2, C_2H_4 and C_2H_6.

Injector and Gas Sampling Valve

Two different types of injectors containing electronic pneumatic control (EPC) are installed for the two detectors. The injector for TCD includes a purged packed inlet while the one for FID contains a split/splitless inlet which has four different working models (split, pulsed split, splitless and pulsed splitless) [152]. In this GC, the purged packed inlet is installed with a packed column[24], and the split/splitless inlet is installed with a capillary column[25]. Both of the injectors can be used for measuring the sample from low to high concentration. However, the sample has to be injected into the columns by a syringe when using these two injectors.

Since the online measurements of gas species produced from the counter-flow flame require a continuous procedure, it means that the sample injection by a syringe is inappropriate for this application. Moreover, its injected volume of the sample is difficult to be kept constant every time, resulting the repeatability and accuracy of the measurements are not good enough. For these reasons, two GSVs[26] with two sample loops are installed on the top of GC for the two injectors. The sample loops have the constant volumes that they can make sure the volume of the injected sample constant at each time. The volume of the loop[27] installed for TCD is 1 ml to make sure the sample is enough for the packed column, and it is a 0.25 ml loop[28] for FID in respect that the column installed is a capillary one.

The GSV can be used under several different models for different applications. In this study, it is used for loading and injecting the sample into GC columns, shown as Fig.3.6. In the beginning, the GSV will be set at the "load" position shown as Fig.3.6a, where the gas sample will be delivered into the sample loop continuously by the vacuum pump first. When the time is enough for filling the loop with the gas sample, the GSV will be switched manually to the "injection" position shown as Fig.3.6b, where the carrier gas will pass through the loop and carry the gas sample into the column for the future analysis. Once

[24] G3591-80017, Mole-sieve 5A column, 1/8 inch × 6 feet (Agilent Technologies, USA)

[25] 113-3133, Carbon-Plot column, 30 m × 0.32 mm × 3.00μm (Agilent Technologies, USA)

[26] H-2C6UWT, 6 port, 2 positions, Manual Valve for 1/16 inch tubing (VICI Valco Instruments Co. Inc., USA)

[27] PS-SL1KCUW, 1ml Sample Loop, 1/16 inch ends with nuts & ferrules(VICI Valco Instruments Co. Inc., USA)

[28] PS-SL250KCUW, 0.25ml Sample Loop, 1/16 inch ends with nuts & ferrules(VICI Valco Instruments Co. Inc., USA)

all the sample inside loop is injected into the column, GSV should be switched back to the "load" position to collect the sample for the next analysis. The load and injection time of the GSVs used for TCD and FID are shown in the Table 3.2 and 3.3

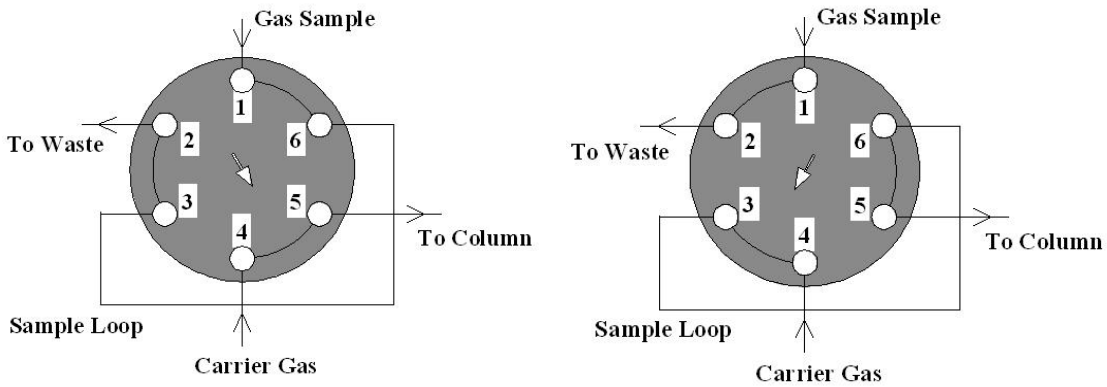

Figure 3.6: Schematic of the gas sampling valve (GSV) for sample injection. a) "Load" position of GSV; b) "Injection" position of GSV [11].

.

3.4.2 GC Methodology

Different parts of GC work under different conditions when analyzing the gas sample. The collection of these operation parameters, such as the oven temperature and the flow rate, is called the GC method [11, 149]. To detect the expected components in the gas sample, well separation of the components in the column is required to make sure that only one component is analyzed by the detector at a certain period. As a result, the oven temperature program as well as the flow rate of the carrier gas are the most important factors for separating the different components. Moreover, the sensitivity of detector is affected by the flow rate of makeup gas which is also a key parameter. Usually, high sensitivity is expected as it can give a good gas signal. The method used in this study for analyzing CO, O_2 and N_2 with TCD is shown as Table 3.2.

To analyze the hydrocarbons such as CH_4, C_2H_2, C_2H_4 and C_2H_6 by FID, the method used in the experiments is shown as Table 3.3. The split/splitless injector is used under the split model to make sure that the sample injected into the capillary column is not overloaded. Moreover, the flow rate of hydrogen, air and makeup gas (helium) should be set at the appropriate range, in order to make the hydrogen-air flame stable. Tests on the

Table 3.2: Analytic method of TCD used in experiments

Oven temperature program	125°C, hold 3 minutes 20°C/min heated to 250°C, hold 3 minutes
Purged packed Inlet	Temperature: 250°C
Column	Mole-sieve 5A packed column Constant flow model Carrier gas (Heilum) flow: 25 ml/min
Detector	Temperature: 300°C Reference gas (Heilum) flow: 45 ml/min Makeup gas (Heilum) flow: 2 ml/min
Gas sampling valve	Load time: 5 minutes Injection time: 2 minutes Injected sample volume: 1 ml

stability of hydrogen-air flame indicate that the flame will be blown out frequently if the total flow rate of makeup gas and carrier gas is too high. The results show that the best flow rate fraction of different gas flows is around 0.75:1:10 (makeup gas plus carrier gas : hydrogen : air).

Once the gas sample is injected into the column, the sample compounds are separated and then detected by the detectors orderly. The qualitative and quantitative analysis for sample mixture can be conducted based on the chromatogram gotten from the GC measurements. Fig.3.7 shows the examples of chromatograms gotten from the measurements by TCD and FID. The peak presented on the chromatogram indicates one component of the sample mixture, and its value shown in x-axis is called retention time. Once the conditions used in the GC method is finalized and kept constant, the retention time for a certain component will also be fixed to help identify the composition of the sample mixture. This is known as qualitative analysis. In this study, the peak order gotten in the experiments by TCD is O_2, N_2, CH_4 and CO, and meanwhile, it is CH_4, C_2H_2, C_2H_4 and C_2H_6 for FID measurement.

GC can also be used to quantitatively analyze the sample components. In the chro-

Table 3.3: Analytic method of FID used in experiments

Oven temperature program	125°C, hold 3 minutes 20°C/min heated to 250°C, hold 3 minutes
Split/splitless Inlet	Temperature: 250°C Split model, Split ratio 27.3:1 Split flow: 109 ml/min
Column	Carbon-Plot capillary column Constant flow model Carrier gas (Heilum) flow: 4 ml/min
Detector	Temperature: 300°C H_2 flow: 40 ml/min, Air flow: 400ml/min Makeup gas (Heilum) : 26 ml/min
Gas Sampling Valve	Load time: 5 minutes Injection time: 2 minutes Injected sample volume: 0.25 ml

matogram, the area between the peak and baseline is proportional to the amount of the component contained in the injected analyte. Therefore, the concentration of one component in the sample can be calculated once the area values of the same component with known amount is provided as the reference. Based on the work principle of GC, it indicates that a constant volume of sample injected into the column is critical in order to measure the accurate concentrations of the sample mixture.

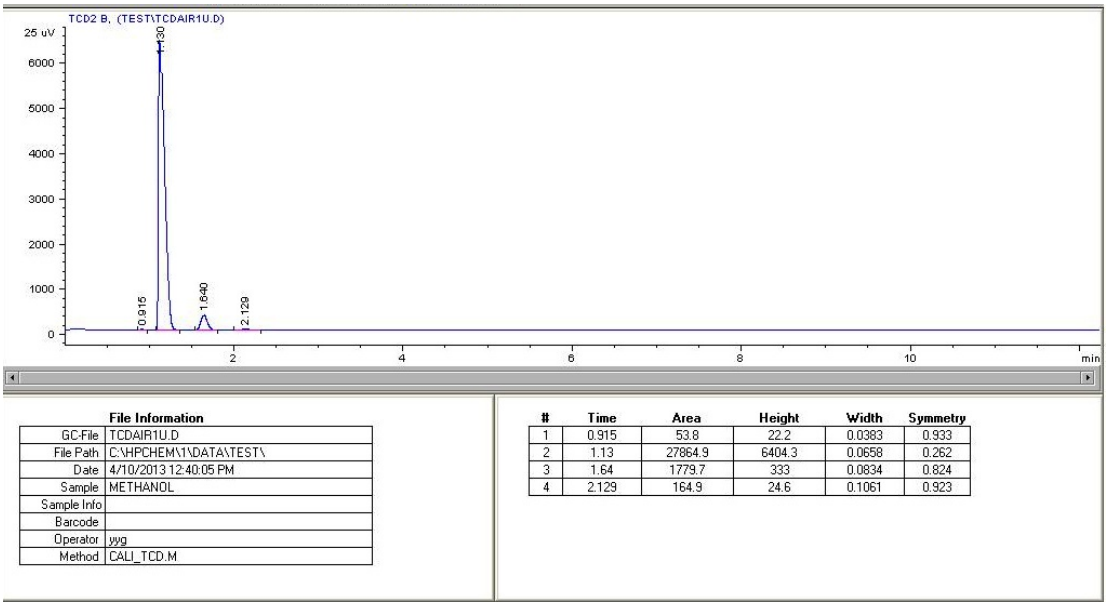

File Information	
GC-File	TCDAIR1U.D
File Path	C:\HPCHEM\1\DATA\TEST\
Date	4/10/2013 12:40:05 PM
Sample	METHANOL
Sample Info	
Barcode	
Operator	yyg
Method	CALI_TCD.M

#	Time	Area	Height	Width	Symmetry
1	0.915	53.8	22.2	0.0383	0.933
2	1.13	27864.9	6404.3	0.0658	0.262
3	1.64	1779.7	333	0.0834	0.824
4	2.129	164.9	24.6	0.1061	0.923

(a)

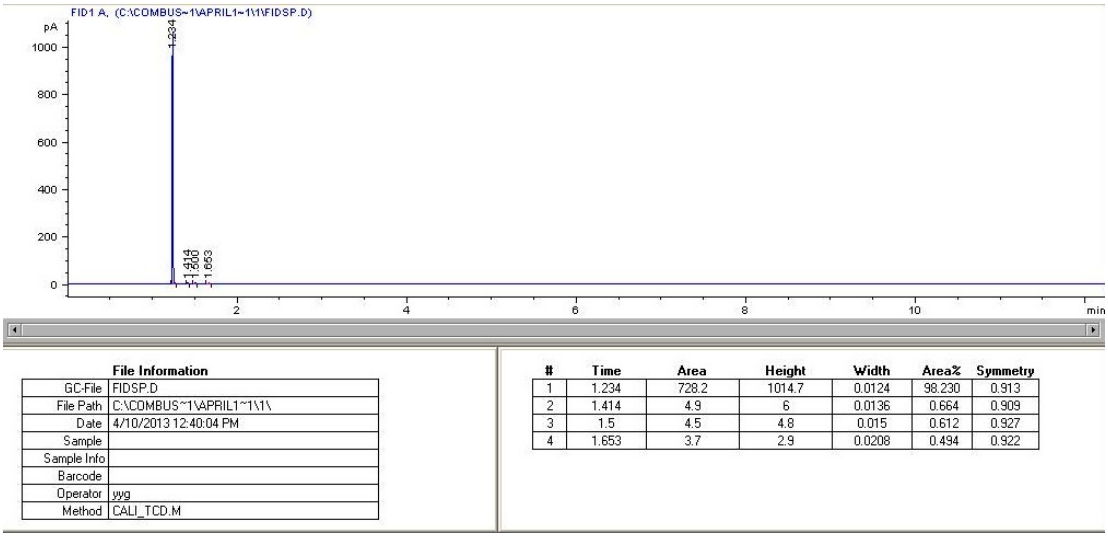

File Information	
GC-File	FIDSP.D
File Path	C:\COMBUS~1\APRIL1~1\1\
Date	4/10/2013 12:40:04 PM
Sample	
Sample Info	
Barcode	
Operator	yyg
Method	CALI_TCD.M

#	Time	Area	Height	Width	Area%	Symmetry
1	1.234	728.2	1014.7	0.0124	98.230	0.913
2	1.414	4.9	6	0.0136	0.664	0.909
3	1.5	4.5	4.8	0.015	0.612	0.927
4	1.653	3.7	2.9	0.0208	0.494	0.922

(b)

Figure 3.7: Schematic of the chromatograms for different components obtained from experimental measurements. a) Chromatogram of the inorganic components measured by TCD; b) Chromatogram of the organic components measured by FID.

GC Calibration

To analyze the gas sample, the reference chromatogram obtained from the known mixture is essential to determine the retention time and peak area of the wanted components. The process to confirm the GC method and get the reference data is called GC calibration. In this study, two calibration gas mixtures gotten from Praxair Inc. are used for calibrating the GC. One mixture contains 4.05% H_2, 9.85% N_2, 0.1026% NO, 0.407% CH_4, 5.07% CO and 0.1006% N_2O in helium (balance gas), and the other one contains 0.5% C_2H_2, 0.499% C_2H_4 and 0.5% C_2H_6 in helium (balance gas). Moreover, GC is also calibrated by the surrounding air to get the reference data for oxygen and nitrogen.

The gas mixture is withdrawn and delivered to GC via the experimental system directly, where the aforementioned sampling procedure and GC methods are used in the calibration process. Since two different gas sampling methods are used in the experiments, the GC calibration process is operated under two different pressures to obtain the related reference data.

Chapter 4

Results and Discussion

In this chapter, the gas profiles obtained from the non-catalytic natural gas combustion using two different sampling methods are compared with a previous study. The results from the measurements are also compared with the CHEMKIN modeling, in order to validate the numerical model and provide the experimental data for the further improvement of the kinetic mechanism.

Iron pentacarbonyl, the catalyst precursor, is added into the counter-flow diffusion flame through the central port of the fuel-side burner. Its effects on pollutant reduction are studied by measuring the generated gas species and comparing them to the initial non-catalytic experimental results. In addition, the concentrations of the injected iron pentacarbonyl are also varied to better understand the effects on pollution control.

4.1 Experimental Studies on the Characteristics of Non-catalytic Natural Gas Combustion

The experimental conditions for studying the characteristics of natural gas in a counter-flow diffusion flame is described in Table 3.1. A blue laminar flame is located at the height of approximately 9 mm above the fuel-side burner, shown in Fig.4.1a. The profiles of the gas species, including CH_4, O_2, N_2, CO and C_2 species, are shown in Fig.4.2∼4.6. These results are measured by two gas sampling methods which are operated at the low pressure of 25"Hg (Method 1) and atmospheric pressure (Method 2), respectively. In these figures, the x-axis shows the height of the sampling point above the surface of the bottom burner (fuel-side burner) which is defined as the zero point, and the y-axis indicates the concentration of the gas species (in this thesis, gas concentration is expressed using mole fraction).

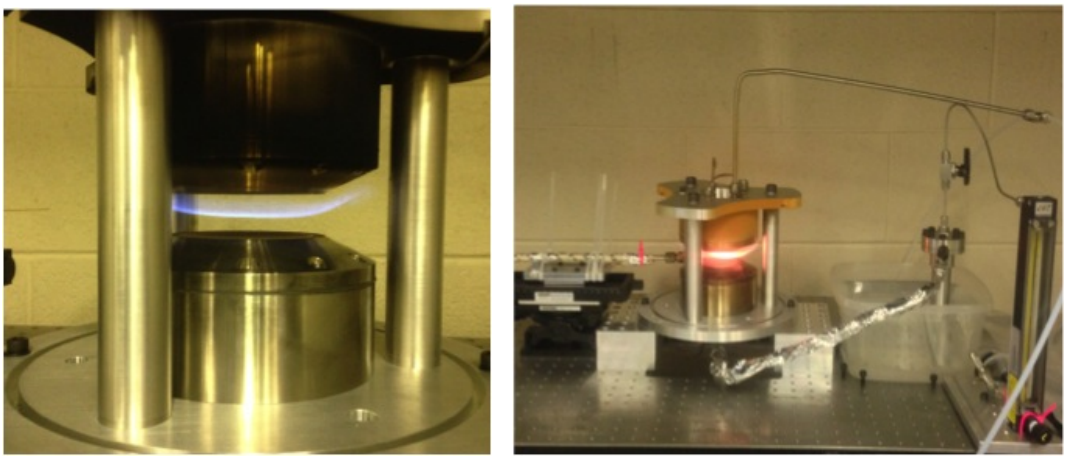

(a) (b)

Figure 4.1: Schematic of the laminar flames in experiments. a) Natural gas combustion without $Fe(CO)_5$ addition; b) Natural gas combustion with $Fe(CO)_5$ addition .

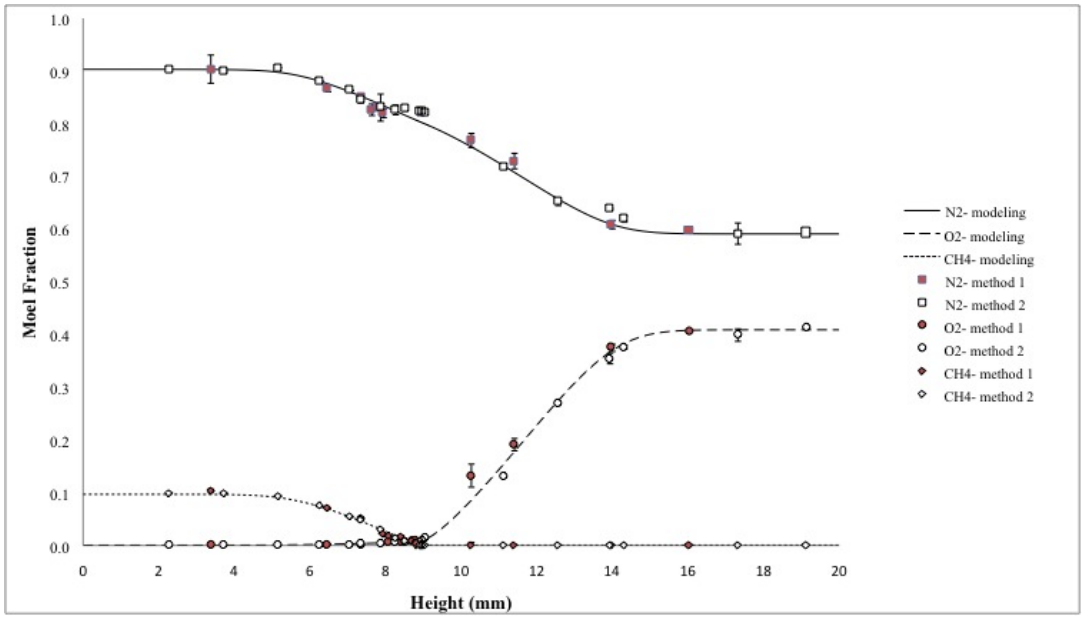

Figure 4.2: Gas profiles of CH_4, O_2 and N_2 from the non-catalytic natural gas combustion measured by experiments and predicted by the numerical simulation. Note: zero point of the height is the location of the bottom burner surface

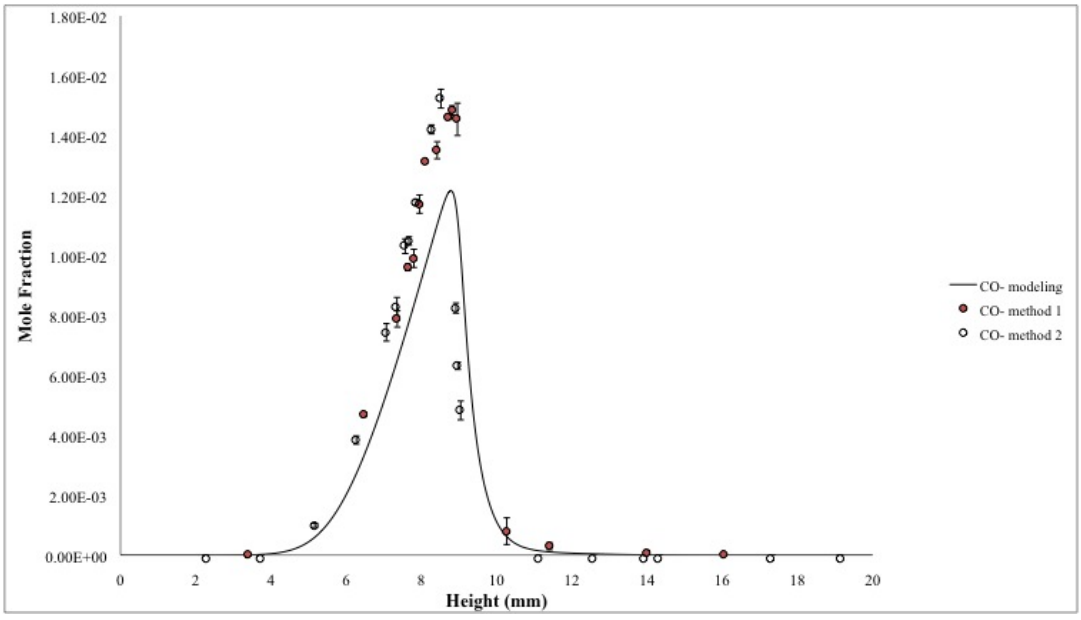

Figure 4.3: CO profile of the non-catalytic natural gas combustion measured by experiments and predicted by the numerical simulation. Note: zero point of the height is the location of the bottom burner surface

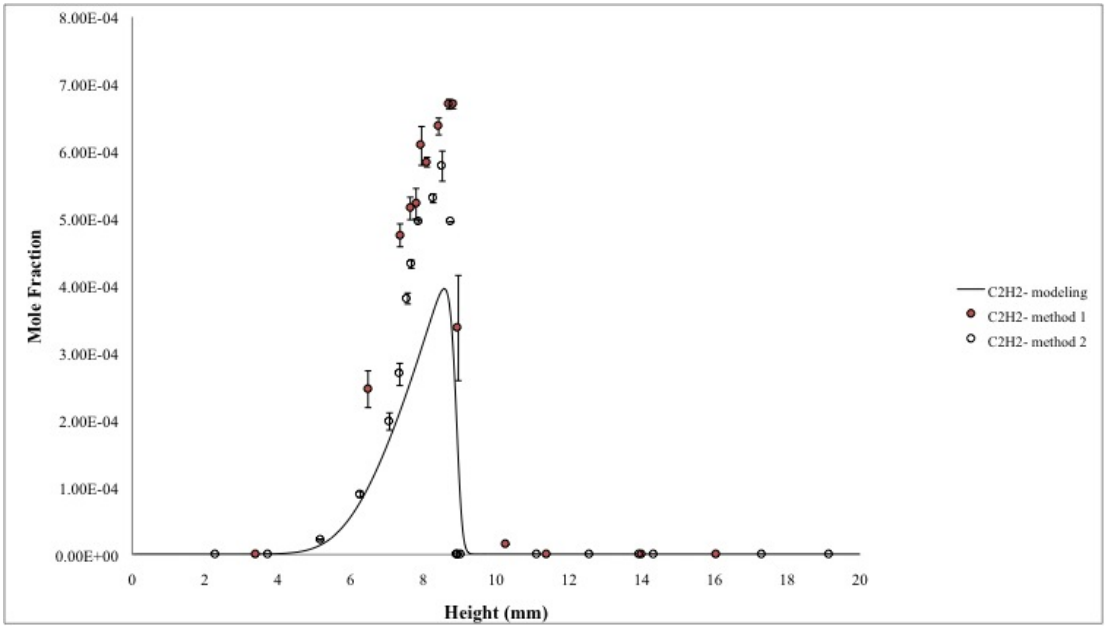

Figure 4.4: C_2H_2 profile of the non-catalytic natural gas combustion measured by experiments and predicted by the numerical simulation. Note: zero point of the height is the location of the bottom burner surface

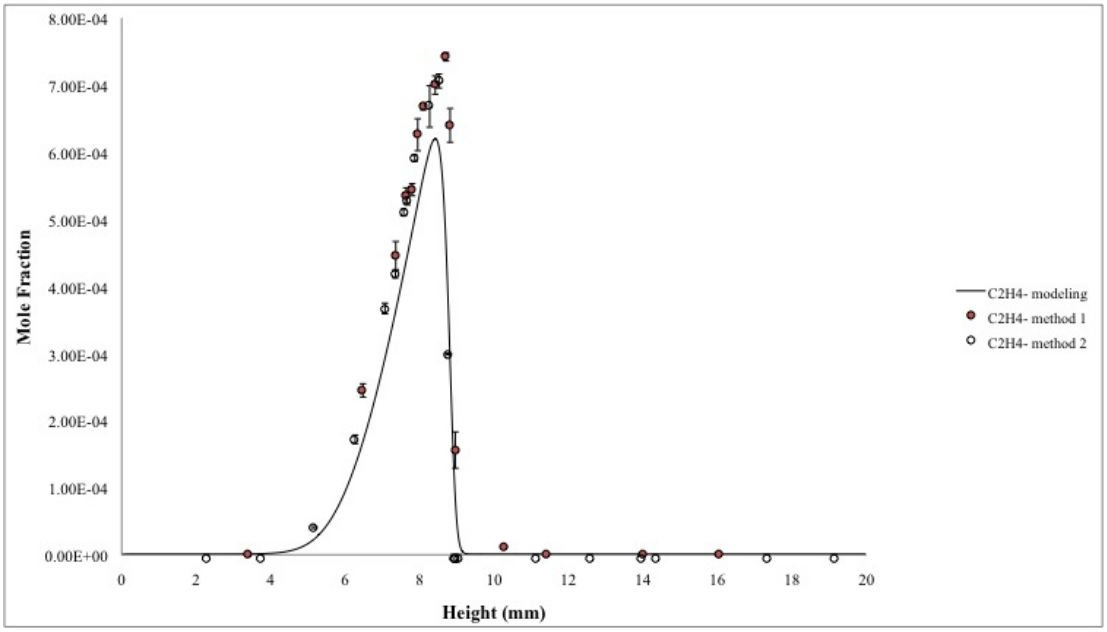

Figure 4.5: C_2H_4 profile of the non-catalytic natural gas combustion measured by experiments and predicted by the numerical simulation. Note: zero point of the height is the location of the bottom burner surface

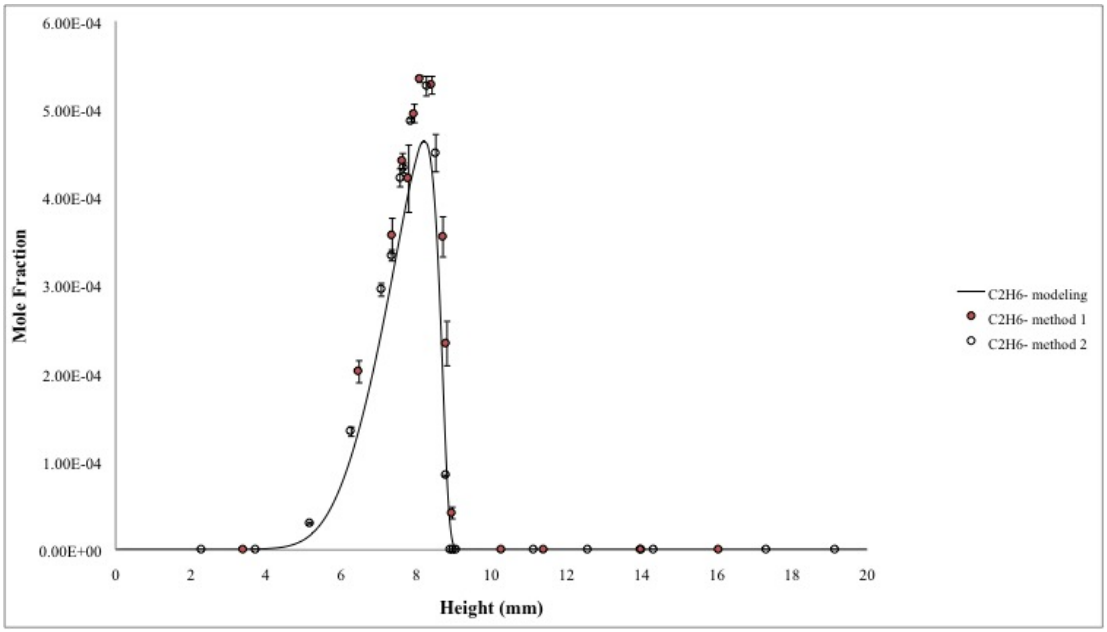

Figure 4.6: C_2H_6 profile of the non-catalytic natural gas combustion measured by experiments and predicted by the numerical simulation. Note: zero point of the height is the location of bottom burner surface

4.1.1 Comparison of the Experimental Results with a Previous Study

The experimental results measured from the counter-flow flame are compared with a previous study conducted by W.A. Hahn and J.O.L. Wendt [32]. The gas profiles of CH_4, O_2 and CO match well in these two experimental studies, which indicates that the measurements of the generated gas species by this experimental system have a high reliability for presenting the structure of the natural gas fuelled laminar flame.

Based on Fig.4.3∼4.6, the results demonstrate the peaks of CO, C_2H_2, C_2H_4 and C_2H_6 are located 0∼0.5 mm below the position of the blue flat flame, and their concentrations drop very quickly in the flame zone. Less formation of these species implies a more complete combustion of natural gas in the flame zone. As the height increases from the bottom burner (fuel side) to the region close to the flame, the chemical reactions among light hydrocarbons become more intense as the temperature increases. Therefore, the concentrations of CO and C_2 species increase subsequently. Once the height increases to the flame location where the equivalence ratio is close to 1, the fuel reacts with the oxidizer completely to generate carbon dioxide and water, resulting in a sharp decrease of all other gas species.

4.1.2 Comparison of the Experimental Results from Different Sampling Methods

To establish an appropriate experimental method which can be used for obtaining accurate measurements from the counter-flow flame, the experimental results obtained by two different sampling methods are compared to evaluate their reliability and practicability under different flame conditions (such as different temperature). The experimental results shown in the above figures demonstrate that the gas profiles measured by method 1 and 2 agree well with each other. The slight peak differences of CO, C_2H_2, C_2H_4 and C_2H_6 measured by the two methods can be ignored, as these small differences may be caused by the experimental operation. The consistent measurements suggest that both of the two sampling methods can be chosen for collecting and measuring the gas species produced from this counter-flow diffusion flame.

Furthermore, the error bars of the measurements by method 1 are bigger than those by method 2, especially at positions close to the flame zone. This indicates the accuracy and repeatability of the measurements by method 1 are slightly lower than method 2. Based on the comparison of the peak areas of the same gas species in the chromatograms measured by the two methods, it can be observed that the peak area measured by method 1 is much smaller due to the dilution of the injected gas sample. As a result, the small area fluctuation can induce a bigger concentration difference for the measurements obtained in method 1. In addition, it is harder to identify the peak area difference if two gas samples have very close concentrations when using method 1, due to the smaller measured peaks. For these reasons, method 2 which injects the gas sample into GC at atmospheric pressure is preferred. The measurements are better especially when the gas concentration is low or when the concentration difference is too small in two different sampling positions.

However, method 2 is much slower than method 1, since in method 2 that it takes several minutes for the pressure to revert from vacuum to atmospheric pressure. When the sample is taken from locations near the flame zone, the pressure recovery time becomes long enough that the sampling probe sometimes gets distorted by the high temperature. The distortion of the microprobe not only induces measurement errors but also shortens the lifespan of the microprobe. In addition, there will be lots of iron particles produced when $Fe(CO)_5$ is added into the flame (will be shown in the later discussion), so that the microprobe quickly becomes clogged. In comparison, method 1 is much faster, so that it can not only save time and experimental cost but also get the acceptable results. Therefore, method 1 is preferred when gas samples are taken from the high temperature reaction zone

or the flame with catalyst addition.

4.1.3 Comparison of the Experimental Results with the Numerical Simulation

As a numerical simulation can be used for predicting the gas emission levels produced by fuel combustion, it can save experimental cost and also conduct further combustion investigation. However, the numerical model usually need to be validated by experimental data to confirm its correctness or to do necessary improvements, so that the simulated results can give correct conclusions. For this reason, the experimental data is compared to the numerical results obtained by CHEMKIN, which was done by Qi [153]. The numerical simulation uses the GRI-3.0 methane combustion mechanism, which includes 53 species and 325 reactions. Based on the comparisons in Fig.4.3∼4.6, the modeling results are found to match with the experimental measurements, especially for the profiles of CH_4, O_2 and N_2. This reveals that the numerical model can be used for predicting the flame structure of natural gas combustion in the counter-flow diffusion burner.

In addition, the measured gas peaks of CO and C_2 species are slightly higher than the predictions. The discrepancy between the experiments and modeling may be caused by the simplification of the 2D flow structure in the numerical model and the inaccuracies of the experimental measurements. In the numerical simulation, the software CHEMKIN can only set up the configuration of the counter-flow flame (such as the distance of the burners, the initial flow rate, the temperature and pressure of the fuel and oxidizer streams) in a simplified manner. However, the real conditions (such as flame disturbance caused by surrounding air flow) in the combustion process are much more complicated than the modeling assumption, resulting in differences between the experiments and modeling. In the experiments, some errors can be caused by the equipment and experimental operation to make the measured gas concentration different from the simulation. Moreover, the discrepancy may also be attributed to the limitation of the chemical mechanism, which needs to be further improved.

4.2 Experimental Studies on the Characteristics of Catalytic Natural Gas Combustion

To evaluate the performance of iron-containing catalysts, iron pentacarbonyl ($Fe(CO)_5$) is vaporized by the carrier gas first and then injected into the counter-flow flame via the central port of the bottom burner. When $Fe(CO)_5$ was added, a stable orange flame was observed (shown as Fig.4.1b) and the colour intensity increased as the concentration of $Fe(CO)_5$ increased. In addition, some orange particles were observed at the outside of both the microprobe and the top burner after the catalytic flame was burnt for a while.

The experimental conditions, such as the carrier gas flow rate and $Fe(CO)_5$ concentration, in the catalytic combustion are shown in Table 4.1. In this study, the concentration of $Fe(CO)_5$ is varied while the carrier gas (N_2) flow rate is kept constant. The total flow rates of fuel and oxidizer are kept at the same values with the initial non-catalytic experiments (shown as the Table 3.1). In addition, the initial experimental results for the non-catalytic natural gas combustion, regarded as the reference, are measured by method 2 (operated at atmospheric pressure) in this section.

Table 4.1: Experimental conditions in the catalytic combustion

Catalytic combustion	1	2	3	4	5	6
Concentration of $Fe(CO)_5$ in the carrier gas (ppm) Note: ppm here signifies mole fraction $\cdot 10^6$	3354	4472	4845	5466	7453	10390
Flow Rate of carrier gas - N_2 (ml/min)	15					

4.2.1 Effects of the Iron-based Catalyst on Pollution Reduction

Effects of the Carrier Gas on the Characteristics of Natural Gas Combustion

In order to add $Fe(CO)_5$ into the flame, a small amount of N_2 is used as the carrier gas and directed into the flame through the central port of the bottom burner. This is different from the initial experiments, where no gas is injected from the central tube. Thus, this difference may lead to some changes to the flame structure. To understand and eliminate

the potential changes on the flame structure caused by the central flow, the gas species are measured when there is a central N_2 stream injected into the flame (without adding any $Fe(CO)_5$). The flow rate of the central N_2 is 15 ml/min. The experimental results are demonstrated in Fig.4.7∼Fig.4.11.

The results imply that the central N_2 stream has no obvious influence on the flame structure, in respect that the flow rate of this central stream is small enough compared with the total flow rate of the N_2 and CH_4 mixture. However, when the flow rate of the central N_2 is increased above 50 ml/min, the flat flame becomes unstable and can even be blown out by the strong central flow. Consequently, these comparisons indicate that any change of the gas profile in the catalytic combustion can be considered to be as the results of adding $Fe(CO)_5$ into the flame, when the central N_2 is controlled at the flow rate of 15 ml/min.

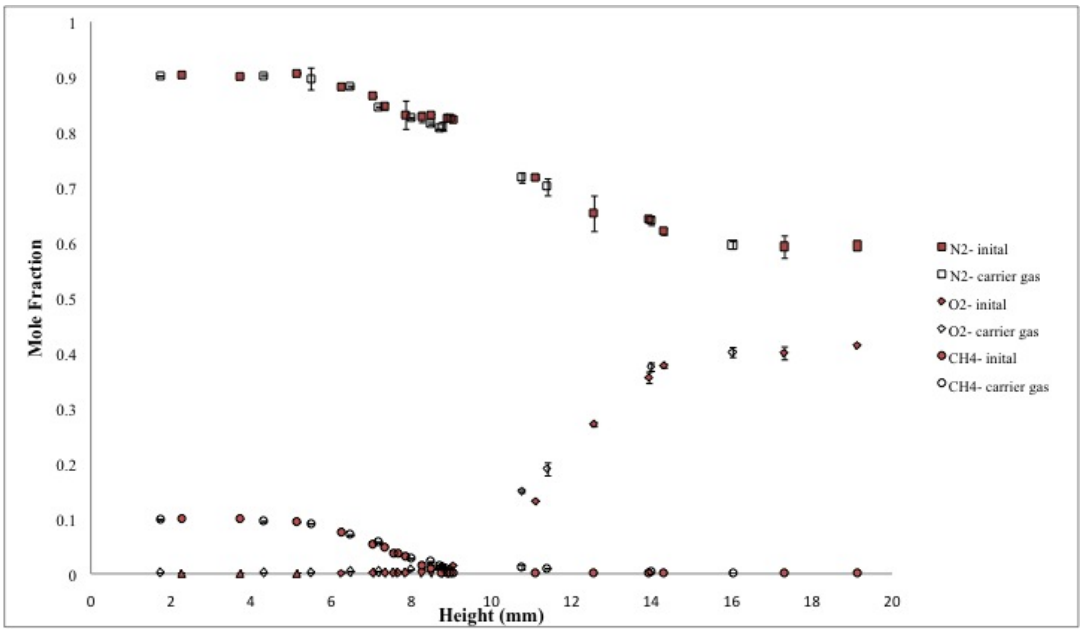

Figure 4.7: Comparison of CH_4, O_2 and N_2 profiles between the experiments with and without the central N_2 injection. Note: The blank points are the results with the central N_2 injection, while the solid points are the initial data obtained by method 2 without the central N_2 injection

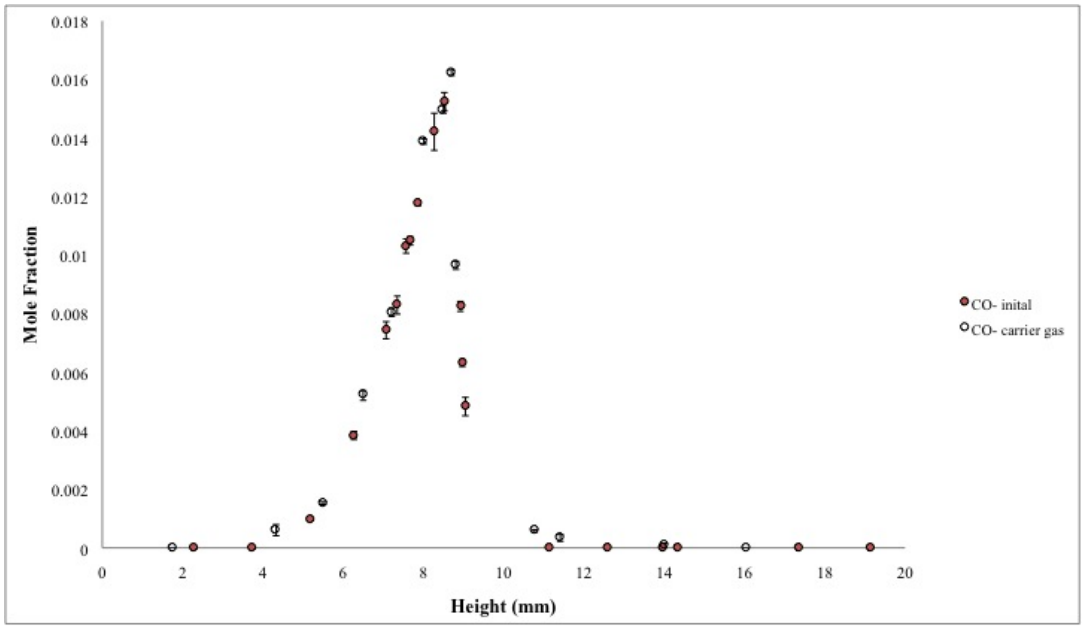

Figure 4.8: Comparison of CO profile between the experiments with and without the central N_2 injection. Note: The blank points are the results with the central N_2 injection, while the solid points are the initial data obtained by method 2 without the central N_2 injection

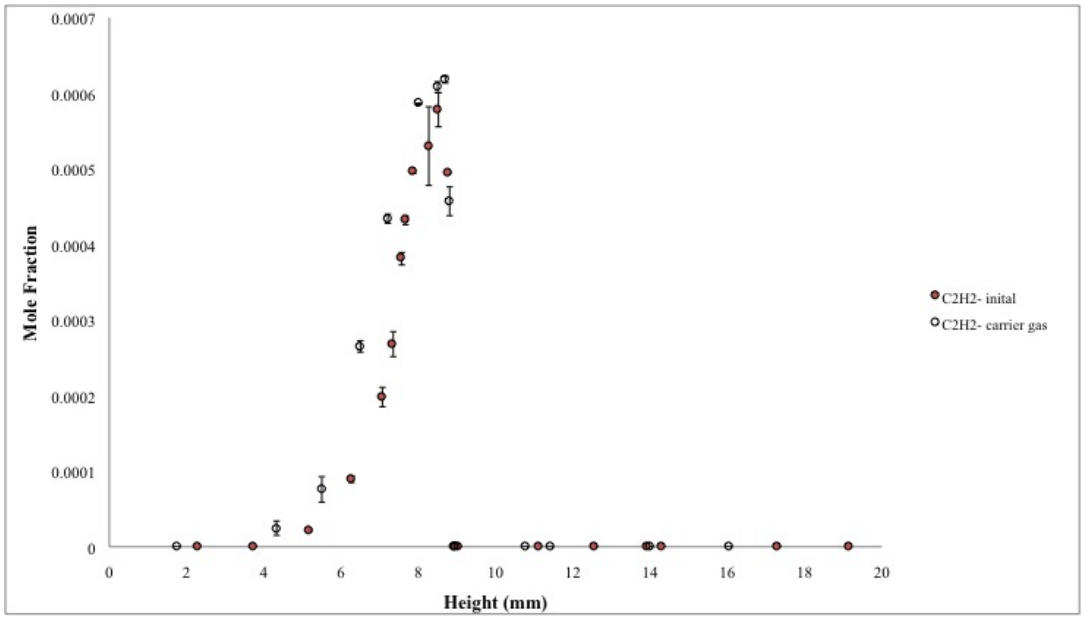

Figure 4.9: Comparison of C_2H_2 profile between the experiments with and without the central N_2 injection. Note: The blank points are the results with the central N_2 injection, while the solid points are the initial data obtained by method 2 without the central N_2 injection

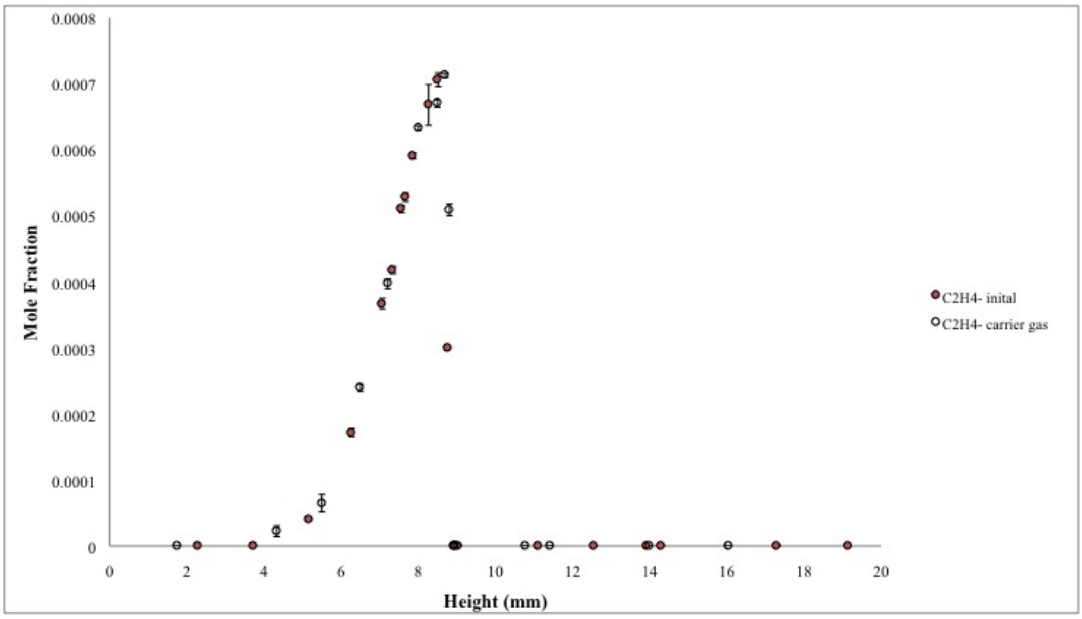

Figure 4.10: Comparison of C_2H_4 profile between the experiments with and without the central N_2 injection. Note: The blank points are the results with the central N_2 injection, while the solid points are the initial data obtained by method 2 without the central N_2 injection

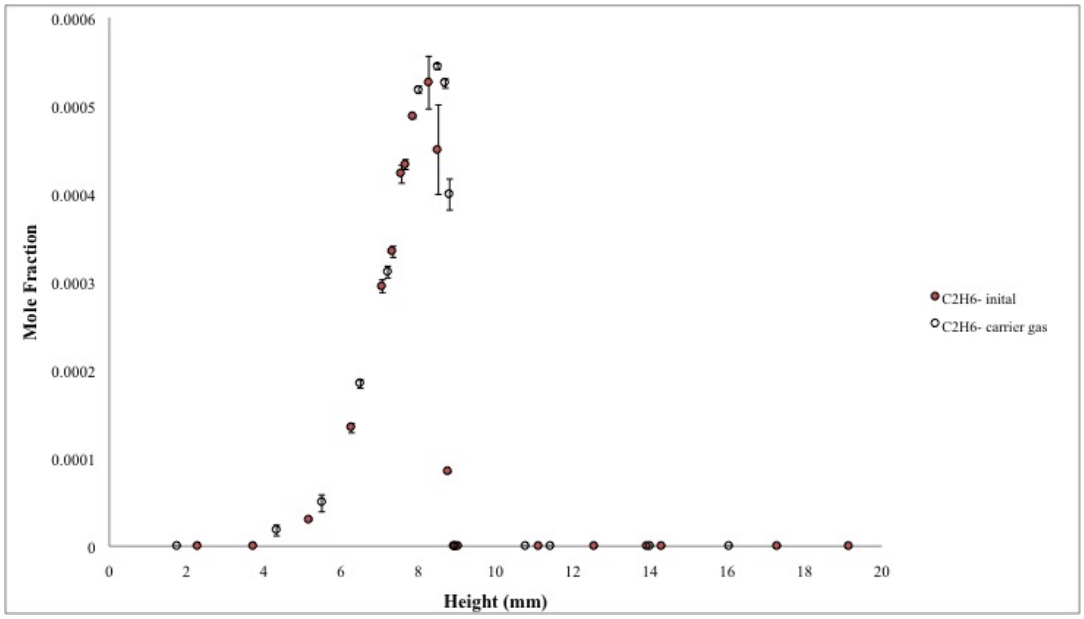

Figure 4.11: Comparison of C_2H_6 profile between the experiments with and without the central N_2 injection. Note: The blank points are the results with the central N_2 injection, while the solid points are the initial data obtained by method 2 without the central N_2 injection

Comparison of the Emissions from the Catalytic and Non-catalytic Combustion

The flame structure of the natural gas combustion after adding $Fe(CO)_5$ is shown in Fig.4.12∼Fig.4.17. These gas profiles are measured in the vertical direction between the two burners when the concentration of $Fe(CO)_5$ in the carrier gas is around 7453 ppm . The experimental parameters are shown as the "catalytic combustion 5" in Table 4.1.

Fig.4.14 to Fig.4.17 indicate that emission of CO and C_2 species can be significantly reduced by $Fe(CO)_5$ compared with the initial data. The reduction of CO, C_2H_2, C_2H_4 and C_2H_6 can reach 80% to 95%. Moreover, the peak values of these gas species are presented 2∼2.5 mm lower than their initial positions without adding $Fe(CO)_5$. This is attributed to the catalytic combustion of methane by the formed iron oxides. After $Fe(CO)_5$ is injected from the fuel side burner, various iron oxides (especially Fe_2O_3) can be created. Previous studies [138, 141] have already shown the formation mechanism of iron oxides. Evidence for this is the presence of orange particles, which are believed to be iron oxides, at the outside of the microprobe during the experimental process. These iron oxides are the major catalysts promoting the complete combustion of methane via surface reactions, which reduce the production of CO and C_2 species. In addition, oxygen and the resulting iron oxides increase as the height increases, and this causes methane to be completely oxidized to CO_2 and water at a lower position compared to the initial experiments. From the methane profile shown in Fig.4.13, it can be found that methane is completely consumed at the height of approximately 8 mm. This is around 1 mm lower than its corresponding position in the initial experiments. Therefore, the concentrations of the major emissions are reduced and meanwhile their peaks move closer to the fuel-side burner, as a result of the addition of $Fe(CO)_5$ into the flame.

Compared with the initial gas profiles shown in Fig.4.13, it illustrates that more O_2 is present below the flame while less is found at the oxidizer side in the catalytic combustion, corresponding to an inverse change of the N_2 profile (shown in Fig.4.12). The increase of oxygen in the fuel side is probably induced by the increasely complete combustion at lower heights, so that more oxygen is saved below the flame. Moreover, as iron atoms can be formed again after iron oxides catalyze the oxidation of methane, some of them may pass through the flame zone and react with the oxygen to induce its concentration reduction in the oxidizer side. During the experimental process, some orange iron particles are found outside of the oxidizer-side top burner, supporting this hypothesis.

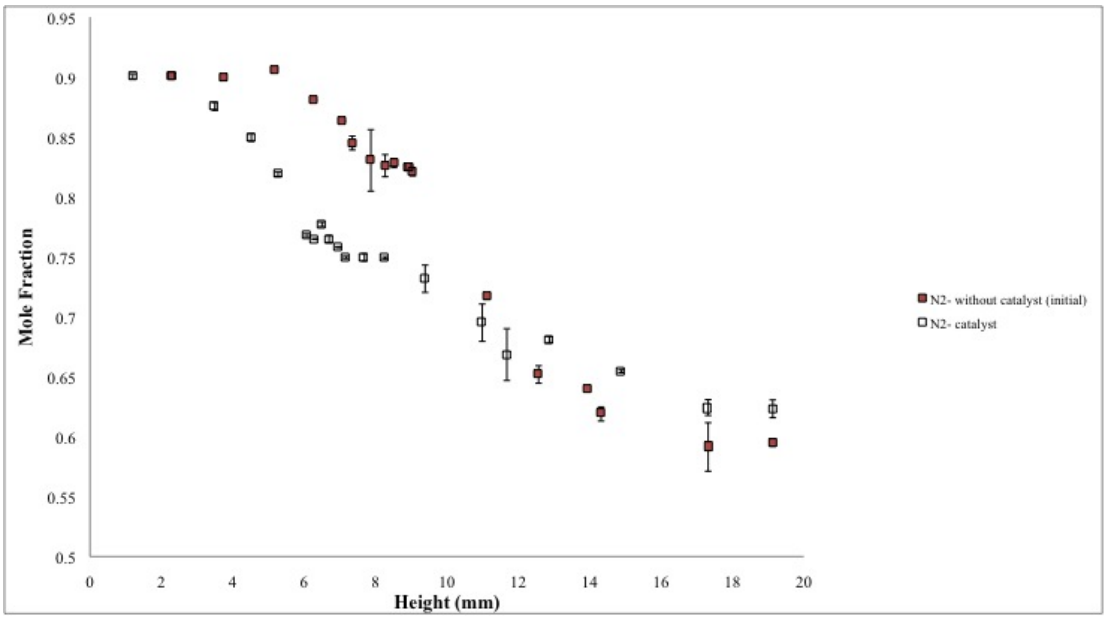

Figure 4.12: N_2 profile measured from the catalytic and non-catalytic combustion. Note: The blank points are the results with $Fe(CO)_5$ addition, while the solid points are the initial data gotten by method 2 without $Fe(CO)_5$ addition

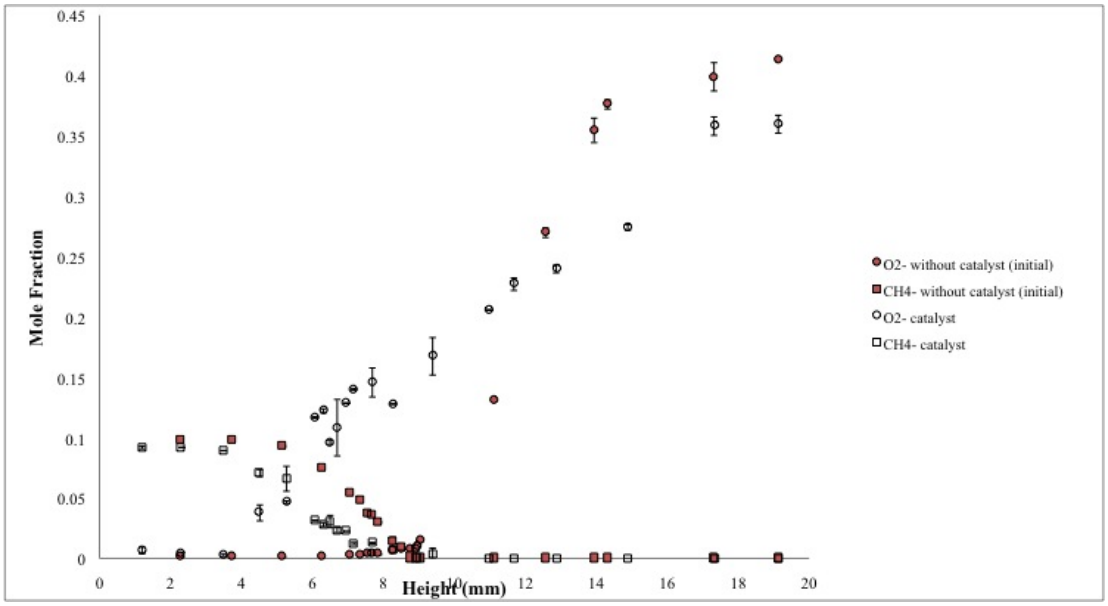

Figure 4.13: Comparison of CH_4 and O_2 profiles measured from the catalytic and non-catalytic combustion. Note: The blank points are the results with $Fe(CO)_5$ addition, while the solid points are the initial data gotten by method 2 without $Fe(CO)_5$ addition

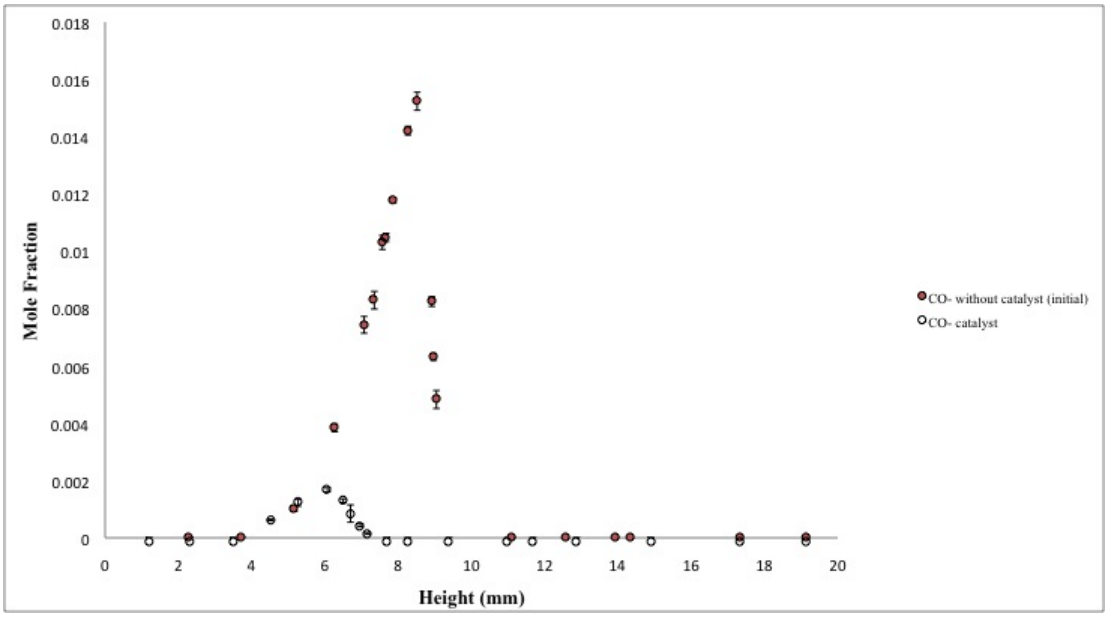

Figure 4.14: CO profiles measured from the catalytic and non-catalytic combustion. Note: The blank points are the results with $Fe(CO)_5$ addition, while the solid points are the initial data gotten by method 2 without $Fe(CO)_5$ addition

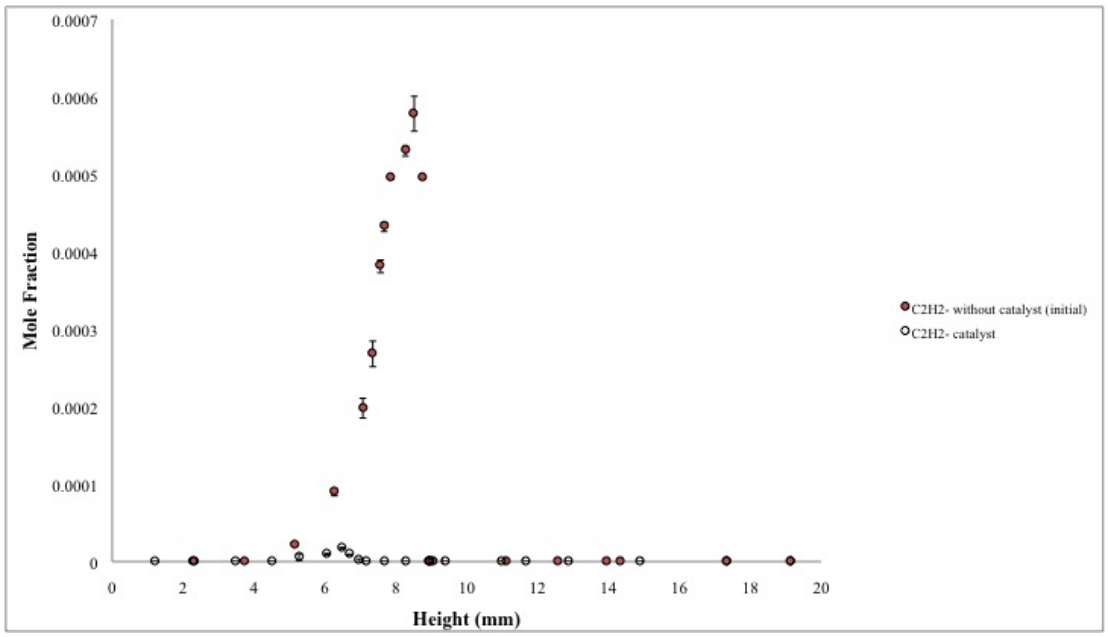

Figure 4.15: C_2H_2 profile measured from the catalytic and non-catalytic combustion. Note: The blank points are the results with $Fe(CO)_5$ addition, while the solid points are the initial data gotten by method 2 without $Fe(CO)_5$ addition

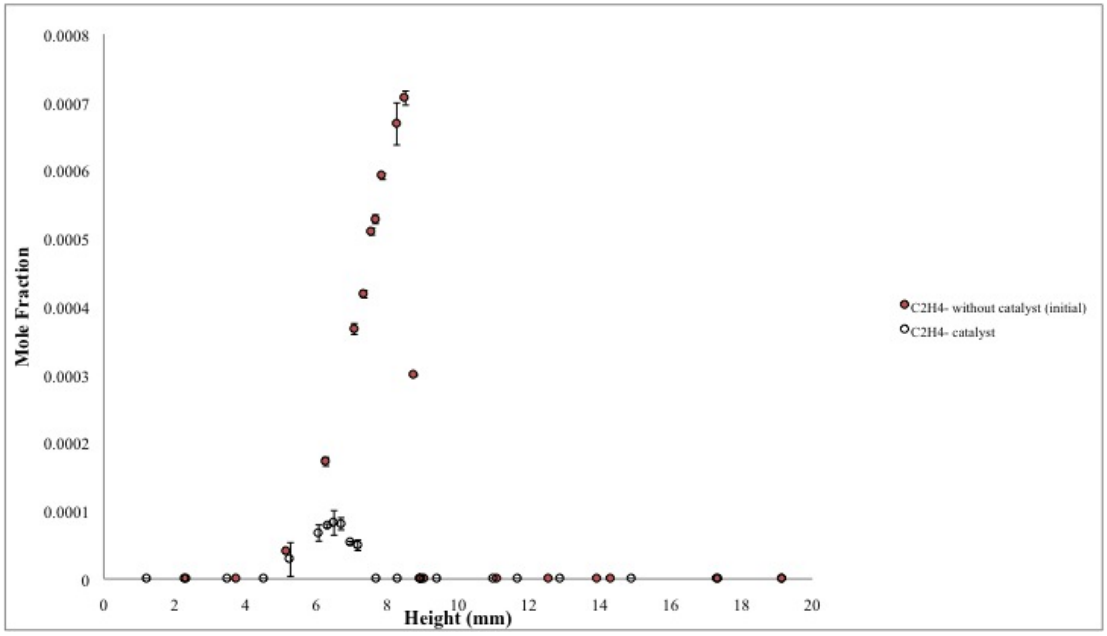

Figure 4.16: C_2H_4 profile measured from the catalytic and non-catalytic combustion. Note: The blank points are the results with $Fe(CO)_5$ addition, while the solid points are the initial data gotten by method 2 without $Fe(CO)_5$ addition

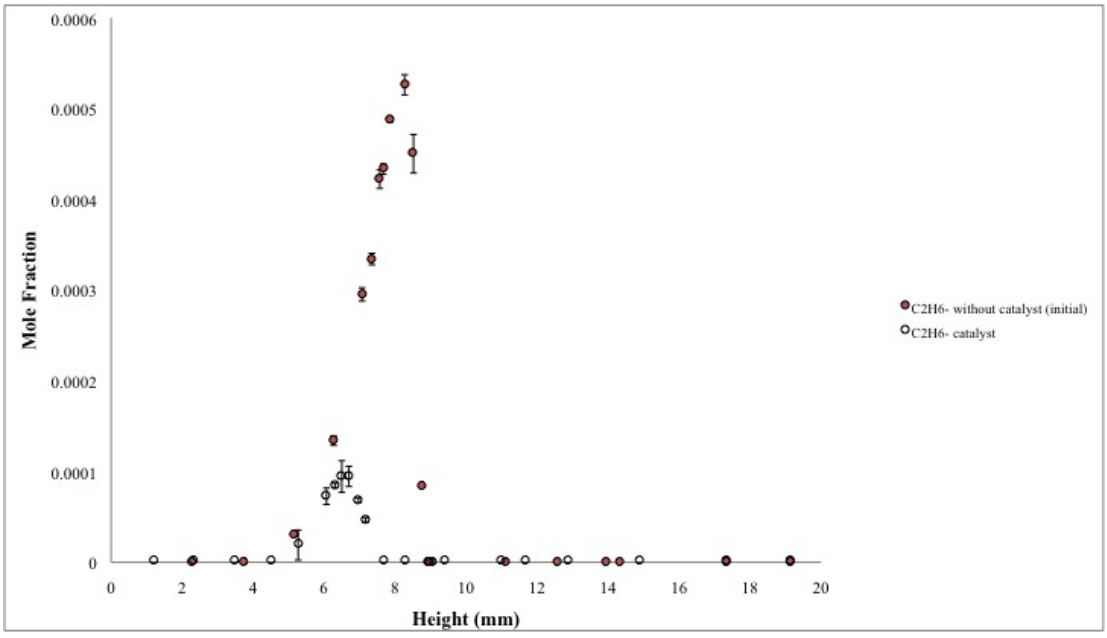

Figure 4.17: C_2H_6 profile measured from the catalytic and non-catalytic combustion. Note: The blank points are the results with $Fe(CO)_5$ addition, while the solid points are the initial data gotten by method 2 without $Fe(CO)_5$ addition

Emissions in the Horizontal Direction

Since $Fe(CO)_5$ is added into the flame through the burner central tube, it is partially mixed with the fuel-side stream at the low position above the bottom burner surface. It is hence interesting to get the gas profiles in the horizontal direction to review the dispersion of $Fe(CO)_5$ in the counter-flow flame. Fig.4.18∼Fig.4.21 are the curves showing the gas profiles of the major emissions in the horizontal direction measured from the catalytic (catalytic combustion 4) and non-catalytic combustion. The gas sample is collected at the height of approximately 8 mm, where the concentrations of emissions in non-catalytic combustion are maximum. In these figures, the x-axis indicates the distance between the microprobe tip and the burner central vertical axis (defined as the zero point), and the y-axis shows the concentration of the generated emissions.

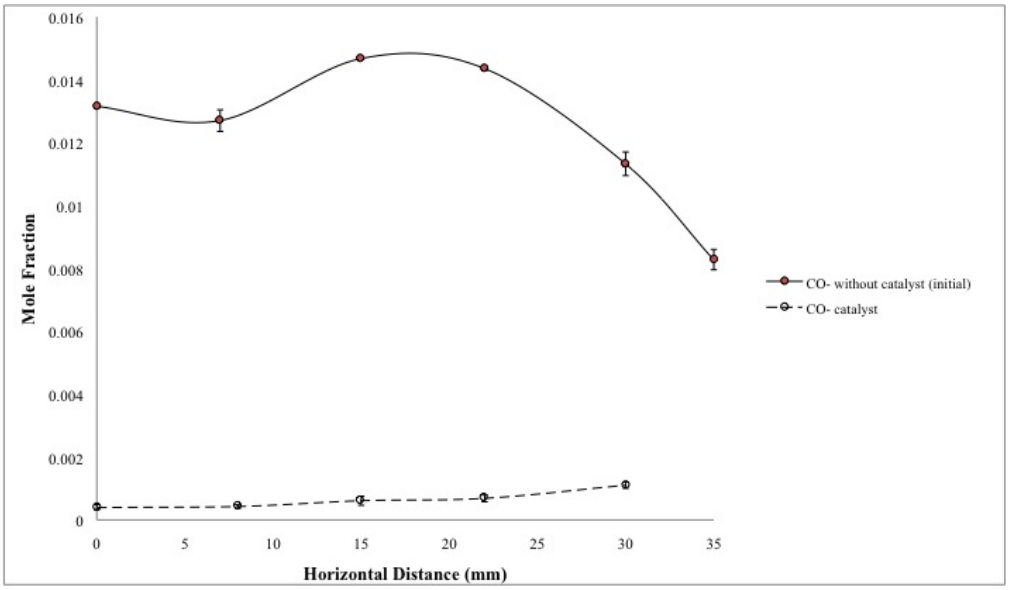

Figure 4.18: CO emission in the horizontal direction measured from the catalytic and non-catalytic combustion. Note: The blank points with dashed line are the data from the catalytic combustion, while the solid points are the initial data from the non-catalytic combustion. (zero point in x-axis is the location of the central vertical axis)

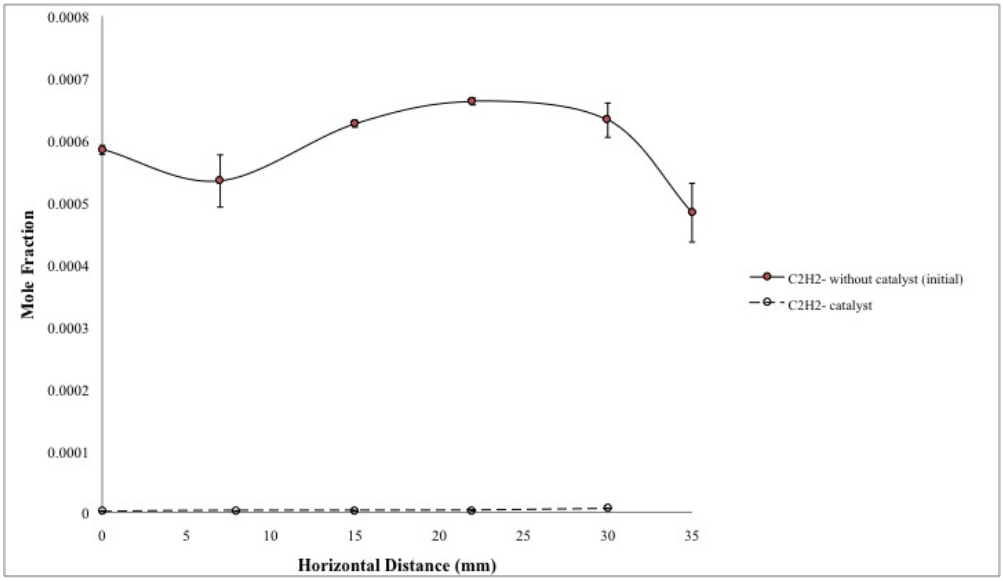

Figure 4.19: C_2H_2 emission in the horizontal direction measured from the catalytic and non-catalytic combustion. Note: The blank points with dashed line are the data from the catalytic combustion, while the solid points are the initial data from the non-catalytic combustion. (zero point in x-axis is the location of the central vertical axis)

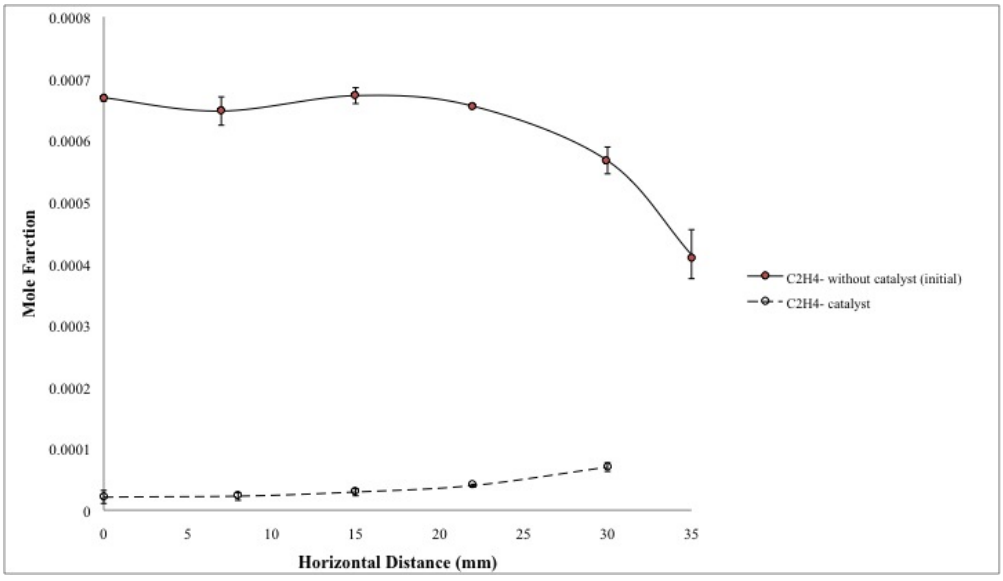

Figure 4.20: C_2H_4 emission in the horizontal direction measured from the catalytic and non-catalytic combustion. Note: The blank points with dashed line are the data from the catalytic combustion, while the solid points are the initial data from the non-catalytic combustion. (zero point in x-axis is the location of the central vertical axis)

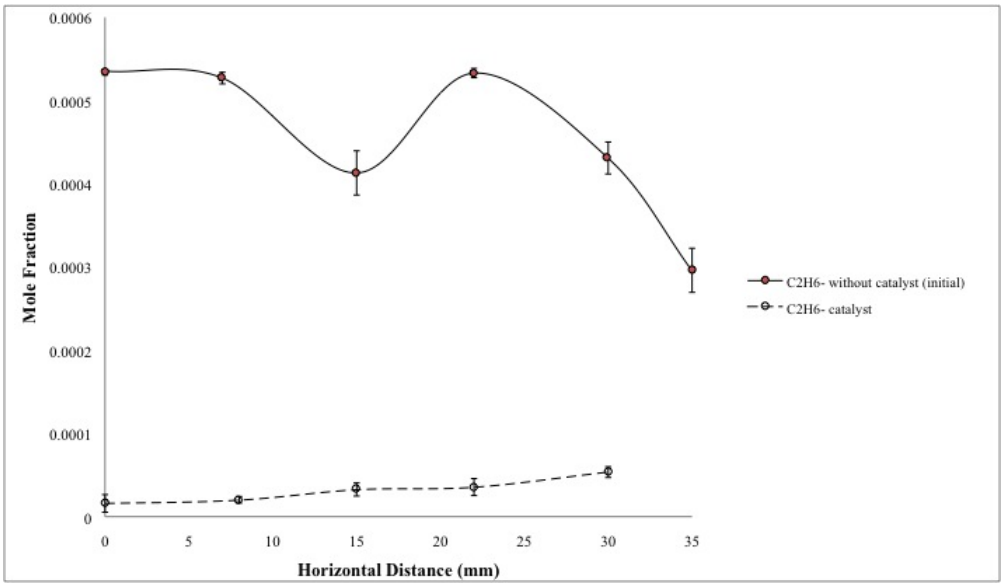

Figure 4.21: C_2H_6 emission in the horizontal direction measured from the catalytic and non-catalytic combustion. Note: The blank points with dashed line are the data from the catalytic combustion, while the solid points are the initial data from the non-catalytic combustion. (zero point in x-axis is the location of the central vertical axis)

Overall, the emissions of CO and C_2 species are significantly reduced by the iron-containing catalysts in the horizontal direction, by comparing their concentration curves obtained from the catalytic combustion with those of the non-catalytic combustion. The reason for this reduction is mainly attributed to the radial dispersion of the catalysts. Furthermore, based on the gas profiles of the catalytic combustion, these emissions are found to be increasing as the sampling points move far away from the central line. The tendency to increase is not very strong close to the central area. These changes indicate that the concentration of iron-containing catalysts is slightly diminishing as it spreads from the central part to the surrounding area radially. All of these findings are significant for evaluating the effectiveness and feasibility of this catalyst injection method in the industrial applications, as the conclusions in this study reveal that the chemical additive ($Fe(CO)_5$) injected into fuel-side stream through the central port can be well transported to the whole flow field when it reaches the height close to the flame.

4.2.2 Effects of the Catalyst Concentration on Pollution Reduction

More experiments were conducted in the thesis to investigate the relationship between the emission reduction and the dosage of the injected $Fe(CO)_5$. Six different concentrations of $Fe(CO)_5$ were injected into the flame. The experimental conditions are described in Table 4.1. During the experiments, the intensity of the orange flame was weaken as less $Fe(CO)_5$ was added. In addition, when compared to the initial flame, its location was found around 1 mm lower in "catalytic combustion 5 and 6". However, this location shift decreased as the catalyst concentration decreased. When the concentration of $Fe(CO)_5$ in the carrier gas was 3354 ppm, there was no measurable change in both the location and colour of the flame compared with the non-catalytic flame.

For the gas emissions, the measured concentrations of CO and C_2 species are shown in Fig.4.22 $\sim$ Fig.4.25. In these figures, the x-axis shows the concentration of $Fe(CO)_5$, and the y-axis shows the concentration of emissions generated from the catalytic combustion. Based on these curves, the emission of CO and C_2 species are lowered as more $Fe(CO)_5$ is added into the counter-flow flame. This is reasonable as the catalytic oxidation of methane is enhanced due to the generation of more iron oxides. When iron oxides are produced, it is believed that these oxides can absorb methane to their surface and catalyze them via the surface chemical reactions. After that, these iron oxides can be reduced to the iron particles, which will absorb oxygen to form the oxides again. This catalytic cycle will repeat during the combustion process. Therefore, more emissions can be generally reduced as more $Fe(CO)_5$ is injected into the methane flame.

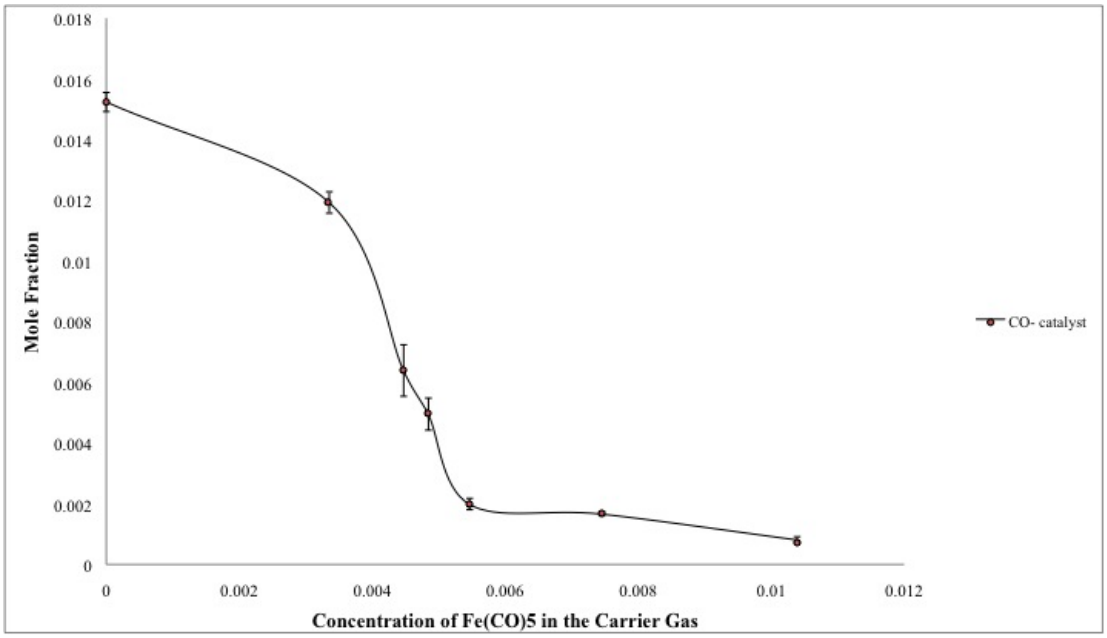

Figure 4.22: CO emission measured from the catalytic combustion of natural gas with different concentrations of $Fe(CO)_5$. Note: the concentration of $Fe(CO)_5$ here is its mole fraction in the carrier gas

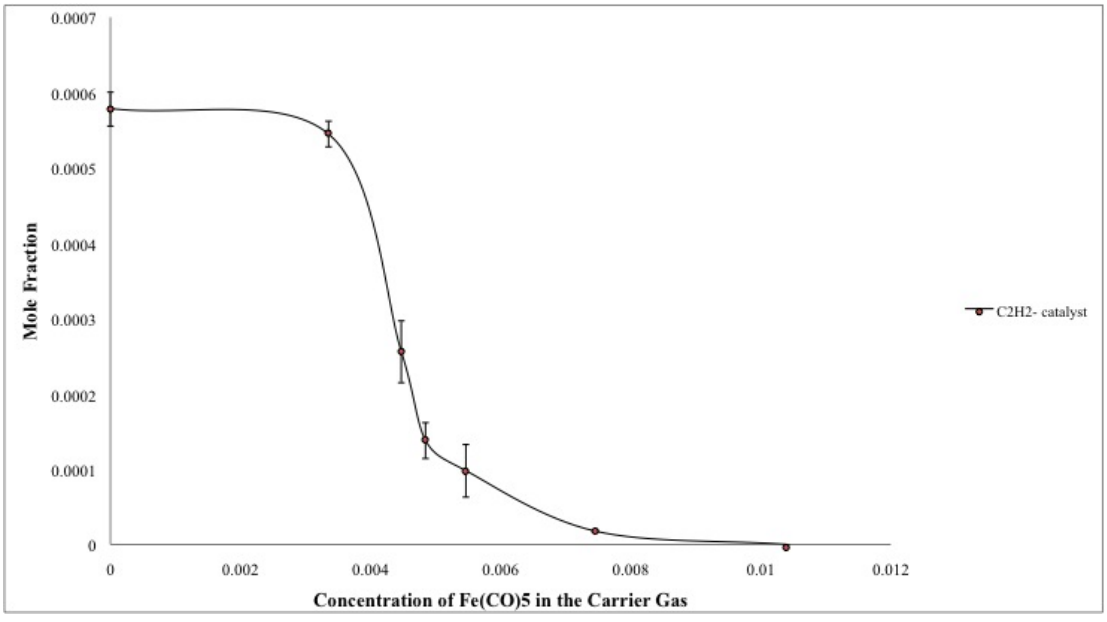

Figure 4.23: C_2H_2 emission measured from the catalytic combustion of natural gas with different concentrations of $Fe(CO)_5$. Note: the concentration of $Fe(CO)_5$ here is its mole fraction in the carrier gas

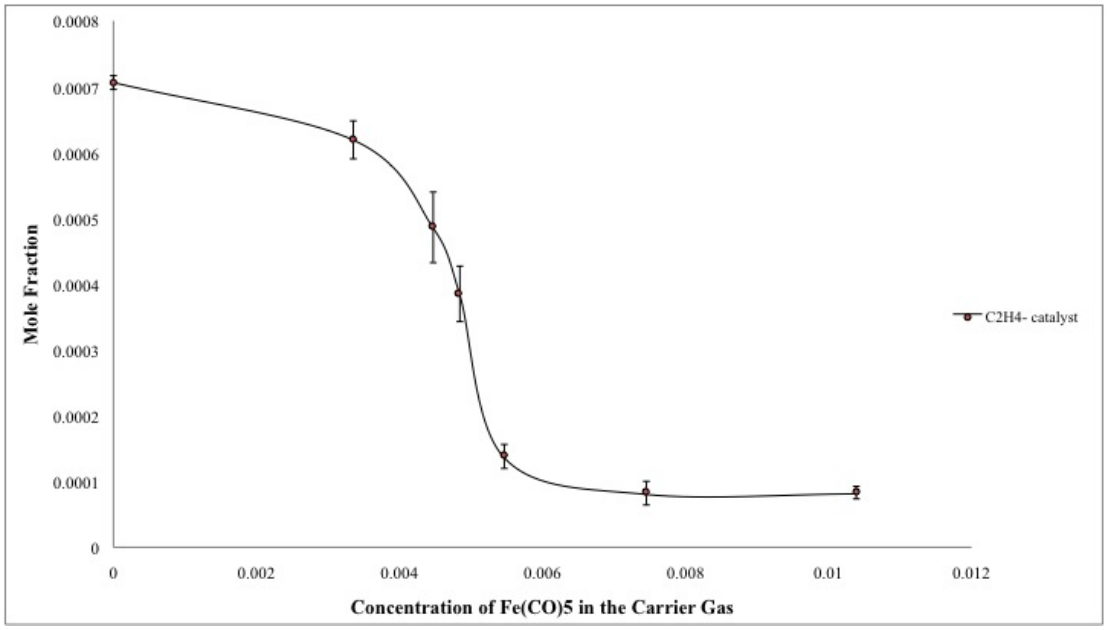

Figure 4.24: C_2H_4 emission measured from the catalytic combustion of natural gas with different concentrations of $Fe(CO)_5$. Note: the concentration of $Fe(CO)_5$ here is its mole fraction in the carrier gas

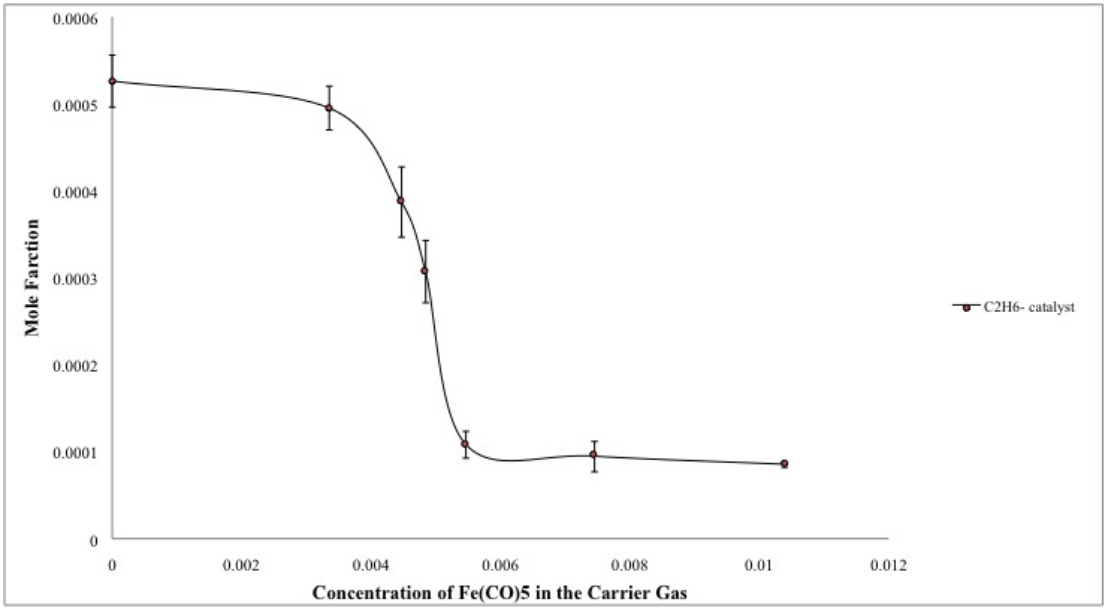

Figure 4.25: C_2H_6 emission measured from the catalytic combustion of natural gas with different concentrations of $Fe(CO)_5$. Note: the concentration of $Fe(CO)_5$ here is its mole fraction in the carrier gas

However, the reduction efficiency of these emissions is lower before the concentration of $Fe(CO)_5$ in the carrier gas reaches a certain level or when its concentration is too high. When the concentration of $Fe(CO)_5$ is too low, the generated iron oxides are not enough to form an efficient catalytic cycle for the complete oxidation of methane species. As a result, the emissions generated from methane combustion is unaffected. This may explain why the major emissions have a slow decline at the beginning of these curves. In addition, when the additive concentration is too high, the iron-containing particles are too much to saturate the catalytic cycle, and thereby it diminishes the emission reduction efficiency. This inhibition of the catalytic efficiency at high concentration of $Fe(CO)_5$ has already been investigated [138, 140]. Based on these analyses, it is suggested that the concentration of $Fe(CO)_5$ should be around 6000ppm in order to get the best performance for emission control, when the catalyst is injected through the central port of the bottom burner.

4.3 Analysis of the Uncertainty in the Experimental Studies

Errors exist in the experimental results of the gas species measured from natural gas combustion. These errors may be caused by not only the system uncertainties but also the experimental operations.

One major source of the uncertainties in the experimental results is caused by the system errors of the equipment used in the study, such as GC and mass flow controllers (MFCs). The errors caused by the GC analysis are considered to be smaller than 4%, based on the results obtained from the GC calibration process. For the flow rates, which are controlled by the MFCs (for fuel and oxidizers) and the rotameters (for carrier gas flow), the uncertainties are 1% of the experimental readings and 2% of the full scales respectively, known as the system errors of these flow meters.

Another source of the system errors come from the uncertainties of gas sampling technology and inaccuracies of the experimental setup. Although the rapid pressure drop inside the microprobe is thought to be a good method for the accurate measurements, it would still cause certain errors in the measured data. These errors can be induced by either the disturbance to the flame when inserting the microprobe or the potential continuous chemical reactions inside the sampling line. In addition, the two burners are ideally separated at a distance of 20 mm, whereas the actual value is smaller than the

design due to the manufacture tolerance.

In addition, the fluctuation caused by the microprobe configuration can introduce some uncertainties to the measurements. On one hand, the vertical position of the microprobe is determined by using a vernier caliper with a high accuracy of 0.01mm to measure the height difference between the sampling point and bottom burner surface. The height of the bottom burner surface is confirmed by adjusting the microprobe so that it makes contact with the burner surface closely. However, errors can be introduced here, as it is quite difficult to make a perfect contact by manual adjustment. On the other hand, the microprobe distorts when it is close to the high temperature flame zone. This is because the material of the probe is silica, which cannot withstand the peak temperature caused by the flat flame for a long time. As a result, the gas sample may be extracted from other positions, which are different from the measured height.

Finally, the counter-flow diffusion burner is an open experimental system which is completely exposed to the surrounding environment. Since this experimental system is a very sensitive one, the surrounding air flux caused by the operator or other factors could lead to some disturbance to the flat flame. The disturbance may induce some changes to the flame structure and even blow out the flame if the surrounding air flow is too strong. Hence, the uncertain environmental factors are potential risks for obtaining inaccurate experimental measurements.

Chapter 5

Conclusions and Recommendations

5.1 Conclusions

The characteristics of a natural gas fired counter-flow flame catalyzed by iron pentacarbonyl are experimentally studied via an online GC. The initial pictures of the gas emissions from the non-catalytic natural gas combustion are established by the experimental measurements. Furthermore, the performance of iron pentacarbonyl on emission reduction is investigated and evaluated in detail.

The experimental system, which is composed of a counter-flow diffusion flame burner and an online GC, is built up and improved for the fundamental combustion studies. The major gas species generated in the non-catalytic combustion including methane (CH_4), oxygen (O_2), nitrogen (N_2), carbon monoxide (CO), acetylene (C_2H_2), ethylene (C_2H_4) and ethane (C_2H_6) are collected and measured by two different gas sampling methods. The experimental results are compared to a previous study, which indicates that the experimental system has a high reliability for measuring the gas species produced by the natural gas fuelled diffusion flame. In addition, the experimental results are also used to validate the numerical simulation by comparing them with the CHEMKIN modeling. The consistency between the results in the comparison implies that the numerical model can be used to predict the gas products by the combustion of natural gas, although the measured concentrations of CO and C_2 species are slightly higher.

The experimental results obtained by the two different sampling methods are compared as well. The analysis indicates that method 2 (operated at atmospheric pressure) is preferred for collecting the gas sample from the counter-flow flame, as it has better repeatability and

stability. However, method 1 (operated under a higher vacuum) is much faster and more economical. Therefore, it is more suitable to collect the sample from the high-temperature zone or the heavy-particle flame.

In the second part of this experimental study, the effects of iron-containing catalysts on pollution reduction are investigated in order to develop the catalytic combustion technology for natural gas. Different amounts of iron pentacarbonyl carried by the nitrogen bypass-flow are directed into the flame through the central port of the bottom burner. The full gas profiles of the major emissions are measured when the concentration of iron pentacarbonyl in the carrier gas is 7453 ppm. Compared to the initial non-catalytic combustion data, the emissions of CO and light C_2 hydrocarbons can be reduced by 80%∼95%. Moreover, their peaks are observed to shift to positions closer to the fuel port. These findings are attributed to the catalytic oxidation of methane by the catalysts formed from the decomposition of iron pentacarbonyl.

Bigger pictures on the performance of iron-based catalysts are drawn by investigating the gas profiles in the horizontal direction. Compared with the baselines of the gas species generated from the non-catalytic combustion, the lower concentration curves illustrate that the catalysts can be radially transported to the edge of the flow field at a height close to flame. Furthermore, the effects of the iron pentacarbonyl concentration on the catalytic efficiency are also demonstrated by drawing the emission curves of CO and C_2 species. Overall, the emission reduction is enhanced when more iron pentacarbonyl is added into the flame, due to the increase of the formed iron-based catalysts. However, when the concentration of iron pentacarbonyl is too low or too high, its efficiency on emission reduction is diminished. The decline is probably caused by the lack of effective catalytic cycle at the low catalyst concentration and the saturation of the catalytic cycle at the high catalyst concentration.

5.2 Recommendations

To further understand the essence of the catalytic natural gas combustion with iron pentacarbonyl addition, some recommendations are proposed for the future experimental research.

- One major pollutant NO_x cannot be detected by GC, although its signal can be found in the GC calibration process. NO_x (mainly NO and NO_2) is highly sensitive

to water, pressure and temperature, which may induce the loss of NO_x during the sampling process. As a result, it fails to inject NO_x into the GC for the sample analysis. Moreover, the GC equipment does not have enough sensitivity to detect NO_x signal, especially when the NO_x content is very low in the gas sample. The calibration results show that the column installed in this GC cannot well separate the peak of NO from the methane signal. As a solution, different types of equipment, such as FTIR and dedicated NO_x analyzer, are suggested to be used for analyzing NO_x in the future experiments.

- In this study, the temperature profile of the counter-flow flame is not obtained. Temperature is an important factor for the fundamental combustion studies, as it may explain the reasons of some experimental findings or suggest the potential experimental tendency. Usually, temperature can be obtained by the intrusive (thermocouples) or non-intrusive (laser detection) technologies. A suitable thermocouple is proposed to get the temperature profile in future studies, although temperature detection limit and uncertainty in the measurements are big challenges in its application.

- More detailed experiments are necessary to study the iron-containing species and other chemical components, such as the intermediate species and carbon dioxide. Due to the absence of experimental data for these critical components, the results in this thesis are hence limited in explaining the details of the catalytic mechanism with iron pentacarbonyl addition. Therefore, the measurements on the formation process of these components are important, as they can not only help understand the reaction pathways but also help improve the numerical model used for predicting the flame structure.

- More studies under different experimental conditions are critical for further understanding the catalytic technology based on iron-containing catalysts. For iron pentacarbonyl, its effects on pollutant reduction, affected by different catalyst concentrations and the partial-mixing injection method, have been investigated. However, the characteristics of the diffusion flame with catalyst addition can also be affected by other factors, such as different strain rates, different fuel/oxidizer ratios and other catalyst injection methods. These factors may give some surprising findings which can help to better understand the performance of iron-based additives for pollution control. Consequently, it is interesting and important to collect more results under different experimental conditions.

- Further improvement and optimization of the experimental apparatus are necessary to obtain data with higher accuracy. Uncertainties in the experimental results are not expected as they can lead to the erroneous conclusions and thus influence the proper application of the iron-based additives. Using the equipment with a higher accuracy or improving the experimental setup are ways to obtain better experimental measurements. For this system, replacing the rotameters with mass flow meters (MFCs), adding shields to the outside of the burners and using digital pressure gauges are possible improvements for reducing experimental errors.

References

[1] R. A. B. Semin, "A technical review of compressed natural gas as an alternative fuel for internal combustion engines," *Am. J. Engg. & Applied Sci*, vol. 1, no. 4, pp. 302–311, 2008.

[2] J. Huang and R. Crookes, "Assessment of simulated biogas as a fuel for the spark ignition engine," *Fuel*, vol. 77, no. 15, pp. 1793–1801, 1998.

[3] R. Thring, "Alternative fuels for spark ignition engines," Southwest Research Institute, Tech. Rep., 1983.

[4] A. M. Namasivayam, "Combustion, performance and emissions characteristics of compression-ignition engines fuelled by sustainable fuels," Ph.D. dissertation, Queen Mary, University of London, 2011.

[5] "Canadian energy overview 2006-energy market assessment," National Energy Board, Canada, Tech. Rep., May 2007.

[6] "Canadian energy overview 2011-energy briefing note," National Energy Board, Canada, Tech. Rep., July 2011.

[7] "Natural gas 1998: Issues and trends," Energy Information Administration, USA, Tech. Rep., April 1999.

[8] I. Glassman and R. Yetter, *Combustion*. Academic press, 2008.

[9] P. Thevenin, "Catalytic combustion of methane," Ph.D. dissertation, KTH, 2002.

[10] J. H. Lee and D. L. Trimm, "Catalytic combustion of methane," *Fuel Processing Technology*, vol. 42, no. 2, pp. 339–359, 1995.

[11] *Agilent 6890 Series Gas Chromatograph Operation Manual Volume 1. General Information*, Agilent Technologies, Inc.

[12] "Energy futures backgrounder: Addendum to canadas energy future: Energy supply and demand projections to 2035," National Energy Board, Canada, Tech. Rep., June 2012.

[13] "Summer energy outlook 2013," National Energy Board, Canada, Tech. Rep., 2013.

[14] "Canadas energy future: Energy supply and demand projections to 2035 - energy market assessment," National Energy Board, Canada, Tech. Rep., November 2011.

[15] B. M. Shasby, "Alternative fuels: Incompletely addressing the problems of the automobile," Ph.D. dissertation, Virginia Polytechnic Institute and State University, 2004.

[16] G. Munde Gopal and S. Dalu Rajendra, "Compressed natural gas as an alternative fuel for spark ignition engine: A review," *International Journal of Engineering and Innovative Technology*, vol. 2, no. 6, 2012.

[17] I. Langmuir, "The mechanism of the catalytic action of platinum in the reactions $2CO + O_2 = 2CO_2$ and $2H_2 + O_2 = 2H_2O$," *Transactions of the Faraday Society*, vol. 17, pp. 621–654, 1922.

[18] T. Choudhary, S. Banerjee, and V. Choudhary, "Catalysts for combustion of methane and lower alkanes," *Applied Catalysis A: General*, vol. 234, no. 1, pp. 1–23, 2002.

[19] A. Barbosa, J. Herguido, and J. Santamaria, "Methane combustion over unsupported iron oxide catalysts," *Catalysis today*, vol. 64, no. 1, pp. 43–50, 2001.

[20] S. Kwon, M. Fan, T. Wheelock, and B. Saha, "Nano-and micro-iron oxide catalysts for controlling the emission of carbon monoxide and methane," *Separation and Purification Technology*, vol. 58, no. 1, pp. 40–48, 2007.

[21] H. Tsuji, "Counterflow diffusion flames," *Progress in energy and combustion science*, vol. 8, no. 2, pp. 93–119, 1982.

[22] NaturalGas.org. (2013, Jun.) Background. [Online]. Available: http://www.naturalgas.org/overview/background.asp

[23] K. Bhandari, A. Bansal, A. Shukla, and M. Khare, "Performance and emissions of natural gas fueled internal combustion engine: A review," *Journal of scientific & industrial research*, vol. 64, no. 5, pp. 333–338, 2005.

[24] H. M. Cho and B.-Q. He, "Spark ignition natural gas enginesa review," *Energy Conversion and Management*, vol. 48, no. 2, pp. 608–618, 2007.

[25] K. Zeng, Z. Huang, B. Liu, L. Liu, D. Jiang, Y. Ren, and J. Wang, "Combustion characteristics of a direct-injection natural gas engine under various fuel injection timings," *Applied thermal engineering*, vol. 26, no. 8, pp. 806–813, 2006.

[26] L. Shenghua, Z. Longbao, W. Ziyan, and R. Jiang, "Combustion characteristics of compressed natural gas/diesel dual-fuel turbocharged compressed ignition engine," *Proceedings of the Institution of Mechanical Engineers, Part D: Journal of Automobile Engineering*, vol. 217, no. 9, pp. 833–838, 2003.

[27] I. Puri, K. Seshadri, M. Smooke, and D. Keyes, "A comparison between numerical calculations and experimental measurements of the structure of a counterflow methane-air diffusion flame," *Combustion science and technology*, vol. 56, no. 1-3, pp. 1–22, 1987.

[28] V. Khanna, R. Goel, and J. Ellzey, "Measurements of emissions and radiation for methane combustion within a porous medium burner," *Combustion science and technology*, vol. 99, no. 1-3, pp. 133–142, 1994.

[29] R. C. Flagan and J. H. Seinfeld, *Fundamentals of air pollution engineering*. Courier Dover Publications, 2012.

[30] K. B. Schnelle and C. A. Brown, *Air pollution control technology handbook*. CRC PressI Llc, 2002.

[31] D. Pershing and J. Wendt, "Relative contributions of volatile nitrogen and char nitrogen to NOx emissions from pulverized coal flames," *Industrial & Engineering Chemistry Process Design and Development*, vol. 18, no. 1, pp. 60–67, 1979.

[32] W. Hahn and J. Wendt, "NO_x formation in flat, laminar, opposed jet methane diffusion flames," in *Symposium (International) on Combustion*, vol. 18, no. 1. Elsevier, 1981, pp. 121–131.

[33] L. G. Blevins and J. P. Gore, "Computed structure of low strain rate partially premixed CH_4/air counterflow flames: implications for no formation," *Combustion and flame*, vol. 116, no. 4, pp. 546–566, 1999.

[34] A. Beltrame, P. Porshnev, W. Merchan-Merchan, A. Saveliev, A. Fridman, L. Kennedy, O. Petrova, S. Zhdanok, F. Amouri, and O. Charon, "Soot and NO formation in methane–oxygen enriched diffusion flames," *Combustion and flame*, vol. 124, no. 1, pp. 295–310, 2001.

[35] V. Dupont and A. Williams, "NO_x mechanisms in rich methane-air flames," *Combustion and flame*, vol. 114, no. 1, pp. 103–118, 1998.

[36] Particulate matter-health. [Online]. Available: http://www.epa.gov/pm/health.html

[37] L. Rubino, "The effect of oxygenated additives on soot precursor formation." Master's thesis, University of Toronto, 2001.

[38] S. M. Sarathy, "Using an opposed flow diffusion flame to study the oxidation of C_4 fatty acid methyl esters," Master's thesis, University of Toronto, 2006.

[39] N. Marinov, W. Pitz, C. Westbrook, A. Lutz, A. Vincitore, and S. Senkan, "Chemical kinetic modeling of a methane opposed-flow diffusion flame and comparison to experiments," in *Symposium (International) on Combustion*, vol. 27, no. 1. Elsevier, 1998, pp. 605–613.

[40] K. C. Smyth, J. H. Miller, R. C. Dorfman, W. G. Mallard, and R. J. Santoro, "Soot inception in a methane/air diffusion flame as characterized by detailed species profiles," *Combustion and Flame*, vol. 62, no. 2, pp. 157–181, 1985.

[41] Y. Wang, Y. Liu, Q. Cao, C. Wang, and D. Che, "Homogeneous combustion of fuel ultra-lean methane–air mixtures: Experimental study and simplified reaction mechanism," *Energy & Fuels*, vol. 25, no. 8, pp. 3437–3445, 2011.

[42] V. Kozlov, A. Lebedev, A. Sekundov, and K. Y. Yakubovskii, "Emission of carbon oxides during the combustion of lean methane-air premixed mixtures," *Russian Journal of Physical Chemistry B*, vol. 4, no. 4, pp. 602–612, 2010.

[43] Y. Fahmy, P. Fornasiero, S. Zinoviev, and S. Miertus, "Air pollution control technologies compendium," United Nations Industrial Development Organization, 2007.

[44] "Control of nitrogen oxide emissions: Selective catalytic reduction (SCR)," U.S. Department of Energy and Southwest Company Services, Inc., Tech. Rep., July 1997.

[45] F. Luck and J. Roiron, "Selective catalytic reduction of NO_x emitted by nitric acid plants," *Catalysis Today*, vol. 4, no. 2, pp. 205–218, 1989.

[46] Z. Zong-rang, "Design optimization of SCR system for coal-fired boilers [j]," *Electric Power*, vol. 11, p. 016, 2005.

[47] M. Koebel, M. Elsener, and T. Marti, "NO_x-reduction in diesel exhaust gas with urea and selective catalytic reduction," *Combustion science and technology*, vol. 121, no. 1-6, pp. 85–102, 1996.

[48] J. D. Peter-Hoblyn, E. N. Balles, T. J. Tarabulski, J. E. Hofmann, and J. M. Valentine, "Urea pyrolysis chamber and process for reducing lean-burn engine NO_x emissions by selective catalytic reduction," Mar. 20 2001, US Patent 6,203,770.

[49] E. Marty and G. H. Martin, "Session 13 waste treatments: Selective non-catalytic reduction of nitrogen oxides."

[50] S. Mahmoudi, J. Baeyens, and J. P. Seville, "NO_x formation and selective non-catalytic reduction (SNCR) in a fluidized bed combustor of biomass," *Biomass and bioenergy*, vol. 34, no. 9, pp. 1393–1409, 2010.

[51] M. Jødal, T. L. Lauridsen, and K. Dam-Johansen, "NO_x removal on a coal-fired utility boiler by selective non-catalytic reduction," *Environmental progress*, vol. 11, no. 4, pp. 296–301, 1992.

[52] C. Nam and B. Gibbs, "Selective non-catalytic reduction of NO_x under diesel engine conditions," *Proceedings of the Combustion Institute*, vol. 28, no. 1, pp. 1203–1209, 2000.

[53] P. W. Groff and B. K. Gullett, "Industrial boiler retrofit for NO_x control: combined selective noncatalytic reduction and selective catalytic reduction," *Environmental progress*, vol. 16, no. 2, pp. 116–120, 1997.

[54] B. K. Gullett, P. W. Groff, M. L. Lin, and J. M. Chen, "NO_x removal with combined selective catalytic reduction and selective noncatalytic reduction: pilot-scale test results," *Air & waste*, vol. 44, no. 10, pp. 1188–1194, 1994.

[55] Y. S. Mok and H.-J. Lee, "Removal of sulfur dioxide and nitrogen oxides by using ozone injection and absorption–reduction technique," *Fuel Processing Technology*, vol. 87, no. 7, pp. 591–597, 2006.

[56] K. Urashima, J.-S. Chang, J.-Y. Park, D.-C. Lee, A. Chakrabarti, and T. Ito, "Reduction of nO_x from natural gas combustion flue gases by corona discharge radical injection techniques [thermal power plant emissions control]," *Industry Applications, IEEE Transactions on*, vol. 34, no. 5, pp. 934–939, 1998.

[57] M. Okubo, N. Arita, T. Kuroki, K. Yoshida, and T. Yamamoto, "Total diesel emission control technology using ozone injection and plasma desorption," *Plasma Chemistry and Plasma Processing*, vol. 28, no. 2, pp. 173–187, 2008.

[58] M. Schoenung and R. K. Hanson, "CO and temperature measurements in a flat flame by laser absorption spectroscopy and probe techniques," *Combustion Science and Technology*, vol. 24, no. 5-6, pp. 227–237, 1980.

[59] M. M. Schorr and J. Chalfin, "Gas turbine NO_x emissions approaching zero–is it worth the price?" *General Electric Power Systems, Schenectady, New York*, pp. 1–6, 1999.

[60] C. E. Maslak, "Water and steam injection in cogeneration system," May 29 1990, US Patent 4,928,478.

[61] C. Wilkes and B. W. Gerhold, "NO_x reduction in a combined gas-steam power plant," Feb. 2 1982, US Patent 4,313,300.

[62] Y. Suzukawa, S. Sugiyama, Y. Hino, M. Ishioka, and I. Mori, "Heat transfer improvement and NO_x reduction by highly preheated air combustion," *Energy Conversion and Management*, vol. 38, no. 10, pp. 1061–1071, 1997.

[63] A. K. Gupta, "Thermal characteristics of gaseous fuel flames using high temperature air," *Transactions-American Society of Mechanical Engineers Journal of Engineering for Gas Turbines and Power*, vol. 126, no. 1, pp. 9–19, 2004.

[64] J. L. Marion, "Advanced overfire air system for NO_x control," Mar. 23 1993, US Patent 5,195,450.

[65] R. E. Donais, T. D. Hellewell, P. D. Kuczma, and J. S. Simon, "Control of staged combustion, low NO_x firing systems with single or multiple levels of overfire air," May 6 1997, US Patent 5,626,085.

[66] L. Smoot, S. Hill, and H. Xu, "NO_x control through reburning1," *Progress in energy and combustion science*, vol. 24, no. 5, pp. 385–408, 1998.

[67] P. Maly, V. Zamansky, L. Ho, and R. Payne, "Alternative fuel reburning," *Fuel*, vol. 78, no. 3, pp. 327–334, 1999.

[68] M. Lapuerta, J. Hernandez, and F. Gimenez, "Evaluation of exhaust gas recirculation as a technique for reducing diesel engine NO_x emissions," *Proceedings of the Institution of Mechanical Engineers, Part D: Journal of Automobile Engineering*, vol. 214, no. 1, pp. 85–93, 2000.

[69] S. J. Bortz, D. E. Shore, N. Garrad, J. Pirkey, and Facchiano, "Ultra-low NO_x rapid mix burner demonstration at con edisons 59th street station," Aug. 25 - 29 1997, present at EPRI-DOE-EPA Combined Utility Air Pollutant Control Symposium.

[70] J. Saint-Just and J. der Kinderen, "Catalytic combustion: from reaction mechanism to commercial applications," *Catalysis today*, vol. 29, no. 1, pp. 387–395, 1996.

[71] R. Burch *et al.*, "Low NO_x options in catalytic combustion and emission control," *Pure and applied chemistry*, vol. 68, no. 2, pp. 377–386, 1996.

[72] B. Enga and D. Thompson, "Catalytic combustion applied to gas turbine technology," *Platinum Metals Review*, vol. 23, no. 4, pp. 134–141, 1979.

[73] S. R. Vatcha, "Low-emission gas turbines using catalytic combustion," *Energy conversion and management*, vol. 38, no. 10, pp. 1327–1334, 1997.

[74] S. R. Vaillant and A. S. Gastec, "Catalytic combustion in a domestic natural gas burner," *Catalysis today*, vol. 47, no. 1, pp. 415–420, 1999.

[75] M. Iamarino, R. Chirone, L. Lisi, R. Pirone, P. Salatino, and G. Russo, "Cu/γ-Al_2O_3 catalyst for the combustion of methane in a fluidized bed reactor," *Catalysis today*, vol. 75, no. 1, pp. 317–324, 2002.

[76] M. Foka, J. Chaouki, C. Guy, and D. Klvana, "Natural gas combustion in a catalytic turbulent fluidized bed," *Chemical engineering science*, vol. 49, no. 24, pp. 4269–4276, 1994.

[77] "Emission control technologies for diesel-power vehicles," Manufacturers of Emission Controls Association, 2007.

[78] J. Neeft, M. Makkee, and J. A. Moulijn, "Diesel particulate emission control," *Fuel processing technology*, vol. 47, no. 1, pp. 1–69, 1996.

[79] O. Deutschmann and A. G. Konstandopoulos, "Catalytic technology for soot and gaseous pollution control," *Handbook of Combustion*, 2010.

[80] S. Deshmukh and D. Vlachos, "A reduced mechanism for methane and one-step rate expressions for fuel-lean catalytic combustion of small alkanes on noble metals," *Combustion and Flame*, vol. 149, no. 4, pp. 366–383, 2007.

[81] A. Mhadeshwar and D. Vlachos, "A catalytic reaction mechanism for methane partial oxidation at short contact times, reforming, and combustion, and for oxygenate decomposition and oxidation on platinum," *Industrial & engineering chemistry research*, vol. 46, no. 16, pp. 5310–5324, 2007.

[82] G. Neri, L. Bonaccorsi, A. Donato, C. Milone, M. G. Musolino, and A. M. Visco, "Catalytic combustion of diesel soot over metal oxide catalysts," *Applied Catalysis B: Environmental*, vol. 11, no. 2, pp. 217–231, 1997.

[83] E. Miró, F. Ravelli, M. Ulla, L. Cornaglia, and C. Querini, "Catalytic combustion of diesel soot on Co, K supported catalysts," *Catalysis Today*, vol. 53, no. 4, pp. 631–638, 1999.

[84] P. Ciambelli, P. Corbo, M. Gambino, V. Palma, and S. Vaccaro, "Catalytic combustion of carbon particulate," *Catalysis Today*, vol. 27, no. 1, pp. 99–106, 1996.

[85] B. A. Van Setten, M. Makkee, and J. A. Moulijn, "Science and technology of catalytic diesel particulate filters," *Catalysis Reviews*, vol. 43, no. 4, pp. 489–564, 2001.

[86] Diesel particulate filters. [Online]. Available: http://www.dieselretrofit.eu/technologies_filters.html

[87] D. Wiznia, G. Geist, and H. Ellis, "Biofuels implementation and emissions analysis," *Yale Department of Mechanical Engineering New Haven, CT*, vol. 6511, 2006.

[88] Y.-F. Y. Yao, "The oxidation of CO and hydrocarbons over noble metal catalysts," *Journal of Catalysis*, vol. 87, no. 1, pp. 152–162, 1984.

[89] G. C. Bond and D. T. Thompson, "Gold-catalysed oxidation of carbon monoxide," *Gold Bulletin*, vol. 33, no. 2, pp. 41–50, 2000.

[90] B. V. Lvov and A. K. Galwey, "Catalytic oxidation of CO on platinum," *Journal of Thermal Analysis and Calorimetry*, vol. 111, no. 1, pp. 145–154, 2013.

[91] J. G. McCarty, M. Gusman, D. Lowe, D. Hildenbrand, and K. Lau, "Stability of supported metal and supported metal oxide combustion catalysts," *Catalysis Today*, vol. 47, no. 1, pp. 5–17, 1999.

[92] T. Baldwin and R. Burch, "Remarkable activity enhancement in the catalytic combustion of methane on supported palladium catalysts," *Catalysis Letters*, vol. 6, no. 1, pp. 131–138, 1990.

[93] H. Widjaja, K. Sekizawa, K. Eguchi, and H. Arai, "Oxidation of methane over pd-supported catalysts," *Catalysis today*, vol. 35, no. 1, pp. 197–202, 1997.

[94] F. Ribeiro, M. Chow, and R. Dallabetta, "Kinetics of the complete oxidation of methane over supported palladium catalysts," *Journal of Catalysis*, vol. 146, no. 2, pp. 537–544, 1994.

[95] Y.-H. Chin and D. E. Resasco, "Catalytic oxidation of methane on supported palladium under lean conditions: Kinetics, structure and properties," *CATALYSIS-LONDON-*, vol. 14, pp. 1–39, 1999.

[96] D. Ciuparu, M. R. Lyubovsky, E. Altman, L. D. Pfefferle, and A. Datye, "Catalytic combustion of methane over palladium-based catalysts," *Catalysis Reviews*, vol. 44, no. 4, pp. 593–649, 2002.

[97] Z. Li and G. B. Hoflund, "A review on complete oxidation of methane at low temperatures," *Journal of Natural Gas Chemistry*, vol. 12, no. 3, pp. 153–160, 2003.

[98] J. H. Lee, D. Trimm, and N. Cant, "The catalytic combustion of methane and hydrogen sulphide," *Catalysis today*, vol. 47, no. 1, pp. 353–357, 1999.

[99] M. Aryafar and F. Zaera, "Kinetic study of the catalytic oxidation of alkanes over nickel, palladium, and platinum foils," *Catalysis Letters*, vol. 48, no. 3-4, pp. 173–183, 1997.

[100] G. Lapisardi, P. Gelin, A. Kaddouri, E. Garbowski, and S. Da Costa, "Pt - Pd bimetallic catalysts for methane emissions abatement," *Topics in Catalysis*, vol. 42, no. 1-4, pp. 461–464, 2007.

[101] R. Abbasi, L. Wu, S. Wanke, and R. Hayes, "Kinetics of methane combustion over Pt and Pt - Pd catalysts," *Chemical Engineering Research and Design*, vol. 90, no. 11, pp. 1930–1942, 2012.

[102] H. Yamamoto and H. Uchida, "Oxidation of methane over Pt and Pd supported on alumina in lean-burn natural-gas engine exhaust," *Catalysis today*, vol. 45, no. 1, pp. 147–151, 1998.

[103] R. Waters, J. Weimer, and J. Smith, "An investigation of the activity of coprecipitated gold catalysts for methane oxidation," *Catalysis letters*, vol. 30, no. 1-4, pp. 181–188, 1994.

[104] R. Grisel, P. Kooyman, and B. Nieuwenhuys, "Influence of the preparation of Au/Al_2o_3 on CH_4 oxidation activity," *Journal of Catalysis*, vol. 191, no. 2, pp. 430–437, 2000.

[105] K. Blick, T. D. Mitrelias, J. S. Hargreaves, G. J. Hutchings, R. W. Joyner, C. J. Kiely, and F. E. Wagner, "Methane oxidation using Au/MgO catalysts," *Catalysis letters*, vol. 50, no. 3-4, pp. 211–218, 1998.

[106] G. Pecchi, P. Reyes, R. Gómez, T. López, and J. Fierro, "Methane combustion on Rh/ZrO_2 catalysts," *Applied Catalysis B: Environmental*, vol. 17, no. 1, pp. L7–L13, 1998.

[107] S. Miao and Y. Deng, "Au-Pt/Co_3O_4 catalyst for methane combustion," *Applied Catalysis B: Environmental*, vol. 31, no. 3, pp. L1–L4, 2001.

[108] M. Bhagiyalakshmi, R. Anuradha, S. Do Park, T. S. Park, W. S. Cha, and H. T. Jang, "Effect of bimetallic Pt-Rh and trimetallic Pt-Pd-Rh catalysts for low temperature catalytic combustion of methane," *Bulletin of the Korean Chemical Society*, vol. 31, no. 1, pp. 120–124, 2010.

[109] C. Kul Ryu, M. Wong Ryoo, I. Soo Ryu, and S. Kyu Kang, "Catalytic combustion of methane over supported bimetallic Pd catalysts: Effects of Ru or Rh addition," *Catalysis today*, vol. 47, no. 1, pp. 141–147, 1999.

[110] M. ClaireáMarion *et al.*, "Catalytic properties of copper oxide supported on zinc aluminate in methane combustion," *Journal of the Chemical Society, Faraday Transactions*, vol. 87, no. 11, pp. 1795–1800, 1991.

[111] P. W. Park and J. S. Ledford, "The influence of surface structure on the catalytic activity of alumina supported copper oxide catalysts. oxidation of carbon monoxide and methane," *Applied Catalysis B: Environmental*, vol. 15, no. 3, pp. 221–231, 1998.

[112] M. I. Zaki, M. A. Hasan, L. Pasupulety, N. E. Fouad, and H. Knözinger, "CO and CH_4 total oxidation over manganese oxide supported on ZrO_2, TiO_2, TiO_2-Al_2O_3 and SiO_2-Al_2O_3 catalysts," *New Journal of Chemistry*, vol. 23, no. 12, pp. 1197–1202, 1999.

[113] T.-c. Xiao, S.-f. Ji, H.-t. Wang, K. S. Coleman, and M. L. Green, "Methane combustion over supported cobalt catalysts," *Journal of Molecular Catalysis A: Chemical*, vol. 175, no. 1, pp. 111–123, 2001.

[114] J. McCarty, Y.-F. Chang, V. Wong, and E. Johansson, "Kinetics of high temperature methane combustion by metal oxide catalysts," *Preprints-American Chemical Society. Division of Petroleum Chemistry*, vol. 42, no. 1, pp. 158–162, 1997.

[115] P. Ciambelli, S. Cimino, L. Lisi, M. Faticanti, G. Minelli, I. Pettiti, and P. Porta, "La, Ca and Fe oxide perovskites: preparation, characterization and catalytic properties for methane combustion," *Applied Catalysis B: Environmental*, vol. 33, no. 3, pp. 193–203, 2001.

[116] H. Arai, T. Yamada, K. Eguchi, and T. Seiyama, "Catalytic combustion of methane over various perovskite-type oxides," *Applied catalysis*, vol. 26, pp. 265–276, 1986.

[117] L. Marchetti and L. Forni, "Catalytic combustion of methane over perovskites," *Applied Catalysis B: Environmental*, vol. 15, no. 3, pp. 179–187, 1998.

[118] B. de Collongue, E. Garbowski, and M. Primet, "Catalytic combustion of methane over bulk and supported $LaCrO_3$ perovskites," *Journal of the Chemical Society, Faraday Transactions*, vol. 87, no. 15, pp. 2493–2499, 1991.

[119] S. Cimino, L. Lisi, R. Pirone, G. Russo, and M. Turco, "Methane combustion on perovskites-based structured catalysts," *Catalysis today*, vol. 59, no. 1, pp. 19–31, 2000.

[120] J. Chen, W. Shi, and J. Li, "Catalytic combustion of methane over cerium-doped cobalt chromite catalysts," *Catalysis Today*, vol. 175, no. 1, pp. 216–222, 2011.

[121] W. Tang, Z. Hu, M. Wang, G. D. Stucky, H. Metiu, and E. W. McFarland, "Methane complete and partial oxidation catalyzed by Pt-doped CeO_2," *Journal of Catalysis*, vol. 273, no. 2, pp. 125–137, 2010.

[122] V. R. Choudhary, B. S. Uphade, and S. G. Pataskar, "Low temperature complete combustion of dilute methane over Mn-doped ZrO_2 catalysts: factors influencing the reactivity of lattice oxygen and methane combustion activity of the catalyst," *Applied Catalysis A: General*, vol. 227, no. 1, pp. 29–41, 2002.

[123] P. Artizzu-Duart, J. Millet, N. Guilhaume, E. Garbowski, and M. Primet, "Catalytic combustion of methane on substituted barium hexaaluminates," *Catalysis Today*, vol. 59, no. 1, pp. 163–177, 2000.

[124] M. Machida, K. Eguchi, and H. Arai, "Catalytic properties of $BaMAl_{11}O_{19-\alpha}$(M= Cr, Mn, Fe, Co, and Ni) for high-temperature catalytic combustion," *Journal of catalysis*, vol. 120, no. 2, pp. 377–386, 1989.

[125] P. Artizzu, N. Guilhaume, E. Garbowski, Y. Brullé, and M. Primet, "Catalytic combustion of methane on copper-substituted barium hexaaluminates," *Catalysis letters*, vol. 51, no. 1-2, pp. 69–75, 1998.

[126] P. Artizzu-Duart, Y. Brulle, F. Gaillard, E. Garbowski, N. Guilhaume, and M. Primet, "Catalytic combustion of methane over copper- and manganese-substituted barium hexaaluminates," *Catalysis today*, vol. 54, no. 1, pp. 181–190, 1999.

[127] F. Gaillard, P. Artizzu, Y. Brulle, and M. Primet, "Catalytic combustion of methane: surface characterization of manganese-substituted barium hexa-aluminate catalysts," *Surface and interface analysis*, vol. 26, no. 5, pp. 367–373, 1998.

[128] M. Baldi, V. S. Escribano, J. M. G. Amores, F. Milella *et al.*, "Characterization of manganese and iron oxides as combustion catalysts for propane and propene," *Applied Catalysis B: Environmental*, vol. 17, no. 3, pp. L175–L182, 1998.

[129] V. Sazonov, Z. Ismagilov, and N. Prokudina, "Catalytic combustion of lean methane - air mixtures," *Catalysis today*, vol. 47, no. 1, pp. 149–153, 1999.

[130] V. Bobolev, M. Y. Gen, V. Mal'tsev, G. Melesov, P. Pokhil, V. Seleznev, A. Stasenko, and S. Chuiko, "Mechanism of action of iron catalysts on the combustion of composite systems," *Combustion, Explosion, and Shock Waves*, vol. 7, no. 3, pp. 317–324, 1971.

[131] A. Brown, J. Hargreaves, and B. Rijniersce, "A study of the effect of sulphation on iron oxide catalysts for methane oxidation," *Catalysis today*, vol. 45, no. 1, pp. 47–54, 1998.

[132] J. Walker, G. Straguzzi, W. Manogue, and G. Schuit, "Carbon monoxide and propene oxidation by iron oxides for auto-emission control," *Journal of Catalysis*, vol. 110, no. 2, pp. 298–309, 1988.

[133] P. Li, D. E. Miser, S. Rabiei, R. T. Yadav, and M. R. Hajaligol, "The removal of carbon monoxide by iron oxide nanoparticles," *Applied Catalysis B: Environmental*, vol. 43, no. 2, pp. 151–162, 2003.

[134] G. T. Linteris, M. D. Rumminger, and V. I. Babushok, "Catalytic inhibition of laminar flames by transition metal compounds," *Progress in Energy and Combustion Science*, vol. 34, no. 3, pp. 288–329, 2008.

[135] M. D. Rumminger, D. Reinelt, V. Babushok, and G. T. Linteris, "Inhibition of flames by iron pentacarbonyl," in *Halon Options Technical Working Conference*, 1998, pp. 145–156.

[136] M. D. Rumminger and G. T. Linteris, "Inhibition of premixed carbon monoxide–hydrogen–oxygen–nitrogen flames by iron pentacarbonyl," *Combustion and Flame*, vol. 120, no. 4, pp. 451–464, 2000.

[137] D. Reinelt and G. Linteris, "Experimental study of the inhibition of premixed and diffusion flames by iron pentacarbonyl," in *Symposium (International) on Combustion*, vol. 26, no. 1. Elsevier, 1996, pp. 1421–1428.

[138] M. Rumminger, D. Reinelt, V. Babushok, and G. Linteris, "Numerical study of the inhibition of premixed and diffusion flames by iron pentacarbonyl," *Combustion and flame*, vol. 116, no. 1, pp. 207–219, 1999.

[139] D. Jensen and G. Jones, "Catalysis of radical recombination in flames by iron," *The Journal of Chemical Physics*, vol. 60, p. 3421, 1974.

[140] M. D. Rumminger and G. T. Linteris, "Numerical modeling of counterflow diffusion flames inhibited by iron pentacarbonyl."

[141] I. Wlokas, A. Faccinetto, B. Tribalet, C. Schulz, and A. Kempf, "Mechanism of iron oxide formation from iron pentacarbonyl-doped low-pressure hydrogen/oxygen flames," *International Journal of Chemical Kinetics*, vol. 45, no. 8, pp. 487–498, 2013.

[142] K. Kim, K. Masiello, and D. Hahn, "Reduction of soot emissions by iron pentacarbonyl in isooctane diffusion flames," *Combustion and Flame*, vol. 154, no. 1, pp. 164–180, 2008.

[143] Burner diagram. [Online]. Available: http://www.flatflame.com/bronze.htm

[144] K. Seshadri, T. Lu, O. Herbinet, S. Humer, U. Niemann, W. J. Pitz, R. Seiser, and C. K. Law, "Experimental and kinetic modeling study of extinction and ignition of methyl decanoate in laminar non-premixed flows," *Proceedings of the Combustion Institute*, vol. 32, no. 1, pp. 1067–1074, 2009.

[145] P. C. Malte and J. C. Kramlich, "Further observations of the effect of sample probes on pollutant gases drawn from flame zones," *Combustion Science and Technology*, vol. 22, no. 5-6, pp. 263–269, 1980.

[146] M. Kassem, M. Qun, and S. Senkan, "Chemical structure of fuel-rich 1,2-$C_2H_4Cl_2/CH_4/O_2$/Ar flames: effects of micro-probe cooling on the sampling of flames of chlorinated hydrocarbons," *Combustion science and technology*, vol. 67, no. 4-6, pp. 147–157, 1986.

[147] R. M. Fristrom and A. A. Westenberg, *Flame structure*. McGraw-Hill New York, 1965, vol. 276.

[148] S. A. Syed, "Oxidation studies of surrogate bio-diesel fuels in opposed flow diffusion flames," Master's thesis, University of Toronto, 2005.

[149] Gas chromatography. [Online]. Available: http://hiq.linde-gas.com/international/web/lg/spg/like35lgspg.nsf/docbyalias/anal_gaschrom

[150] *Agilent 6890 Series Gas Chromatograph Site Preparation and Installation Manual*, Agilent Technologies, Inc.

[151] *Agilent 6890 Series Gas Chromatograph Operation Manual Volume 3. Detectors*, Agilent Technologies, Inc.

[152] *Agilent 6890 Series Gas Chromatograph Operation Manual Volume 2. Inlet*, Agilent Technologies, Inc.

[153] K. Pan, H. Qi, A. Patro, H. Zhu, S. Xiong, and J. Wen, "Characterization of a counter-flow laminar flame for studying natural gas catalytic combustionl," Combustion Institute - Canadian Section, 2013.

[154] S. Senkan and M. Castaldi, "Formation of polycyclic aromatic hydrocarbons (PAH) in methane combustion: comparative new results from premixed flames," *Combustion and flame*, vol. 107, no. 1, pp. 141–150, 1996.

[155] Y. Yoshioka, K. Sano, and K. Teshima, "NO_x removal from diesel engine exhaust by ozone injection method," *Journal of Advanced Oxidation Technologies*, vol. 6, no. 2, pp. 143–149, 2003.

[156] A. Gupta, S. Bolz, and T. Hasegawa, "Effect of air preheat temperature and oxygen concentration on flame structure and emission," *Journal of Energy Resources Technology-Transactions of The ASME*, vol. 121, no. 3, pp. 209–216, 1999.